博士論文

Morphological Analysis on
Two-dimensional Lipid Membrane Transition
(二次元脂質膜の形態変化解析)

髙橋 慧

Abstract

This doctoral thesis has been submitted to Department of Basic Science, Graduate School of Arts and Sciences, The University of Tokyo.

The thesis focuses on revealing the potential of a model biomembrane by using two-dimensional solid-sustained lipid membranes. Perturbation to the two-dimensional lipid membranes induced the membrane transition the mode of which has not been reported yet. A reconstituted two-dimensional membrane composed of natural lipids from an amoeba cell was newly developed and it buckled autonomously in the presence of the amoeba cell cytosol (Chapter 2). A constituted two-dimensional membrane composed of commercially available lipids exhibited the micrometer-sized pore formation after injection of the cytosol (Chapter 3). A two-dimensional membrane of a newly-designed DNA-lipid conjugate showed the 2D-3D transition which was triggered by heat stimulation (Chapter 4). The current studies include the development of the methodology for construction of two-dimensional model biomembrane in terms of synthetic biology and soft matter science.

Table of Contents

Chapter 4

Construction of Lipid Membrane of DNA-lipid Conjugate and 2D-3D Transition by Heat Stimulation **40**

Chapter 5

General Conclusion **50**

Reference **53**

Acknowledgement **59**

List of Publication **60**

List of Figures

Chapter 1 General Introduction

The general introduction for this thesis is written in this chapter. It includes the scientific attitudes and viewpoints for our understanding to the big problem "What is Life ?", reviewing the classical definitions of the life (1.1). Then, "The RNA World" and "The lipid world" hypotheses are discussed as the significant concepts for experimentalists approaching the nature and origin of life (1.2). Finally, the importance of model construction of membrane and the perturbing approach of its transition is remarked as the scope of this thesis (1.3).

1.1   The Classical Definition of Life

Human beings have been interested in nature and have tried to answer the two big questions; "What is the constituent of substances which are surrounding us?" and "What has happened to the boundary of the universe?" [1]. These correspond to the root meaning of natural science.[1] The former question drives us to the microscopic scientific attitude, and the latter question opens our eyes to macroscopic one. In natural science, when the length and the velocity of matter in the one-body system are raised, we face to understand different type of physics (Figure 1.1 (A)) [2]. The theories of the Quantum Mechanics and the General Theory of Relativity are self-consistent in each field. Even though the microscopic and macroscopic viewpoints and their comprehension (especially physics) have been progressed by the researchers, it should be noted that a problem how the two distinct viewpoints are connected remains in the many-body system. Hence the question of "What kind of mechanism can explain the phenomenon for connecting from microscopic interaction to macro world?" is very important and the Statistical Mechanics has been explored so far in terms of the many-body system (Figure 1.1 (B)). The Statistical Mechanics can connect the Quantum Mechanics and Thermodynamics as well as Field Theory. These theories for superconductivity or superfluidity in low temperature and time-independent state are established and amazing to us as the emergence of the elaborate theories to answer such remained questions.
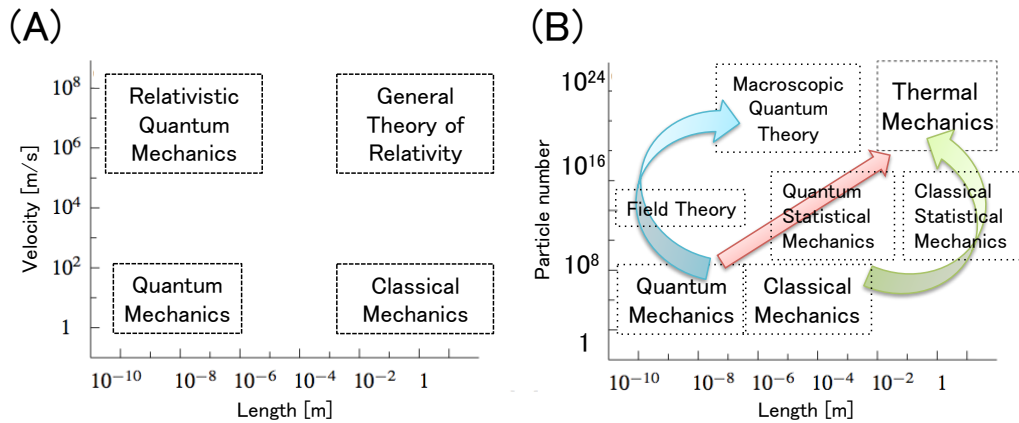
Figure 1.1: The Map of Textbooks (A) in one-body physics and (B) in many-body physics.

---

[1]at least for people who love science.

However, the question of the nature seen in our daily life and familiar to us (especially our bodies) is "Life system" or "Creation" and it is still unclear and remained as the big question of the many-body system. It has many species of molecules and they constitute in the time-dependent, dissipative system. The molecules are based on soft materials, for instance, macromolecules, colloidal particles, liquid crystals, surface-active agents, etc. The soft material is related to abundant forms of life system. Since the soft materials in a non-equilibrium and non-linear state are so complicated, the understanding in terms of the many-body system is an important issue in natural sciences especially physics. Many physicists have proposed the mechanism of soft materials in such state and the life system by their formula and languages [3].

This attitude and attempts of physicists and scientists have started since 1944 when Erwin Schrödinger published the book titled as "What is life?" [4]. First, he remarked that the stability of the life system is controlled by stable genes in his book. And, he introduced an aperiodic crystal with the following paragraph:

To give the statement life and colour, let me anticipate what will be explained in much more detail later, namely, that the most essential part of a living cell-the chromosome fibre may suitably be called an aperiodic crystal. In physics we have dealt hitherto only with periodic crystals. ... Organic chemistry, indeed, in investigating more and more complicated molecules, has come very much nearer to that 'aperiodic crystal' which, in my opinion, is the material carrier of life.

In other words, the life system containing genes must be unstable by physical thinking. He thus implied that information on genes makes the life system stable. Second, he concluded that the life system evades thermodynamic equilibrium state in a decay process from the initial states. According to the second law of thermodynamics, the following equation is expressed;

$$\oint (dq/T) \leqslant 0 \tag{1.1.1}$$

in which the dq notation indicates that any one infinitesimal step is reversible, and T represents (and is used to define in fact) absolute temperature. It is thus possible to define a new state function, S "entropy" which satisfies the definition of an exact differential;

$$dS := \frac{dq}{T} \tag{1.1.2}$$

In the irreversible process, entropy is created in the system, more entropy is extracted from the system than that added to it ($dS < 0$). On the other hand, in the reversible process, no entropy is created and the amount of entropy added is equal to the amount of entropy extracted from it ($dS = 0$) [5]. Does the life violate the second law of thermodynamics? Schrödinger explained that the life system evades the thermodynamic equilibrium by homeostatically maintaining negative entropy (today this quantity is called as information) in a circumstance of an open system.

Recently, the second law of thermodynamics including the mutual information $\langle I \rangle$ by the feedback controller [6, 7] was obtained;

$$\Delta F \leqslant \langle W \rangle + k_B T \langle I \rangle \tag{1.1.3}$$

where $\langle W \rangle$ is the statistical average of work W performed on a thermodynamic system, ΔF is the free-energy difference, k_B is Boltzmann's constant. Namely this formula corresponds to the principle of maximum work including Shannon Information. For elaborating the second law of thermodynamics, we thus have to consider information $\langle I \rangle$ which is related to the so-called Maxwell's demon. All life have their unique information based on the sequences of DNA and other biological molecules. The descendants in the life have received the information of the ancestors, namely, the life system experiences its history from the starting point of its origin. Hence, this law is plausibly related to the life system closely.

While the scientists have accepted the aforementioned statements of Schrödinger about the definition of the life system, several working definitions of life have been raised and discussed with the origin of life since late 20$^{\text{th}}$ century. National Aeronautics and Space Administration (NASA) has adopted the statement that "life is a self-sustained chemical system capable of undergoing Darwinian evolution", which was proposed by Gerald F. Joyce in 1994. Furthermore, Kepa Ruiz-Mirazo proposed the definition of life as "A living being is any autonomous system with open-ended evolutionary capacities" [8]. In addition, the group of Joan D. Oliver and Randall S. Perry remarked that "Life is the sum total of events which allows an autonomous system to respond to external and internal changes and to renew itself from which in such a way as to promote its own continuation" [9]. These are summarized by Dr. Takashi Nakada [10].[2]

There is also a practical drawback to Darwin's definitions. One of the activities of astrobiologists is *in situ* exploration for life on planets other than the Earth. They face to answer the following questions; how long would we wait for discovery of a system being "capable" of Darwinian evolution, and if so, under what conditions? [11]. To speak typically, a simple commonsense of "The Classical Definition of Life" has been acceptable to scientists. According to this, life have the following four properties.

[**A**] **Self-replication**
[**B**] **Energetic Metabolism**
[**C**] **Compartment**
[**D**] **Capability to Evolve**

Every life systems or creations have the ability to move keeping these four properties. When we look at Joyce's definition of life, this lacks [**B**] **Energetic Metabolism** and [**C**] **Compartment**. In the case of Ruiz-Mirazo's definition of life, [**B**] **Energetic Metabolism** is missing. Oliver and Perry's definition does not include [**D**] **Capability to Evolve**. Among these, [**C**] **Compartment** is to be noted as an important and understandable factor because the life system needs geometric borderline as living bodies are working and moving. Namely, the [**C**] **Compartment** of the life system is independent from time other than three factors [**A**],[**B**], and [**D**]. These factors are the functions of time. Since the searching of time-independent factors is also the first attitude for the natural science, this thesis focuses on the role of [**C**] **Compartment**, which is composed of lipid membrane.

Some astrobiologists have raised interesting standpoints to the definition of life. Some of them consider habitability of life system in our universe (Figure 1.2 (A)) [12]. Creations or life systems obtaining chemical or thermal energy as food make their borderline which has the difference of membrane voltage and the potential in Coulomb's energy (Figure 1.2 (B)). The particular range of the energy and the membrane voltage can define the life system.

This remark on the habitability of life system seems to be rambunctious to the definition of life, but it would be useful for the exploration on new extremophile life or creatures in the universe. Life system is maintained by the habitable circumstances as a dissipative structure.

Hence the studies on the definition of life and life system may contain the laws of physics established up to date and also those hitherto unknown. Namely, the difference of life system and non-life system is related to the answer to the question "What is life?" and it will be established as the unique theory on life system. In other words,[3]

$$\text{Life Phenomenon} \smallsetminus \text{Non-equilibrium Statistical Thermodynamics} \quad \Leftrightarrow: \quad \text{Theory Unique to Life} \qquad (1.1.4)$$

Therefore, the exploration on the definition of life needs not only our comprehension by non-equilibrium statistical thermodynamics but also the new concept and idea beyond such theories.[4] In order to consider the first step of the

---

[2]http://www2.tba.t-com.ne.jp/nakada/takashi/origlife/index.html
[3]$B \smallsetminus A$ termed the set-theoretic difference of B and A.
[4]Obviously, we have not even know the first thing about Non-equilibrium theory.
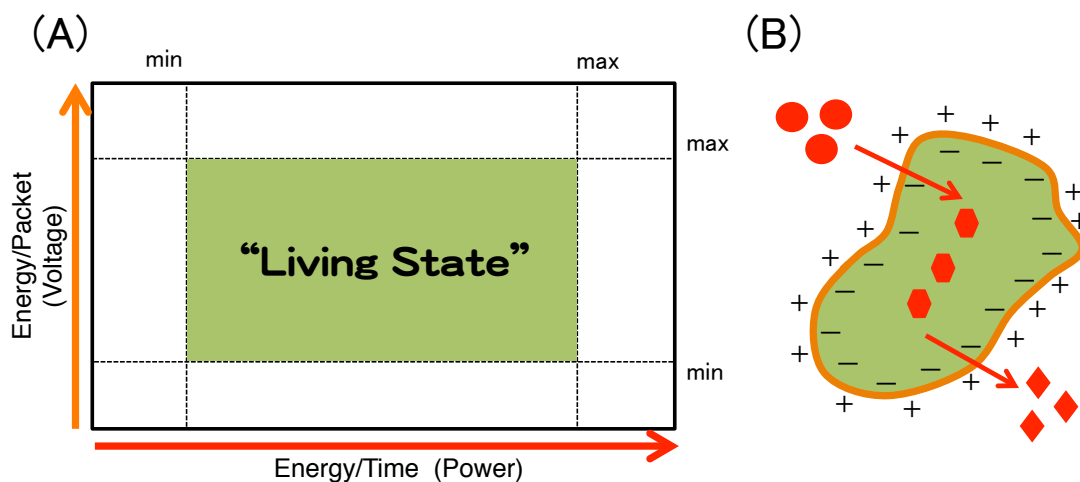
Figure 1.2: Definition and discharging waste of life in terms of habitability by astrobiologist. Schematic illustrations for (A) habitability maintained by an energy balance and (B) living body taking such energy as foods.

exploration, the lipid membrane as [C] **Compartment** is the best choice than other elemental features [A],[B], and [D] of the classical definition of life due to aforementioned discussion.

1.2 "The World" hypotheses for the Origin of Life

The exploration on the definition of life has strongly been linked with the investigation on the origin of life. Because life system has "emerged" and "continued" till now on the Earth. Here several hypotheses are briefly reviewed.

Many researchers accept an idea that the first living cell had some predecessors of the so-called "RNA world" [13, 14]. The RNA world is way of thinking that the beginning of life system can consist of the only RNA and its interaction because RNA have many important roles on chemical reaction networks. For example, an RNA molecule, which was found in *Tetrahymena*, was proved to have catalytic function [15]. The RNA catalysts, called as ribozymes, have been studied since then, because they were found throughout all domains of life system. Joyce's group provided the self-replication system of RNA [16, 17, 18, 19]. A ribozyme catalyzes the RNA production, which the produced RNA catalyzes the original ribozyme, namely, the RNA synthesis from two types of oligonucleotide substrates were mutually catalyzed (Figure 1.3). This undergoes the self-sustained exponential amplification of RNA in the absence of proteins or other biological materials. RNA molecules have information of life system and the sequence of RNA is changed by outer perturbation. Namely, They have three properties of "The Classical Definition of Life", [A] **Self-replication**, [B] **Energetic Metabolism**, and [D] **Capability to Evolve.**

However, RNA molecules do not have the property [C] **Compartment**.

As explained the previous section, the membrane as the borderline of life system is very important. On the Earth, the compartment of life system is composed of lipid membrane. The lipid membrane is merely governed the laws of physic established up to date, hence, consideration about difference between the laws of physics and life system is to be focused using lipid membrane.

Lipid membrane consists of the compartment or boundary for life, and further, senses and moves. For example, self-propelled oil droplets (Figure 1.4) realize one of fundamental and conceptual characteristics of cells, that is, the motion which is of importance for definition of life [20, 21]. The mechanism of the self-propelled oil droplets is based
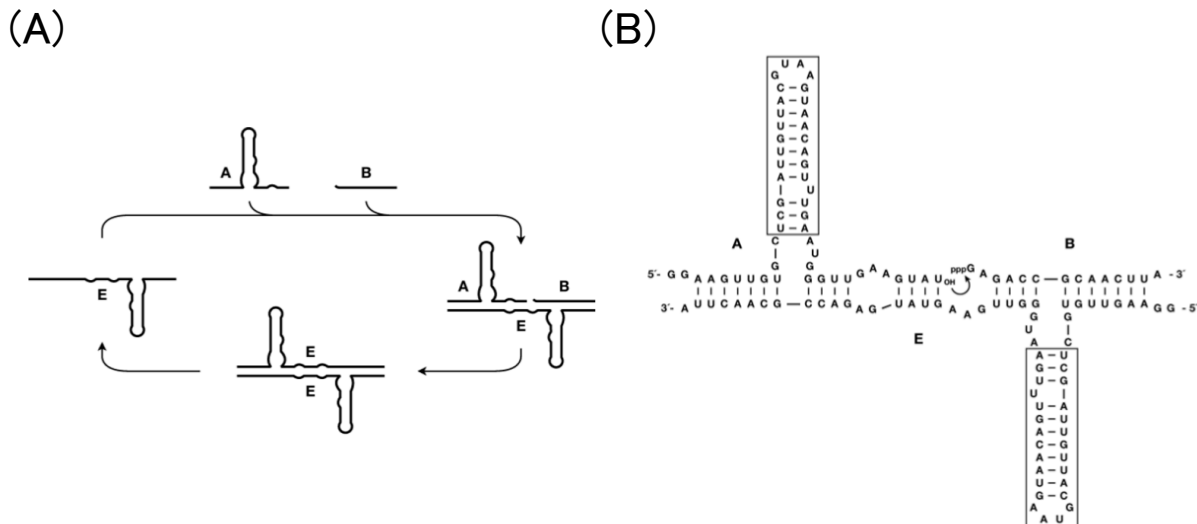
Figure 1.3: Self-sustained replication of an RNA enzyme. (A) The self-replication cycle, involving an RNA enzyme **E** that binds two RNA substrates (**A** and **B**) and catalyzes their ligation to form a new copy of **E**. The **E·E** complex dissociates to provide two copies of **E** to begin the next replication cycle. (B) Sequence and secondary structure of the **E·A·B** complex. Curved arrow indicates the site of ligation. Boxed region indicates the central stem-loop that can be replaced by an aptamer domain. [18]

on the Marangoni effect, spontaneous initiation of flow around the droplet surface due to the surfactant adsorption on the droplet surface, and the autonomous sustainability of surfactant adsorption and chemical reaction to the oil droplet which stays at the surfactant-rich environment. Namely, the self-propelled oil droplet exhibits an open chemical system with a supply of fresh material and energy, which is essential for the sustenance of the system. Such ability to move with keeping four properties of "The Classical Definition of Life" is clearly important in considering the life system. The cells having ability to move can modify their environment through metabolizing the environmental resources, maintaining their bodies, and producing wastes. In the chemical and biological sense, a chemical model for a cell plausibly need to avoid no-reaction by its ability to move.

Such chemical model links to another idea on the origin of life, "The Lipid World" [22]. The Lipid World is a hypothesis in which the lipid aggregates behave like the life system by only lipid interactions and molecular conversion.[5] But, the mechanism of the self-propelled oil droplet is not adopted in self-motion of real cells. On the other hand, lipid directly contributes to the real cells as the component of [**C**] **Compartment**.

A particular type of [**C**] **Compartment** composed of lipid is called as "vesicle", which is formed *in vitro* in an aqueous medium. The interior of the vesicle is a small aqueous pool and the boundary of the vesicle is constituted by thin layers (membranes) of lipid. The lipid is one of amphiphiles containing hydrophilic and hydrophobic parts and often forms bilayer membrane. Amphiphilic block copolymers also form vesicles in the aqueous medium [23, 24]. The amphiphiles in the vesicle membrane are arranged so that the hydrophilic parts are in contact with the aqueous medium and the hydrophobic parts associate to form the interior in the membrane. In the case of unilamellar vesicles composed of conventional biomembrane phospholipids, which have one hydrophilic head group and two lipophilic chains, the vesicle is constructed with one single bilayer membrane [25]. This structure resembles to that of biomembranes in cells. Therefore, while the oil droplets have not drawn attention as the compartment related to the definition of life, vesicles are the outstanding boundary taken the origin of life into accounts and are used for the compartment of cell models especially in synthetic biology.

As aforementioned, the RNA World lacks of [**C**] **Compartment** property in spite of being significant as physics and material science. The Lipid World is too simple and far away from real life system. How can we approach the model

---

[5]However, lipid roles do not have the [**D**]**Capability to Evolve** in obvious. Lipid can "study" at the highest.
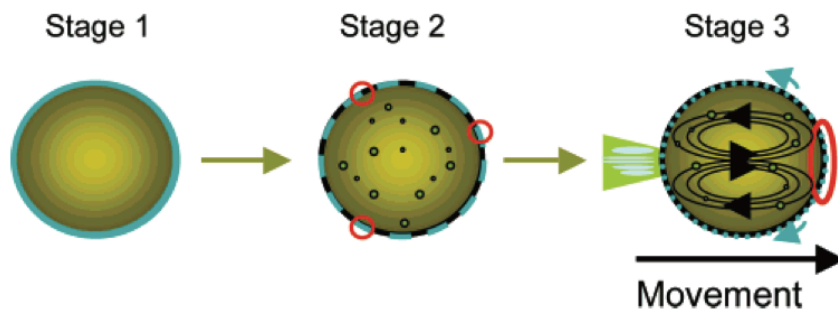
Figure 1.4: Schematic model of the initial stages in oil droplet movement. Stage 1: A fresh oil droplet (amber sphere) is introduced to the aqueous phase. The droplet appears symmetric and is coated in surfactant (blue line), and the oil phase is clear. Stage 2: Internal structures form within the oil droplet and begin to move as spontaneous oscillations exposing precursor to the water phase. Potential sites of hydrolysis are shown in red circles. The oil droplet now appears turbid. Stage 3: Symmetry is broken, convection begins (arrows within the oil), surfactant (blue) moves to the anterior pole (blue arrows), and hydrolysis of precursor is localized (red circle). The blue lines behind the droplet represent surfactant coming off the interface.[20]

of the origin of life and definition of life? The answer to this question is suggested in this thesis; [C] **Compartment** related to both life and non-life phenomenon with a viewpoint of their continuity (Figure 1.5). For example, virus does not have a metabolism but they have envelopes or membranes. Vesicles have only membranes as compartment. Hence, the study of lipid membrane is an acceptable and powerful candidate contributing for the one of the classical definition of life as [C] **Compartment**.

Moreover, in order to avoid the scientific mistake and wrong model for the life system, not only the pure and chemically well-known materials but also the crude and biological materials and their reaction are equally investigated in a macroscopic viewpoint.

1.3   Perturbing Approach for Membrane Deformation in two-dimensional system

The gap between the life and non-life systems has drawn much attention as aforementioned in not only scientific researcher groups but also our society. The gap could be assigned to crossover or phase transition, however we have no answer. As the natural science challenged and revealed what is the difference among ice, water and moisture 100 years ago, we now focus on this gap. For studying this gap, the previous sections dealt with the constructive approach and modeling (Figure 1.6). There still remains a risk that many model candidates cannot link to the real life system. However, we have three prescriptions, **Construction**, **Reconstruction** and **Knockout** of the life system. Hence, it is very intrinsic and somehow short-cutting to combine the three prescriptions.

There are two platforms of self-assembly using lipid membranes. One is the closed lipid membrane which encapsulates the compounds and enzymes which interact the lipids and further cause the membrane deformation through their biochemical reaction network. Molecular cell biology and synthetic biology have succeeded in this sense. The spatial-temporal localization and reaction activity using fluorescent or photoluminescent probes are evaluated in living cells and vesicles installed the proteins and gene circuits [26, 27, 28]. To investigate the initial state of the membrane deformation "emergence" in their methods, the timing of the first stage of their biochemical reaction network is regulated by the membrane-penetrating substrates such as isopropyl β-$_{D}$-1-thiogalactopyranoside. Heat stimulation for starting the biochemical reactions is also used in the vesicle platform researches in synthetic biology. However, these strategies contains the interference of the lipid membrane as a side-effect and the difficulty to set the "t = 0" at the biochemical reaction network due to the chemical/heat stimulation diffusion. These are still challenging issues
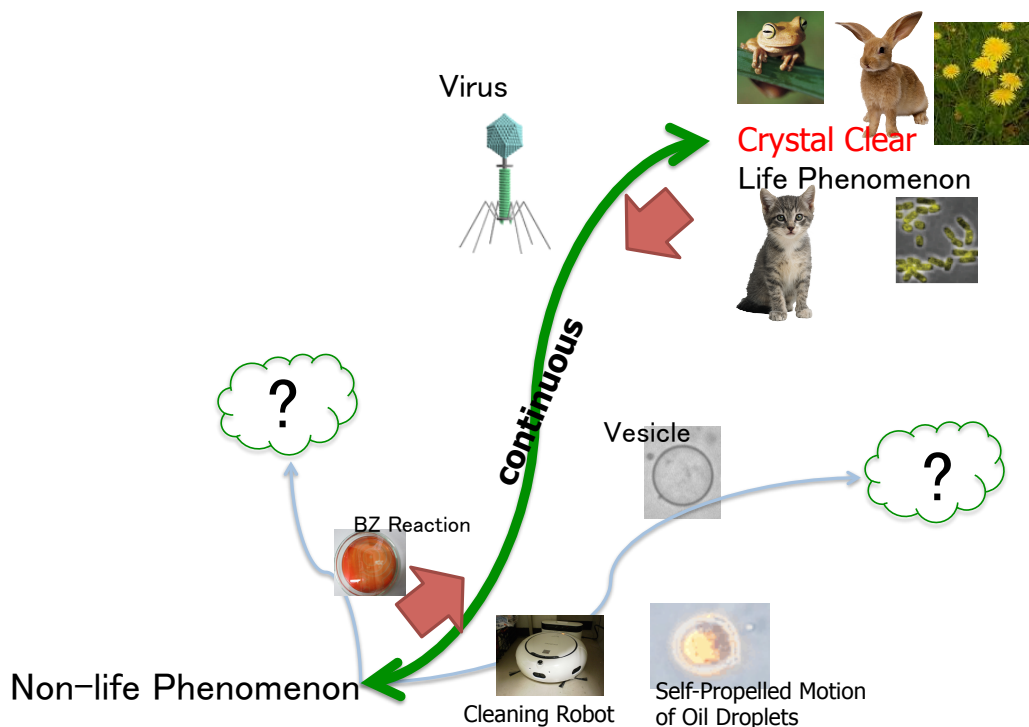
Figure 1.5: Illustration of the distribution of Life and Non-life phenomena in nature.

to be overwhelmed and the more controllable platform using lipid membranes is requisite. Hence, in this thesis, the other platform, two-dimensional solid-sustained lipid membrane, is focused. The two-dimensional lipid membrane is so open system that the timing of the injection of the reactive compounds and enzymes is directly assigned to "t = 0". One can also perform the sequential addition or activation (and exclusion or inactivation) of these compounds or enzymes using additives and drug molecules. Removing the encapsulation effect is enable us to focus on the elements and fundamental processes on [C] **Compartment**.

According to the discussions in this chapter, the scope of this thesis is to construct the methodology approaching the gap between the Life and Non-life system using two-dimensional solid-sustained lipid membrane which is related to the compartments considering the definition of the life system. Namely, this thesis explores two prescriptions; **Construction** and **Reconstruction**. By morphological analysis of the lipid membrane transition, the behavior difference of the extracted crude lipid membrane, purified lipid membrane, and artificial lipid membrane were examined.

In Chapter 2, the reconstitution of the micrometer-sized crude lipid membrane from *Dictyostelium discoideum* is explained. The cytosol extracted from *Dictyostelium discodeum* provides the protein localizing behavior on the membrane and the patch of the membrane exhibited an autonomous buckling.

In Chapter 3, purified lipids were utilized for constitution of the two-dimensional lipid membrane through the small unilamellar vesicle ruptured method. The injected cytosol extracted from *Dictyostelium discoideum* induced the membrane pore formation.

Chapter 4 focuses on the constitution of artificial lipid membrane which is conceived from model of the of the origin of life. A newly designed DNA-bearing lipid was synthesized and its two-dimensional lipid membrane exhibited the 2D-3D transition by heat stimulation. This phenomenon is discussed in terms of connection with information and compartment for constitution of RNA world completely.

Finally the significance of current findings and the future work of this thesis is discussed in Chapter 5.
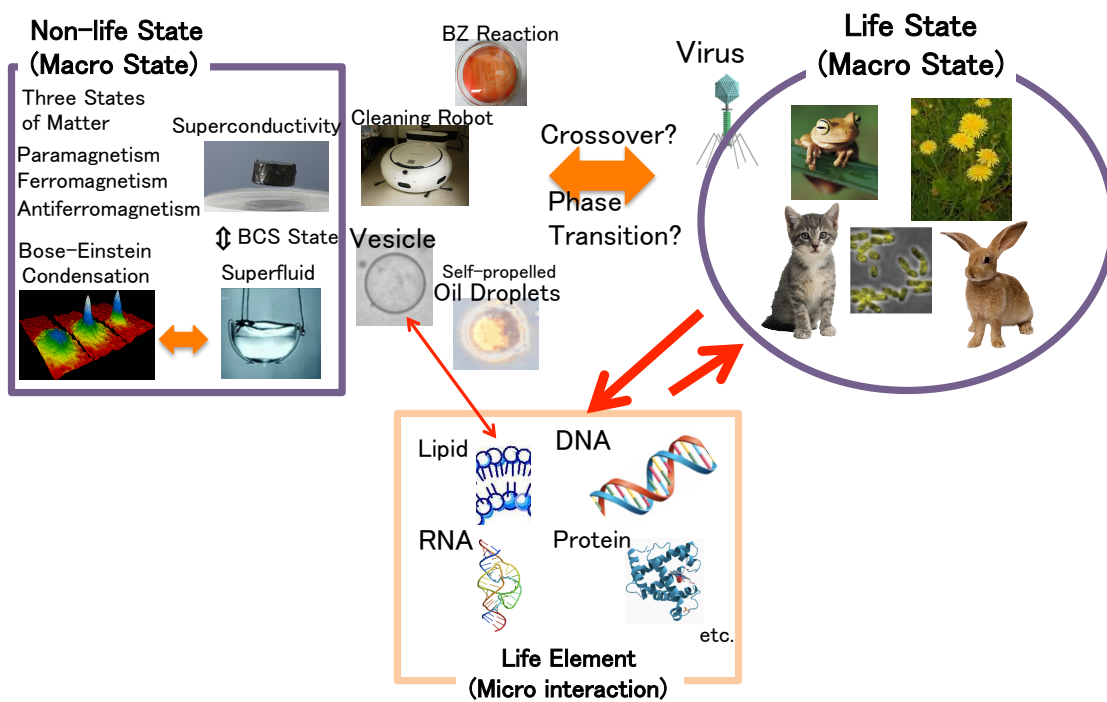
Figure 1.6: Conceptual Illustration of One of the final goals answering "What is Life?".

Chapter 2 Reconstitution of Lipid Membrane from Amoeba Cells and Its Buckling

2.1 Introduction
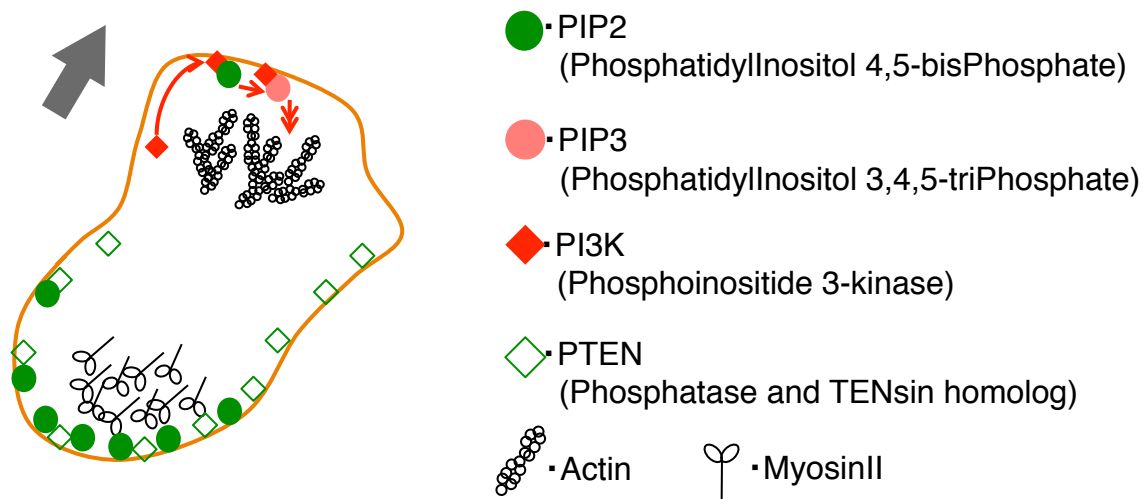
Figure 2.1: Amoeba motion at *Dictyostelium*. Translocation of PIP2 and PIP3 in cell membrane is related to determination of the anterior and posterior sides of the cell motion.

As explained in the previous chapter, the membrane i.e. [C] **Compartment** from "the Classical Definition of Life" should be maintained in the ability to move for living body which keeps the four properties. For the cell motion or dynamics, amoeba locomotion is fundamental mode. By the precise observation on cells exhibiting amoeba motion in the spatio-temporally high-resolution microscopy, the following model is now considered and accepted. Phosphatidylinositol signaling, in particular the interaction between 1-stearoyl-2-arachidonoyl-*sn*-glycero-3-phospho-(1'-*myo*-inositol-4',5'-bisphosphate) (PIP2) and 1-stearoyl-2-arachidonoyl-*sn*-glycero-3-phospho-(1'-*myo*-inositol-3',4',5'-bisphosphate) (PIP3)[1] in cell membrane, controls amoeba locomotion (Figure 2.1). PIP3 activates F-actin polymerization at forward end of a cell. On the other hand, PIP2 activates Myosin-2 contraction at posterior end of a cell. Figure 2.2 describes the reaction network in so-called phosphatidylinositol signaling [29, 30, 31, 32]. However, the mechanisms of asymmetric localization of these signal-associated proteins is not fully comprehended yet in the molecular biology methods. Here, a new system of two-dimensional reconstituted membrane is introduced to challenge this difficulty.

Reconstitution approaches have been adopted to understand such complex biological functions. Prof. van Oudenaarden's group reported that lipid vesicles coated with the Listeria monocytogenes virulence protein ActA are propelled by in vitro actin polymerization [33]. Prof. Takeuchi's group developed self-propelled beads modified with flagella [34]. Prof. Sonobe's group showed that an actomyosin fraction moves like an amoeba containing sol-gel conversion of a cytoplasmic extract [35]. These approaches have been established by using only a part of the chemical reaction networks related to the cell machinery.

When one focuses on using the whole system of biochemical reaction networks for the cell machinery reconstitution,

---

[1]18:0-20:4 PI(4,5)P2 and18:0-20:4 PI(3,4,5)P3 is usual abbreviation.
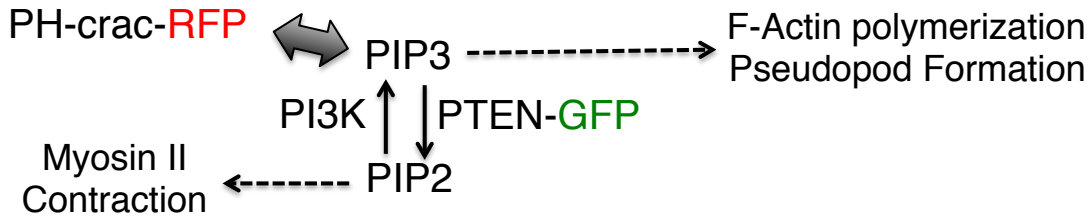
Figure 2.2: Scheme of phosphatidylinositol signaling network in *Dictyostelium*.

change of geometrical configuration and orientation of the components has drawn much attention for exploring the frangibility of the system. Especially, for an amoeba motion reconstructed system, the *in vitro* self-organization of lipid membranes and proteins in a micrometer-sized reaction surface or two-dimensional plane is important.

When one aims to examine amoeba motion, the problem that the parameter space composed of the lipids and proteins related to amoeba motion is too vast to investigate often arises because each component should be completely purified and mixed in a sequential manner. Hence this obstacle is overcame by using lipids and cytosol extracted from an amoeba cell and constructing micrometer-sized substrate-contacting lipid-protein membrane patches. The constructed system enables us to not only examine the essence of the membrane-assisted biochemical machinery of amoeba motion without the cell complexity, but also to avoid the practical difficulty of incomplete encapsulation of cytosol extracts in the case of vesicle-type biochemical machinery. The current purpose is thus to construct an amoeba motion reconstructed system consisting of the cytosolic extract and the lipid membrane film of *Dictyostelium discoideum* (Figure 2.3).

This reconstructed system provides us two achievements which have not delivered in the previous studies. First, the membrane deformations, including membrane buckling, are closely related to amoeba motion which highly functionalized with the coupling of cellular mechanics and sensors [36]. Conventionally, the buckling of a cell membrane is examined by using a narrow glass capillary with the inner diameter of several micrometers. The aspiration through the glass capillary attached on the cell membrane induces locally the cell membrane deformation (and even the transformation of the whole cell body) [37]. This observation method and morphological analysis cannot access directly to the spontaneous interaction between the lipid membrane and the enzymes and compounds of the cytosol of the amoeba cell. Thus the reconstruction study for the membrane buckling of cell is necessary by using the lipid and cytosol extracted from the amoeba cells. Since there is still a difficulty to realize the membrane deformation triggered by the simple injection of the cytosol to the lipid membrane, the lipid patch the size of which is in the range of cellular size must be formed. Second, the conventional molecular cell biology or biophysics have inevitably focused on the dynamics of amoeba cell in living state, namely, the biochemical machinery of the cell dynamics has maintained as the amoeba cells through their history. However, these researches are limited within the living state and do not able us to investigate the initial stage of the amoeba motion in the manner which is independent from the cell living states. The question how the biochemical machinery of the amoeba motion is constructed is to be answered through reconstruction of membrane deformation phenomena, such as membrane buckling, in the spatio-temporarily controlled manner. The reconstructed system using the lipid and cytosol from amoeba cells is two-dimensional and open so that these requirements are fulfilled.

I have three steps in the protocol for reconstruction method. First, the lipid and cytosolic extracts from *Dictyostelium discoideum* (*Dictyostelium*), are focused because *Dictyostelium* is a type of amoeba that sprightly shows amoeba motion at room temperature (20 - 23 °C). The experiment can be undergone without heating or cooling from room temperature. Second, I adopt the spin coating method to prepare a lipid membrane film constructed on a substrate because lipid mixtures extracted from living cells can hardly form well-defined membrane structures, such as single
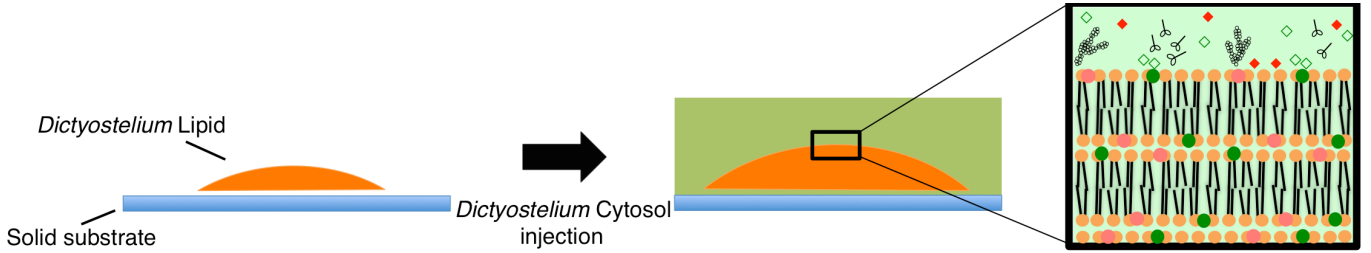
Figure 2.3: Schematic illustration of the micrometer-sized membrane machinery consisting of lipids and a cytosolic extract both of which are extracted from *Dictyostelium discoideum*.

bilayer membranes, supported on a substrate. The spin coating method produces micrometer-sized patches with a thickness of several micrometer when the membrane-forming components are heterogeneous, resulting from the interaction between the organic solvent and the solutes [38]. Third, in order to trace the transformation of such lipid membrane film in a three-dimensional manner after the addition of the cytosolic extract, the time lapse observations using a confocal laser scanning fluorescence microscope was performed.

2.2 Materials and Methods

2.2.1 Cell culture

AX4 cells of the *Dictyostelium discoideum* axenic strain were cultured in modified HL5 medium under shaking at 155 rpm at 22 °C [39]. The AX4 cells co-expressing the Pleckstrin homology domain of cytosolic regulator of adenylyl cyclase (PH-crac) tagged with RFP (PH-crac-RFP) and the phosphatase and tensin homolog deleted from chromosome 10 (PTEN) tagged GFP (PTEN-GFP) were cultured in modified HL5 medium containing G418 (30 μg/mL, Wako) and Hygromycin B (60 μg/mL, Calbiochem) [40].

2.2.2 Cytosol extraction

Cytosolic extracts were prepared from AX4 cells according to the protocol described elsewhere [41, 42]. The cells, which were numbered at 7×10^6 cells mL^{-1} were harvested, washed two times with 80 mL of phosphate buffer (PB), and re-suspended in 500 μL of PB. Cells were disrupted by nitrogen decompression using a cell disruption vessel (model 4639, Parr Instrument, IL, USA) on ice. Cell lysate was centrifuged at 16000 $\times$ g for 30 min at 4 °C. The supernatant was isolated and centrifuged again. The supernatant was transferred to a microtube and kept on ice until just before use. When I examined LY294002 as an inhibitor assay, a dimethyl sulfoxide solution (2 μL) of LY294002 (final concentration of 40 μM) was added to the cell suspension of PB (250 μL) with shaking for 30 min just before use for the extraction.

2.2.3 Lipid extraction

Lipid extraction was performed according to the protocol of Bartles's group [43] with slight modifications. AX4 cells were harvested, washed two times with 80 mL of PB, and re-suspended in phosphate buffered saline (PBS) to prepare the cell dispersion of 4.0×10^8 cells mL^{-1}. The dispersion was quickly frozen once in liquid nitrogen and freeze-thawed in an ice water bath. Lysates were centrifuged at 50,000 $\times$ g for 45 min at 4 °C. Pellets were homogenized by a pipette in Milli-Q water. The homogenate was centrifuged again, and the washed pellets were drained and dispersed in a mixed organic solvent (CHCl$_3$/MeOH (2:1, v/v)). The volume of the organic solvent was 2250 μL per 4×10^8 cells. The organic dispersion was centrifuged at 2000 $\times$ g for 5 min at 4 °C. The organic layer was transferred to a glass

bottle by an acute Pasteur pipette and the solvent was removed by nitrogen gas blowing. The residue was suspended in 938 μL of CHCl$_3$/saturated NaCl aq (2:1, v/v) and the suspension was centrifuged at 2000 $\times$ g for 5 min at 4 °C. The organic layer was transferred to a glass bottle by an acute Pasteur pipette.

2.2.4 Spin coating and microscopy observation

On a square-type cover glass (18 mm $\times$18 mm, thickness; 0.12 - 0.17 mm, MATSUNAMI, Japan), 60 μL of the organic lipid solution was dropped and it was spin coated at 300 rpm for 3 min using a spin coater (MIKASA, JAPAN). As a reference experiment, a chloroform solution (60 μL) of 1-palmitoyl-2-oleoyl-3-sn-glycero-3-phosphocholine (POPC, 0.45 mM, Wako, Tokyo, Japan), 1,2-hexadecanoyl-3-sn-glycerophosphatidylinositol-(3,4,5)-trisphosphate (PIP3, 10 mol%, Avanti Polar Lipids, U.S.A.), and TexasRed®-1,2-dihexadecanoyl-sn-glycero-3-phosphoethanolamine triethylammonium salt (TexasRed-DHPE, 0.1 mol%, Invitrogen, U.S.A.) was dropped and spin coated in the same manner. The lipid membrane film formed on the cover glass was shaded from light and set in a desiccator, and the residual organic solvent was completely removed from the lipid membrane film under reduced pressure at room temperature for 17 hours. To assemble a chamber, the cover glass was attached to a perforated dish with double-sided tape (Frame Seal, thickness; 280 μm, BIO-RAD, MA, USA). The chamber was placed on a microscope stage and the lipid membrane film was pre-wetted by 50 μL of PBS for 10 min. After injection of 25 μL of the extracted cytosol, the lipid membrane film was observed under a confocal laser scanning fluorescence and bright field microscope (A1R$^+$, Nikon, Japan) equipped with a 60$\times$ objective lens. Red and green fluorescence images were obtained through the corresponding band-pass filter and dichroic mirror units (excitation; 562 nm, emission; 570 - 620 nm and excitation; 487 nm, emission; 500 - 550 nm). The time interval for time lapse image acquisition was set to 6 sec. To determine the area of lipid membrane patch formed on the cover glass, the histogram of each Green and Red fluorescence intensity of all pixels on the captured image frame was analyzed by ImageJ (NIH, USA) and found two peaks in the histogram. Since one peak with lower fluorescence intensity was caused by the noise from the detector and the scattered light, the area of pixels where the intensity was in the range of the other peak distribution with larger intensity was measured.

2.2.5 Phalloidin staining and observation

For visualization of F-actin, I used Alexa488-labeled phalloidin (Invitrogen, U.S.A.). 30 min after injection of the cytosol, the lipid membrane film was fixed with 3.7 % formalin in PBS for 10 min. The formalin-fixed film was washed three times by 3 mL of PBS and stained by 50 μL of 5 units/mL Alexa488-labeled phalloidin dissolved in PBS for 20 min, and washed three times by PBS. The stained film was observed under a confocal laser scanning fluorescence microscope (CSU-X1, IX81, Olympus, Japan) equipped with a 100$\times$ objective lens. Red and green fluorescence images were obtained by using the corresponding band-pass filter and dichroic mirror units (excitation; 520 - 550 nm, emission; > 580 nm and excitation 470 - 490 nm, emission; 510 - 550 nm).

2.3 Results

2.3.1 Micrometer-sized patches of lipid membrane film prepared by spin coating

The spin coating method for the lipid membrane film supported on a glass substrate conventionally enables us to prepare heterogeneous films using a lipid mixture [38]. After extraction of the lipid mixture from the wild-type *Dictyostelium*, AX4 cells, the light microscopy clarified the lipid membrane film of *Dictyostelium* prepared by the spin coating method on the millimeter scale by light microscopy. A lipid membrane film pattern on the cover glass was observed (Figure 2.4(a)), which was held by the aspiration pores of the spin coat holder (Figure 2.4(b)). The lipid membrane film pattern was consisted of 25 islands (approximately 2.5 - 3.0 mm in diameter) which contained several patches on the micrometer scale (black spots shown in Figure 2.4(a)). In order to visualize such patches precisely,

both the bright field microscopy images and the autofluorescence images of the lipid membrane film were obtained by using confocal laser scanning fluorescence microscopy. Two sets of autofluorescence images were obtained by using two irradiation lasers and the corresponding band-pass filter and dichroic mirror units (see 2.2.4 Spin Coating and Microscopy Observation). Figure 2.4(c) shows the reconstructed images of the bright field microscopy and autofluorescence images of one of the patches. The regions between the islands were also covered with very thin lipid membranes by a peak existence of autofluorescence intensity measuring z-series at Figure 2.6 (A). Judging from the image analysis and taking into account the diffraction limit of light and the special resolution, the sizes of the patches were in the range of 2.7 to 3.2 $\times$ 10^4 μm^2 and the size range was observed reproducibly; at least 4 out of 5 runs in all processes, from lipid extraction to film preparation by spin coating.

(a) cover glass with *Dictyostelium* lipid membrane film

(b) Photograph of the cover glass holder

(c) Reconstructed image of the typical patch
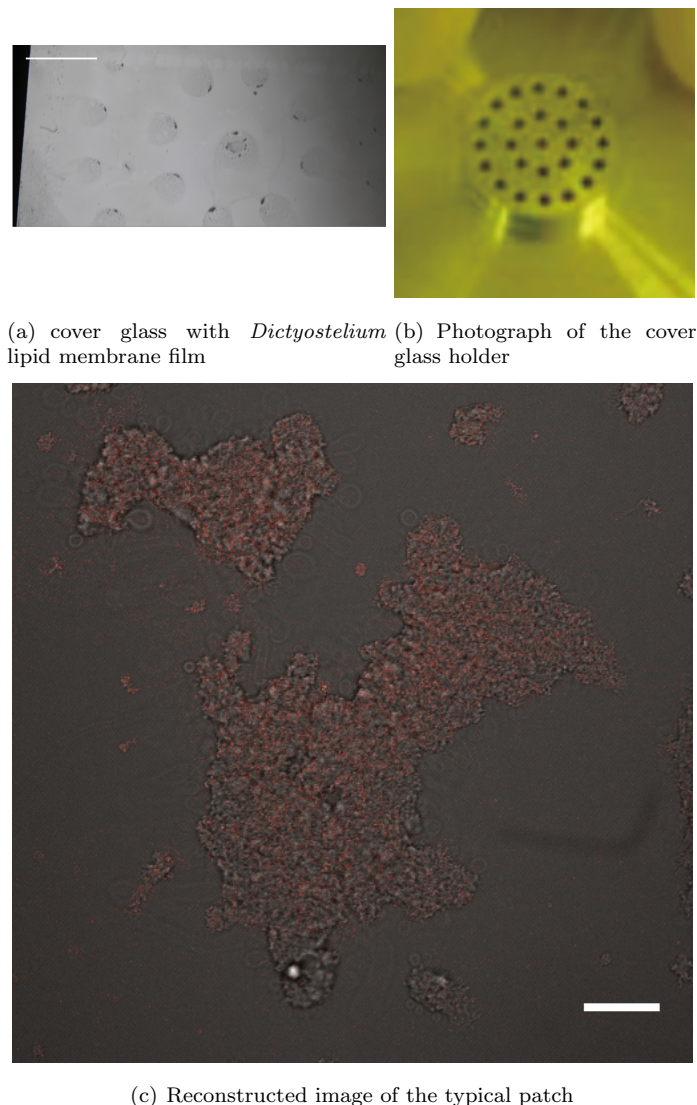
Figure 2.4: Lipid membrane film formed by the spin coating. (a) Bright field microscopy image of the cover glass with *Dictyostelium* lipid membrane film prepared by spin coating (bar = 3 mm). (b) Photograph of the cover glass holder. (c) Reconstructed image of the bright field microscopy image and the autofluorescence images of the typical patch of *Dictyostelium* lipid membrane film (bar = 30 μm).
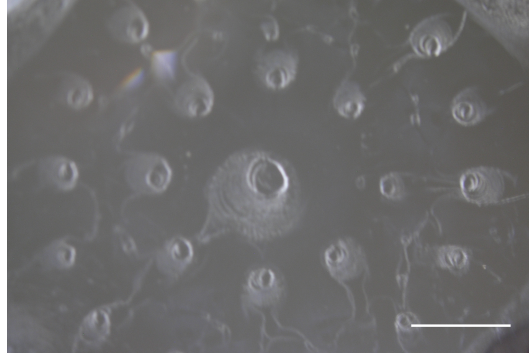
Figure 2.5: Bright field microscopy image of the cover glass with lipid membrane film of POPC containing PIP3 (10 mol%) prepared by the spin coating. Bar = 3 mm
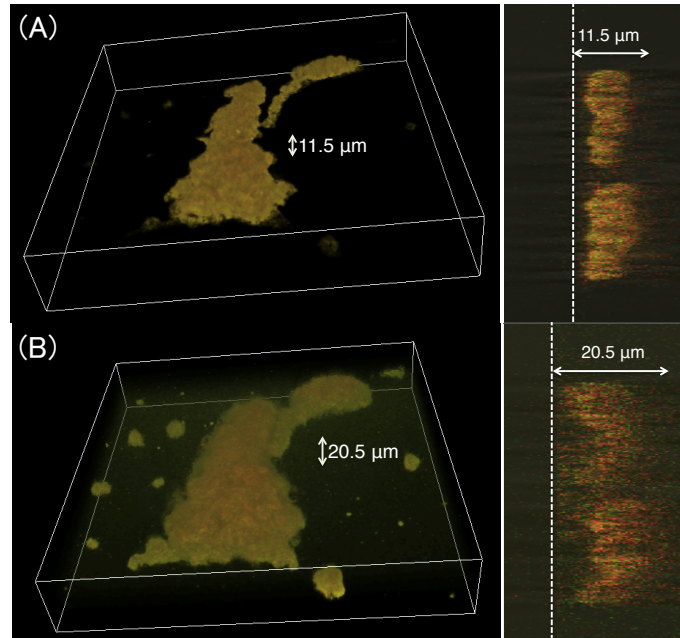
Figure 2.6: 3D-merged reconstructed images of the autofluorescence images of a typical *Dictyostelium* lipid patch obtained by confocal laser scanning fluorescence microscopy with both Red and Green detection modes before (A) and 30 minutes after (B) injection of cytosol extract. The volume size of observation space is 210 μm $\times$ 210 μm $\times$ 37.5 μm. Each x-z plane cross- section of the 3D merged reconstructed image was attached in the right column. Dashed lines correspond to the surface of the glass slide. The height indicates the distance between the surface of the glass slide and the peak top position of the autofluorescence images.

2.3.2 Buckling of lipid membrane patch after injection of cytosol extract

After setting up a chamber attaching the cover glass to a dish by a double sided tape, I injected the cytosol (25 μL) extracted from AX4 cells. As shown in Figure 2.6, the buckling of the lipid film patch was traced immediately after wetting the *Dictyostelium* patch by PBS and following injection of the AX4 cytosol (Figure 2.7). The *Dictyostelium* lipid patch exhibited autonomous transformation for the initial 10 min, resulting in the swelling in the x-y plane. Moreover, I observed a mesh-like structure after the transformation in the bright field microscopy images. The cytosol of genetically modified *Dictyostelium* cells, containing the Pleckstrin homology domain of cytosolic regulator of adenylyl cyclase (PH-crac) tagged with RFP (PH-crac-RFP) and the phosphatase and tensin homolog deleted from chromosome 10 (PTEN) tagged GFP (PTEN-GFP), was injected. The initial lipid membrane, with a maximum height of 10.5 μm on average (Figure 2.8 (A)) under treatment with PBS for 1 min for pre-wetting started to buckle after 10 min in the chamber. In 25 min, *Dictyostelium* lipid patch stopped buckling and an equilibrium state was reached 30 min after *Dictyostelium* cytosol injection into the chamber (Figure 2.9 (A)). The average maximum height of lipid patches was 15.5 μm as seen in 3D reconstructed images. Figure 2.8 (B) shows that PH-crac-RFP and PTEN-GFP localized on micrometer-sized patch of lipid membrane, were mutually exclusive. In particular, GFP fluorescence was enriched at the edge of the patch and surrounded the RFP-fluorescing regions inside the patch (Figure 2.8 (C)). Taking into account the fluorescence intensity of the confocal fluorescence images of the patch at each z-position (interval = 0.5 μm), I evaluated the change in the width and height of the patch before and 30 min after cytosol injection. By measuring the fluorescence intensity profile along the z- position in both Red and Green modes (Figure 2.8 (D), (E), (F), and (G)), I found that the height of the patch increased 30 minutes after cytosol injection (Figure 2.8 (F) and (G)). The maximum thickness of the patch increased by a factor of 2.1 $\pm$ 0.4 after cytosol injection, indicating that membrane deformation and buckling dynamics took place after cytosol injection (Figure 2.10).

Then, the time course changes in the fluorescence intensity of *Dictyostelium* lipid patches in Red and Green modes were analysed with cytosols containing PH-crac-RFP and PTEN-GFP. The mean fluorescence intensity of Green and Red modes of all pixels on each image frame (Red mode, Figure 2.9 (B); Green mode, Figure 2.9 (C)) increased immediately after cytosol injection (t = 30 sec.). When I compared the initial increase in fluorescence intensity in the range of 30 - 180 sec., I found that PTEN-GFP was localized faster than PH-crac-RFP reproducibly. Because, the vertical axis of Figure 2.9 (B) is the same as one of Figure 2.9 (C). As a reference experiment, I injected *Dictyostelium* cytosol containing PTEN-GFP and PH-crac-RFP to the chamber of lipid patches composed of a POPC/PIP3 membrane, and the fluorescence image obtained in the same procedure showed that PTEN-GFP localized on the patches and its localization speed was similar to that observed in the case of *Dictyostelium* lipid patch (Figure 2.9 (D)). Because the lipid patch of POPC/PIP3 was stained with TexasRed-DHPE, I omitted the change in Red fluorescence in this reference experiment.
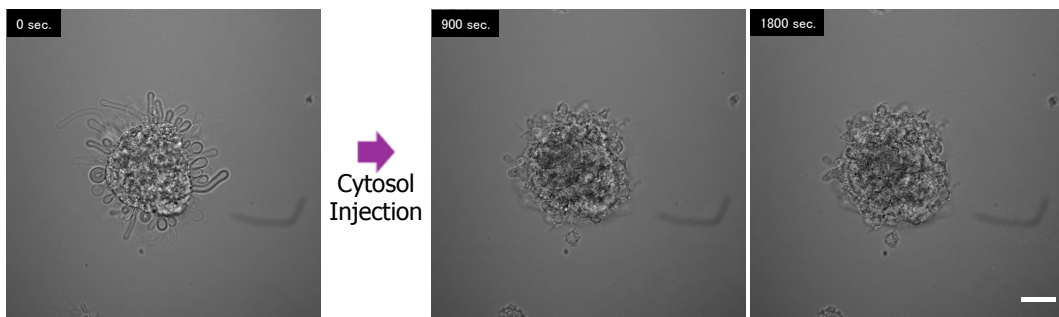
Figure 2.7: Time-course change of bright field microscopy images of *Dictyostelium* lipid patch. The buckling motion of the lipid patch occurred remarkably for initial 900 seconds after injection of AX4 cytosol (24 - 30 sec.). Bar = 30 μm.
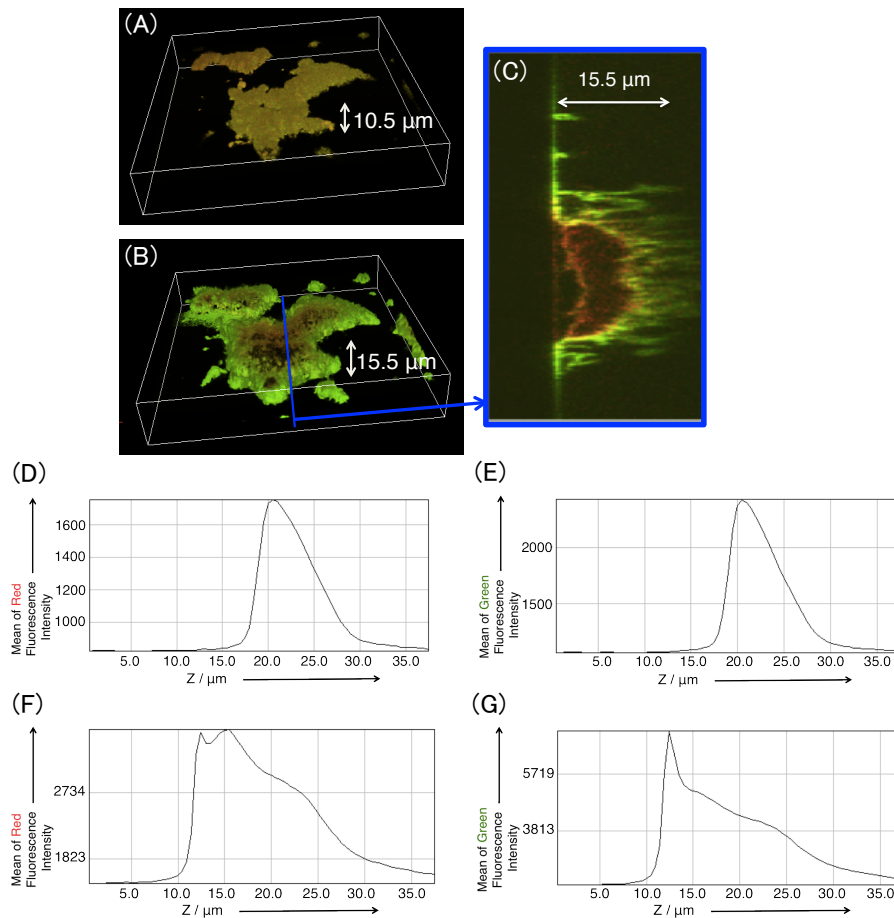
Figure 2.8: *Dictyostelium* lipid membrane before cytosol injection and after one. (A) 3D merge of reconstructed fluorescence images of a typical patch of the *Dictyostelium* lipid membrane film obtained by confocal laser scanning fluorescence microscopy, with both Red and Green fluorescence filter units, before injection of cytosol extract. The volume size of observation space is 210 μm × 210 μm × 37.5 μm. The mean fluorescence intensity of each Red and Green fluorescence image was plotted along the z position in (D) and (E) respectively. (B) 3D merge of reconstructed fluorescence images and (C) the cross-section reconstructed fluorescence images of a typical patch of the lipid membrane film obtained by confocal laser scanning fluorescence microscopy with both Red and Green fluorescence filter units, 30 minutes after injection of the cytosol extract of PH-crac-RFP/PTEN-GFP co-expressing cells. The mean fluorescence intensity of each Red and Green fluorescence image was plotted along z position in (F) and (G), respectively. The height shown in (A-C) indicates the distance between the surface of the glass slide and the peak top position of the autofluorescence images.
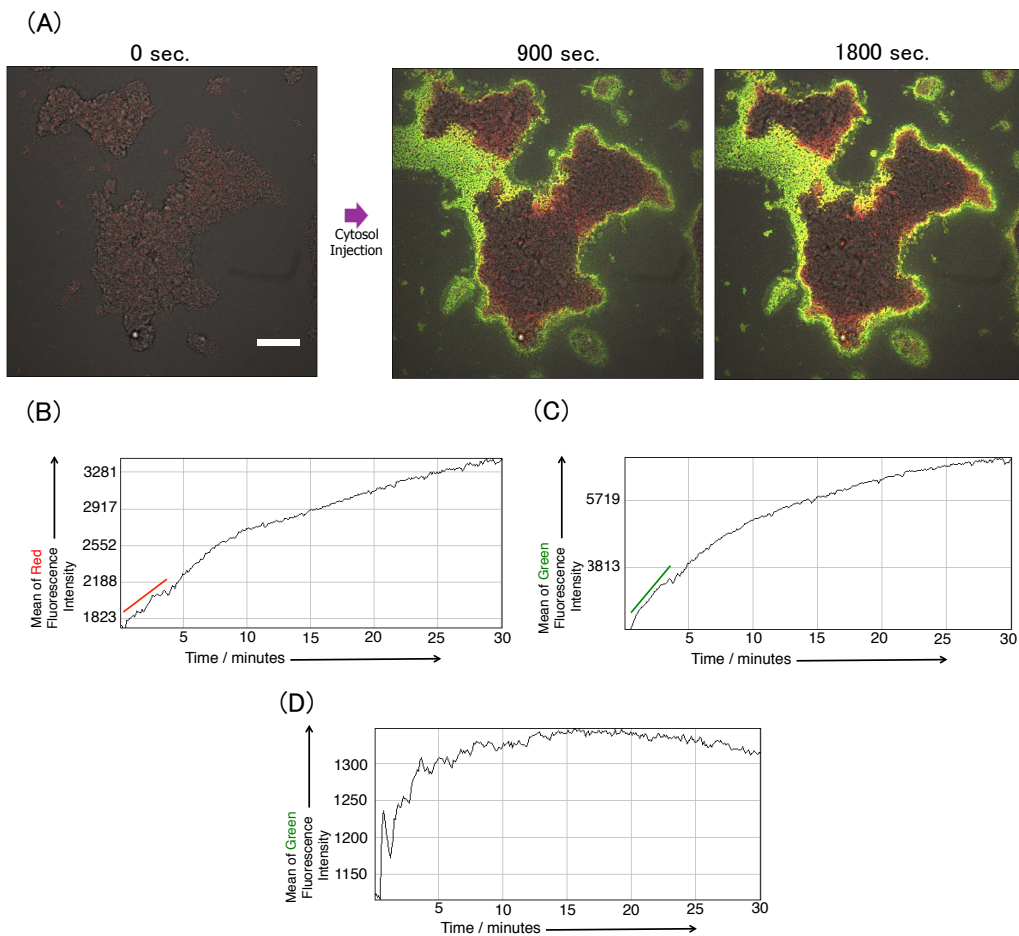
Figure 2.9: (A) Microscopy obsevation of the time-course change of *Dictyostelium* lipid patch. I captured the movie by the confocal laser scanning fluorescence microscopy with both Red and Green detection modes and the typical bright field microscopy. The PTEN-GFP and PH-crac-RFP localization on the *Dictyostelium* lipid patch occurred after injection of cytosol extract of PH-crac-RFP/PTEN-GFP co-expressing cells (24 - 30 sec.). bar = 30 μm. Time course change of the mean fluorescence intensity analysed by fluorescence images (z position; two image frames ($\sim$ 1 μm) above the glass slide) of a typical patch of the *Dictyostelium* lipid membrane film obtained by confocal laser scanning fluorescence microscopy images with both Red (B) and Green (C) fluorescence detection filter units after injection of the cytosol extract of PH-crac-RFP/PTEN-GFP co-expressing cells. The slope in the range of 30 - 180 sec. is depicted in each diagram. (D) Time course change of the mean fluorescence intensity analysed by fluorescence images (z position; two image frames ($\sim$ 1 μm) above the glass slide) of a typical patch of the POPC/PIP3 membrane film obtained by confocal laser scanning fluorescence microscopy images with Green fluorescence detection filter units after injection of the cytosol extract of PH-crac-RFP/PTEN-GFP co-expressing cells.
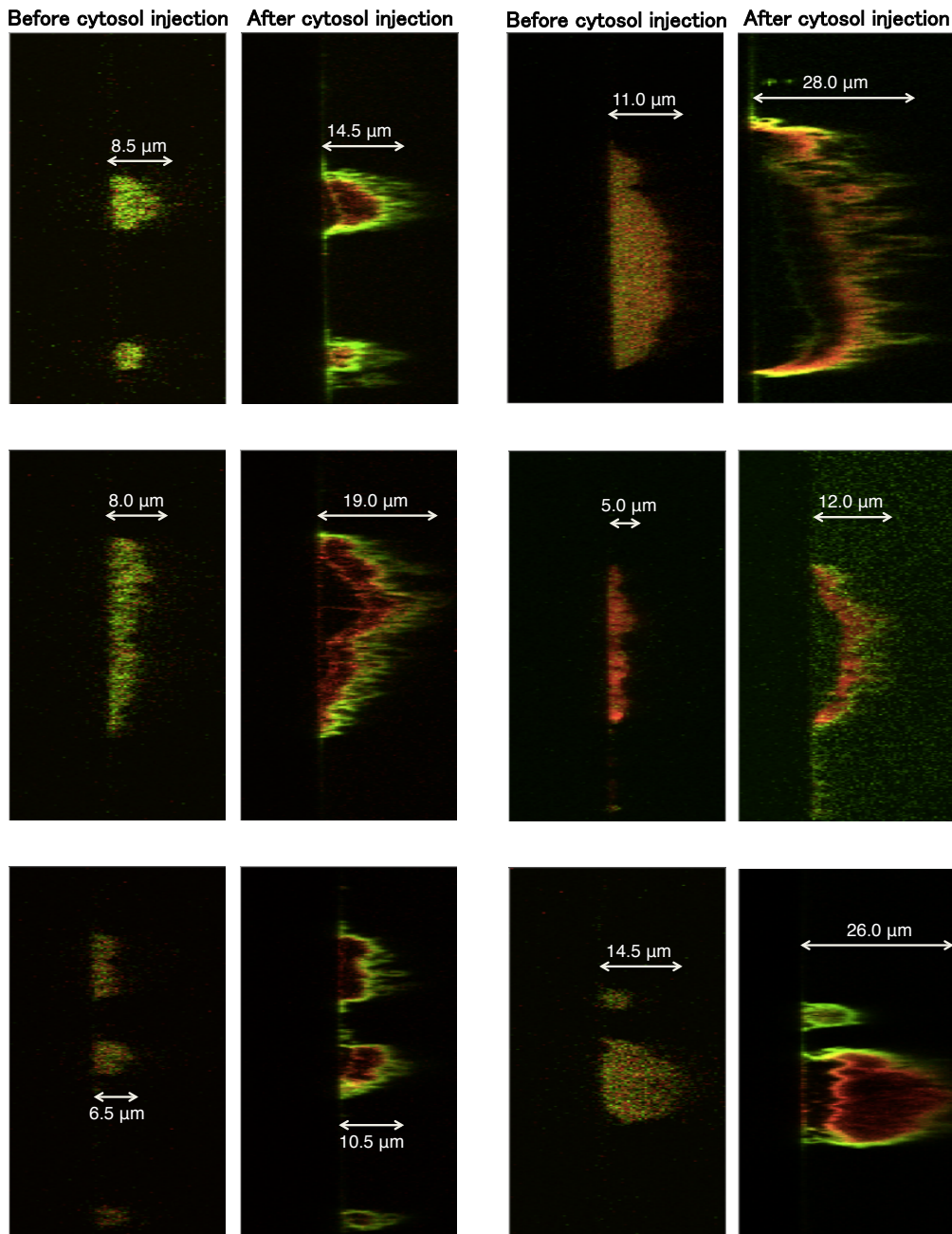
Figure 2.10: The cross-sections of 3D merged reconstructed fluorescence images of lipid membrane patches obtained by confocal laser scanning fluorescence microscopy with both Red and Green fluorescence filter units, before and 30 minutes after injection of the cytosol extract of PH-crac-RFP/PTEN-GFP co-expressing cells. The size of observation space is 37.5 μm $\times$ 210 μm. The six patches were constructed independently in each chamber and undergone the injection of the cytosol. The cytosol was extracted and stocked in same day (left) and different days (right).
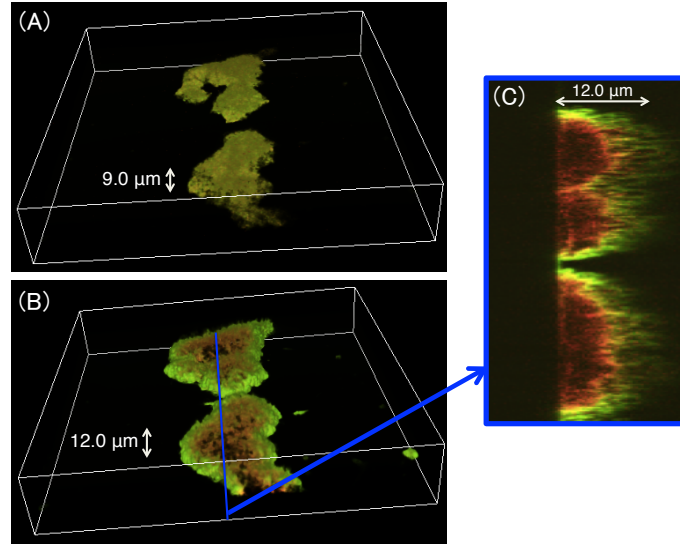
Figure 2.11: *Dictyostelium* lipid patches before cytosol injection extracted from *Dictyostelium* cell starved in the presence of LY294002 and after one. (A) 3D merge of reconstructed fluorescence images of a typical patch of the *Dictyostelium* lipid membrane film obtained by confocal laser scanning fluorescence microscopy, with both Red and Green fluorescence filter units, before injection of cytosol extracted from *Dictyostelium* cell which starved in the presence of 40 μM LY294002 for 30 minutes. The volume size of observation space is 210 μm $\times$ 210 μm $\times$ 37.5 μm. (B) 3D merge of reconstructed fluorescence images and (C) the cross-section reconstructed fluorescence images of a typical patch of the lipid membrane film obtained by confocal laser scanning fluorescence microscopy with both Red and Green fluorescence filter units, 30 minutes after injection of the cytosol extract of PH-crac-RFP/PTEN-GFP co-expressing cell which starved in the presence of 40 μM LY294002 for 30 minutes. The height shown in (A-C) indicates the distance between the surface of the glass slide and the peak top position of the autofluorescence images.

To evaluate the effect of LY294002 to the membrane deformation observed here, the PH-crac-RFP/PTEN-GFP co-expressing cell had starved with 40 μM LY294002 and the cytosol was extracted and injected to two-dimensional reconstituted membrane. LY294002 is an inhibitor of PI3K. At concentration higher than 30 μM, LY294002 effectively inhibited translocation of PH-domain to the plasma membrane of the cells responding to chemoattractant stimulation [44]. The initial lipid membrane, with a maximum height of 9.0 μm on average (Figure 2.11 (A)) under treatment with PBS for 1 min for pre-wetting started to buckle after 10 min in the chamber. *Dictyostelium* lipid patch stopped buckling and an equilibrium state was reached 30 min after injection of the cytosol extracted cells starved with LY294002. The average maximum height of lipid patches was 12.0 μm as judged in 3D reconstructed images. Figure 2.11 (B) shows that PH-crac-RFP and PTEN-GFP localized on the micrometer-sized patches of lipid membrane were mutually exclusive. In particular, GFP fluorescence was enriched at the edge of the patch and surrounded the RFP-fluorescing regions inside the patch (Figure 2.11 (C)). The maximum thickness of the patch increased by a factor of 1.7 $\pm$ 0.6 after injection of the cytosol extracted cells staved with LY294002, indicating that membrane deformation and buckling dynamics took place after this cytosol injection (Figure 2.11). These results have almost same tendency evaluated in the Figure 2.8.

To take advantage of this two-dimensional reconstructed system, the injection of the mixture of the cytosol and 40 μM LY294002 was examined (Figure 2.12). As shown in Figure 2.12 (A) and (B), the buckling of the lipid film patch was traced immediately after wetting the *Dictyostelium* lipid patch by PBS and following injection of the mixture of AX4 cytosol and LY294002. Moreover, the mixture of the cytosol extracted from PH-crac-RFP/PTEN-GFP co-expressing cell and 40 μM LY294002 was also examined and it was found that PH-crac-RFP and PTEN-GFP localized on the *Dictyostelium* lipid patch. These results indicate that, in spite of the injection of the cytosol treated directly with LY294002, membrane buckling was still active.
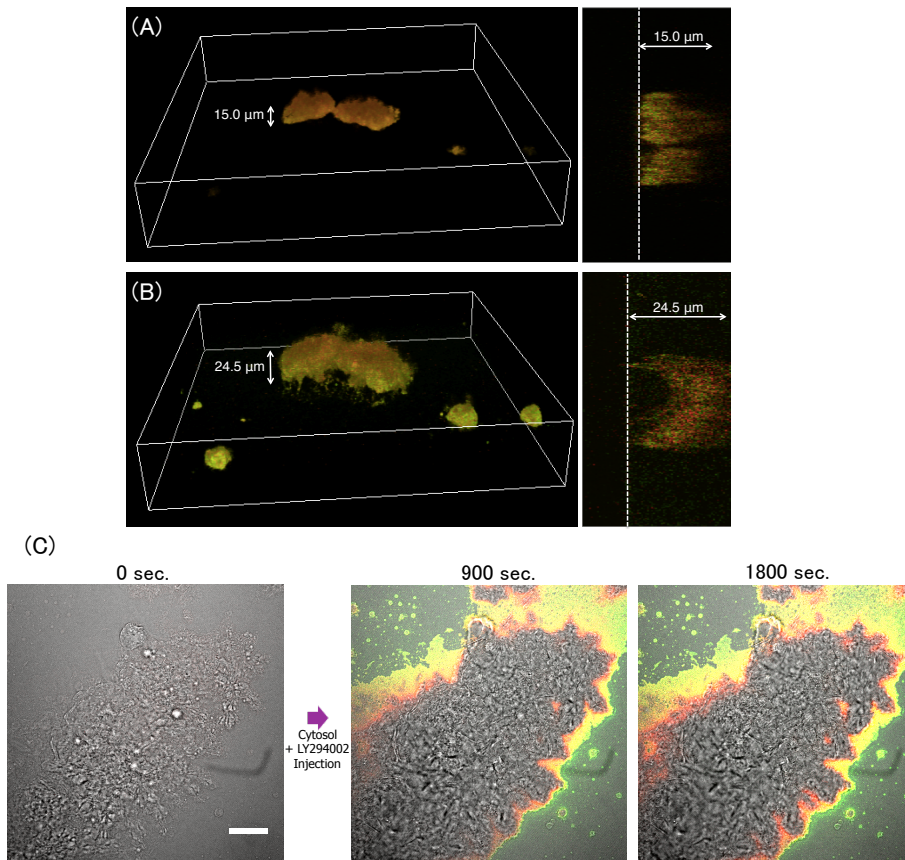
Figure 2.12: *Dictyostelium* lipid patches in the presence of the mixture of the cytosol and LY294002. 3D-merged reconstructed images of the autofluorescence images of a typical *Dictyostelium* lipid patch obtained by confocal laser scanning fluorescence microscopy with both Red and Green detection modes before (A) and 30 minutes after injection of the mixture of the cytosol extract and 40 μM LY294002 (B). The volume size of observation space is 210 μm $\times$ 210 μm $\times$ 37.5 μm. Each x-z plane cross-section of the 3D merged reconstructed image was attached in the right column. Dashed lines correspond to the surface of the glass slide. The height indicates the distance between the surface of the glass slide and the peak top position of the autofluorescence images. Microscopy observation of the time-course change of *Dictyostelium* lipid patch after the injection of the mixture of the cytosol extracted from PH-crac-RFP/PTEN-GFP co-expressing cell and 40 μM LY294002 (C). Time-laps observation was performed by the confocal laser scanning fluorescence microscopy with both Red and Green detection modes and the typical bright field microscopy. The PTEN-GFP and PH-crac-RFP localization on the *Dictyostelium* lipid patch occurred after injection (24 - 30 sec). Bar = 30 μm.
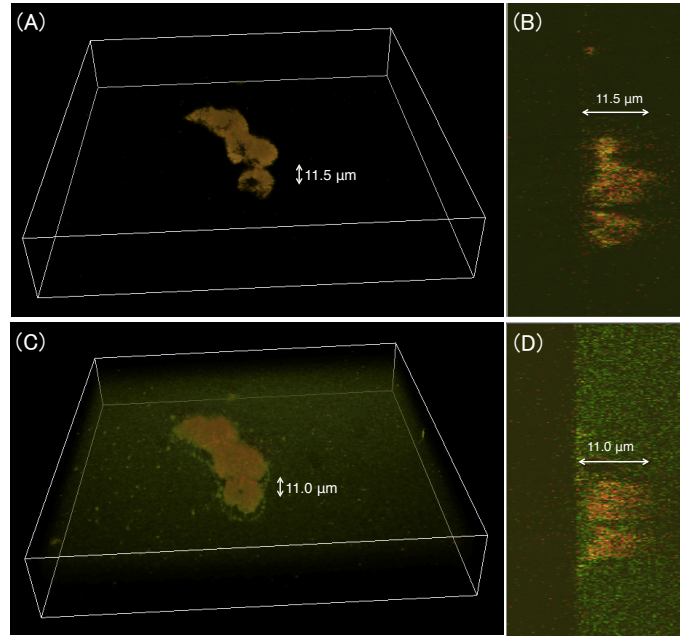
Figure 2.13: 3D-merged reconstructed images of the autofluorescence images of a typical *Dictyostelium* lipid patch obtained by confocal laser scanning fluorescence microscopy with both Red and Green detection modes before (A,B) and 30 minutes after (C,D) injection of cytosol extract, which had been treated at 65 °C for 1 hour just before use, of PTEN-GFP/PH-crac-RFP co-expressing cells. The volume size of observation space is 210 μm $\times$ 210 μm $\times$ 37.5 μm. Each x-z plane cross-section of the 3D merged reconstructed image was attached in the right column (B,D). The height indicates the distance between the surface of the glass slide and the peak top position of the autofluorescence images.

In another reference experiment, I injected *Dictyostelium* cytosol from PH-crac-RFP/PTEN-GFP co-expressing cells treated at 65 °C for 1 hour into the chamber of *Dictyostelium* lipid patches. Figure 2.13 shows the autofluorescence images of the *Dictyostelium* lipid patch before and 30 minutes after cytosol injection. Analysed by time course change of the mean fluorescence intensity (z position; two image frames ($\sim$ 1 μm) above the glass slide), GFP fluorescence increased and the edge of each patch fluoresced 10 min after cytosol injection. Moreover, PTEN-GFP localization in the patch occurred but membrane thickness did not increase. When I injected the cytosol, which had been exposed to either autoclave processing or phosphate buffer treatment into the *Dictyostelium* lipid patch, no patch deformation was observed in either case. The POPC supported membrane on the cover glass remained unaltered after injection of cytosol of *Dictyostelium* cytosol from PH-crac-RFP/PTEN-GFP co-expressing cells.

It is known that F-actin polymerizes on *Dictyostelium* lipid membranes as a result of the downstream chemical reaction network of phosphatidylinositides, known as PIP signalling [45]. I used phalloidin staining to visualize the localization of F-actin polymerization and bundling in the *Dictyostelium* lipid patch in the current study. After formalin fixing, the confocal laser scanning fluorescence microscopy images of the *Dictyostelium* lipid patches showed F-actin localization and polymerization in the patches (Figure 2.14 (A)). No F-actin polymerization occurred on the POPC supported membrane (Figure 2.14 (B)), indicating that the *Dictyostelium* lipid patch accumulated phosphatidylinositides.
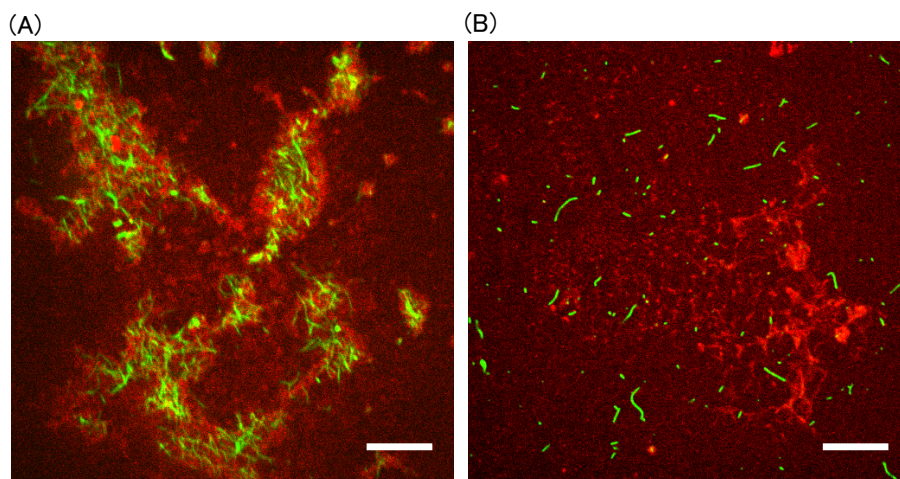
Figure 2.14: Confocal laser scanning fluorescence microscopy images of the *Dictyostelium* lipid patch (A) and POPC membrane film (B) after cytosol extract injection and following phalloidin staining. Bar = 10 μm.

2.4 Discussion

2.4.1 Lipid film patches prepared by spin coating

There are several methods for lipid membrane film preparations, such as casting [46], the spin coating [38, 47], Langmuir-Blodgett membrane formation [48, 49, 50], and vesicle rupture [50, 51, 52]. The casting and spin coating methods are conventionally adopted in requesting membrane films composed of any kinds of lipids or mixtures. In the Langmuir-Blodgett membrane method, the formation of a lipid monolayer on a water surface is essential for the lipid molecular structure and the composition of lipid mixture. The vesicle rupture method relies on the stability of the lipid bilayer membrane for the formation of small unilamellar vesicles as the initial protocol step. The water-in-oil droplet template method is based on formation of stable water-in-oil droplets and the monolayers are stacked in layer-by-layer manner by using a microfluidic system. These last three methods have drawn much attention in terms of preparing single, well-defined bilayer membranes on a substrate. In the current study, the lipid mixture extracted from AX4 cells contains a various kinds of lipids as described later. Thus, the adoption of the Langmuir-Blodgett membrane and the vesicle rupture methods is not worthwhile for the preparation of the lipid membrane film. In fact, previous reports on small unilamellar vesicles revealed that the components of each vesicle are dispersed even in one batch of the vesicle dispersion of lipid mixture [53, 54]. Though I actually tried small unilamellar vesicle ruptured method, its method did not afford such lipid membrane film using the lipid mixture extracted from AX4 cells[2]. Besides, the casting method, where an organic lipid solution is dropped onto a substrate and the solvent is removed resulting in the multilayer membrane structure, also has the issue of regulating membrane formation under the evaporation of the solvent. Particularly, the control of lipid membrane film formation is likely difficult due to the wetting and de-wetting process of the solvent and the solubility of lipids. The spin coating method facilitates the preparation of lipid membrane films using lipids extracted from AX4 cells and allows the control of the organic solution thickness, dissolving lipids before solvent evaporation occurs and resulting in several types of lipid membrane films on the substrate. The micrometer-sized patches of organic thin film are also formed by the spin coating method by means of micro-fabricated surfaces [59, 60] chemically modified substrate surfaces [61, 62] and differences in solubility between each solute in the organic solution [63]. It is noted that the spin coater holder, which has pores (pore size = 3.1 mm) of negative pressure to hold the cover glass induced the concave surface of the cover glass. The membrane film was formed at each position in the vicinity of the holder pores. As far as we know, this process may serve as the fourth technique for the preparation

---

[2]Charge interactions between vesicles and substrate are very important for vesicle ruptured method [55]. *Dictyostelium* lipids contain various lipids as reported in previous articles [56, 57, 58]. Because, charge interactions were not occurred unfortunately. But, I also described ruptured method case of the vesicle based POPC with *Dictyostelium* cytosol in Chapter 3.

of film patches in which the positions of patches are controlled by the holder pores without fabricating, modifying, and arranging the chemical properties of the solution components. After spin coating, the concave surface of the cover glass was covered by a thin layer of the organic solution, and then the further evaporation of the solvent resulted in the island formation with large thin film at each concave surface. The diameter of the island was approximately 3 mm in the current study. The sizes of the lipid film patches at each island were in the range of 2.7 to 3.2 $\times$ 10^4 μm^2. When a chloroform solution of 1-palmitoyl-2-oleoyl-3-sn-glycero-3-phosphocholine (POPC) and 10 mol % of 1,2-hexadecanoyl-3-sn-glycerophosphatidylinositol-(3,4,5) trisphosphate (PIP3) was dropped and spin-coated, islands and lipid membrane patches were also formed at the positions of the holder pores after solvent evaporation (Figure 2.5). Based on the micrograph of the patches, the contrast of the patches was stronger than that of the thin film island, indicating that the lamellarity of the patches was greater than that of the thin film. The mechanism of patch formation is interpreted as follows. Since PIP3 is likely insoluble in chloroform, the patches were primarily composed of PIP3 and grew in a thin layer in the organic solution after spin coating. During the evaporation of the solvent, POPC, the solubility of which is greater than that of PIP3, gradually self-assembled to form a thin film, which covered the concave surface including the patches. This process resembles the patch formation from heterogeneous lipid solutions in the spin coating method [64, 65, 66].

As reported in previous articles [56, 57, 58], lipids extracted from *Dictyostelium discoideum* contain phosphatidylcholines, phosphatidylethanolamines, phosphatidic acids, and phosphatidylinositides. According to the thin layer chromatograms reported in these articles, phosphatidylcholines and phosphatidylethanolamines have a higher affinity to organic solvents such as chloroform compared to phosphatidic acids and phosphatidylinositides. These results suggest that the *Dictyostelium* lipid patches formed on the cover glass contain the core structure of low-solubility lipids (phosphatidic acids, phosphatidylinositides, and so on) and the film layer contains high-solubility lipids (phosphatidylcholines, phosphatidylethanolamines, and so on). Moreover, the size of the patch is influenced by the initial step of *Dictyostelium* lipid extraction, namely the volume ratio of CHCl$_3$/MeOH (2:1, v/v) and the number of AX4 cells. I could systematically optimize the ratio as mentioned in the "2.2 Materials and Methods" to obtain a patch size in the range of 2.7 to 3.2 $\times$ 10^4 μm^2. The thickness of the patches was 10.5 μm on average, judging by 3D constructed images of the autofluorescence images obtained by confocal laser scanning fluorescence microscopy. Thus, the patches by observing their deformation or the construction of micrometer-scale amoeba motion system were applied for further experiments.

2.4.2   Autonomous buckling of the *Dictyostelium* lipid patch

The transformation of the lipid membrane film during hydration and swelling after aqueous solution injection has been discussed in the process of forming vesicles, which are closed lipid bilayer membranes. Vesicle formation consists of two steps: the separation step of stacked membranes and the swelling step of the separated membranes. The separation step of lipid membranes on a substrate was analyzed by atomic force microscopy [69], THz spectroscopy [70], neutron scattering [71]. The swelling step of lipid membranes was clarified in the formation of giant vesicles under the application of an alternative voltage [25].

In the separation step, the hydration of stacked membranes starts when water and water-soluble molecules penetrate or percolate into the stacked membranes of the lipid thin film. Next, the lamellar phase of the lyotropic liquid crystals in the lipid molecules emerges in the lipid thin film. The lipid membranes become elastic, retaining their tension and fluctuating in water. The fluctuating membranes gradually transform in order to minimize their bending energy and to maintain a thermodynamically stable shape: rippled plain lamella, dome-like, mushroom-like, and plain lamella connected with closed membranes via a bottleneck structure, in the swelling step. When an external shear force is applied to the bottleneck, the vesicle is formed at the stacked lipid membranes supported by a substrate. Even though the formation of vesicles was observed, the diameter of which were several micrometer at the path of lipid membrane film immediately after the pre-wetting and the injection of cytosol, it should be noted that the cytosol induced the patch buckling and the transformation of the dome-like shape, which is several tens of micrometers in diameter.

The buckling of lipid membrane films to form such large dome-like shapes from plain lamella is conventionally observed in the so-called electroformation method of giant vesicles [67]. Under the application of an alternative voltage, after the injection of water or buffered solution into the lipid membrane film, the swelling process of the lipid membrane film is controlled by the electrocataphoresis of the membrane and the addition of water and water-soluble substances into the intermembrane space. Thus, the control of the external voltage and time interval can afford the formation of the dome-like and spherical shapes of giant unilamellar vesicles. In this study, the buckling of the lipid membrane film patch composed of *Dictyostelium* lipid autonomously took place under no external forces or stimuli after cytosol injection. I interpret the buckling mechanism of the lipid membrane film patch as follows.

The cytosol of *Dictyostelium discoideum* contains various types of membrane-binding proteins and/or lipid-conversion enzymes such as phospholipases, lipases, and phosphokinases. Since PH-crac and PTEN play important roles in membrane deformation during amoeba motion [30], I focused on their adsorbing process onto the *Dictyostelium* lipid patch by means of PTEN tagged by GFP (PTEN-GFP) and PH-crac tagged by RFP (PH-crac-RFP). As shown in Figure 2.9 (B) and (C), in the initial stage immediately after cytosol injection, PTEN-GFP adsorbed more rapidly than PH-crac-RFP. Since PTEN-GFP adsorbed onto the POPC patch, which contained 10 mol% PIP3, it is implied that PTEN likely adsorbed onto the lipid membrane film. It is known that in living *Dictyostelium discoideum* cells, PTEN is one of the phosphokinases for phosphatidylinositides and tends to bind to the cell membrane during the resting mode of cells [31]. On the other hand, PH-crac tends to stay in the cytosol of resting cells and forms a lipid-protein complex with phosphatidylinositides when it adsorbs to the cell membrane [32, 29]. Because the amount of phosphatidylinositides is much smaller than that of other phospholipids in *Dictyostelium* lipid [32, 57], the initial adsorbing process of PH-crac on the *Dictyostelium* lipid patch is slower than that of PTEN. When the amount of adsorbed PH-crac gradually increases and the lipid-protein complex formation begins in the *Dictyostelium* lipid patch, it likely accumulates inside of the *Dictyostelium* lipid patch. This is probably because the phosphatidylinositides are organized primarily inside the patch and also, PH-crac competes with PTEN, which adsorbs and covers the *Dictyostelium* lipid patch to bind to the phosphatidylinositides. As a result, mutually exclusive distributions of PTEN-GFP and PH-crac-RFP were observed in the buckled *Dictyostelium* lipid patch. The trigger of the buckling is rationally induced by an increase in inner pressure and membrane instability induced by the accumulation of PH-crac and its complex with lipids. The *Dictyostelium* lipid patch is then buckled and grows to become a dome-like shape because of unbalanced osmotic pressure. As reference experiments, when I injected a cytosol, which had been treated at 65 °C for 1 hour just before use, I observed an increase in the fluorescence intensity of PTEN-GFP in the *Dictyostelium* lipid patch but no buckling (Figure 2.13). This indicates that only the adsorbed PTEN on the patch had no potential to induce buckling. After treating the cell culture with LY294002 before the extraction, I injected the extracted cytosol to the *Dictyostelium* lipid patch and observed the buckling and dome-like shape of the patch. The result implied that the activity of phosphatidylinositol-3-kinase (PI3K), which is one of the phosphokinases for phosphatidylinositides and is inhibited by LY294002, exerts less influence on membrane buckling than PTEN and PH-crac. While LY294002 is toxic to the amoeba cells and inhibits the amoeba motion of the cells, the two-dimensional reconstructed system revealed that LY294002 does not influence to the membrane buckling of the *Dictyostelium* lipid patch regardless of the treatment processes; (i) the cells starving in the presence of LY294002 and (ii) the mixing of an extracted cytosol with LY294002. It is plausible that the inhibition effect by LY294002 is related to not only the each component of the biochemical machinery (lipid molecule in membrane, compound and enzyme in cytosol) but also the three dimensional structure of the cell body giving a feedback to the cytosol organization. The membrane buckling observed in the current two-dimensional reconstructed system was observed so reproductively because it is open and undergoes no such feedback.

In order to clarify the phosphatidylinositides accumulation in the *Dictyostelium* lipid patch, I performed phalloidin staining for F-actin polymerization and bundle formation in the buckled *Dictyostelium* lipid patch because these chemical reactions occur at the sites of phosphatidylinositides aggregation accumulated in the *Dictyostelium discoideum* cell membrane [68]. Since bundles of polymerized F-actin were observed in the *Dictyostelium* lipid patch, it was confirmed

that the *Dictyostelium* lipid patch contains phosphatidylinositides after cytosol injection. It implies that, among the phosphatidylinositides, 1,2-dialkyl-3-sn- glycerophosphatidylinositol-(4,5)-diphosphate, which is the product from 1,2-dialkyl-3-sn-glycerophosphatidylinositol- (3,4,5)-triphosphate by PI3K, is less effective than PIP3 for the PTEN-GFP adsorbing behaviour and PH-crac-RFP accumulation.

To summarize the above experimental results, the buckling and dome-like shape of the *Dictyostelium* lipid patch after cytosol injection occur due to the formation of lipid-protein complexes at both the outer and inner regions of the patch.

2.4.3   Significance of the current reconstituted system

The formation of the micrometer-sized lipid-protein patch from *Dictyostelium discoideum* in the current study brought us two achievements for constructing the membrane-assisted biochemical machinery. One achievement is the pre-organization of the *Dictyostelium* lipid patches. The reconstitution of the lipid-protein membrane film from *Escherichia coli* has been already established by using commercially available lipid mixtures [72]. This is because the lipid mixture extracted from *Escherichia coli* facilitates the formation of lipid membrane films supported on a substrate through the vesicle rupture method. There have been reports of lipid-protein patch formed via the break-off of living cells fixed on a substrate [73]. These lipid-protein patches have only directed the focus on the adsorbing and localizing behaviours of proteins on the lipid membrane film. Thus, such setup for research is not applicable in studying membrane film dynamics and deformation, including buckling, because the membrane film is anchored and/or fixed onto the substrate. In the current study, the spin coating method enabled us to form pre-organized lipid patches from *Dictyostelium discoideum* on the micrometer scale using a substrate holder with aspiration pores. It is to be noted that this pre-organization likely induces not only the adsorption and localization of proteins in the cytosol but also the subsequent buckling of the lipid-protein patch. Moreover, when I compare the buckling of the *Dictyostelium* lipid patch with no deformation on the POPC film patch containing PIP3 under the cytosol, the membrane deformation observed *in vivo* could be linked with one-to-many or many-to-many interactions between proteins and lipids. I remark that the current study realized the membrane-assisted biochemical machinery through the self-organization of proteins and lipid membranes.

The other achievement is the constitution of the lipid-protein membrane film, showings three-dimensional dynamic behaviours. The closed bilayer formation to prepare vesicles using natural lipids has been adopted to investigate the adsorbing and localizing behaviours of proteins. Even though such vesicles have drawn attention in terms of artificial cell modelling, it is difficult to construct a membrane-assisted biochemical machinery to be tuned or modified inside after the encapsulation of the cytosol. The current 2D-system is one solution to this issue. Even though the thickness of the *Dictyostelium* lipid patch was evaluated to be 10.5 μm and the patch contained the stacked lipid layers, I observed the autonomous buckling of the lipid membrane film for the first time by the injection of the cytosol. Moreover, in the current system, one can provide a drug, LY294002, to the cytosol at any timing and amount. Conventionally the effect of LY294002 on amoeba cells and their motion has investigated in the living cells, i.e. encapsulated system, and it has been difficult to clarify the timing "t = 0" of the drug's effect on the biochemical machinery and its control. Therefore, this phenomenon is crucial for the continuing development of the membrane-assisted biochemical machinery demonstrating spatially and temporally controlled buckling and movement under chemical stimuli in an open system. The current **Reconstruction** method is a powerful tool to construct micrometer-sized membrane-assisted biochemical machinery.

2.5 Summary

The current study aimed at **Reconstruction** method of membrane-assisted biochemical machinery using the lipid and cytosol extracted from *Dictyostelium discoideum* separately. The micrometer-sized lipid membrane film was prepared by the spin coating method and the buckling of the *Dictyostelium* lipid patch formed on the glass substrate was observed under a confocal laser scanning fluorescence microscope after adsorption and localization of the proteins. The mechanism of buckling was discussed on the basis of the swelling behavior derived from the accumulation of proteins in the patch.

Chapter 3 Reconstitution of Supported Lipid Bilayer and Its Transition by Amoeba Cytosol

3.1 Introduction

In Chapter 1, the classical definition of life has been reviewed and the four properties of life are described as the inevitable elements on the definition. Even in cell motion, the four properties are maintained in the amoeba cell through its history. However, Chapter 2 has demonstrated that the membrane deformation related to the amoeba motion, i.e. membrane buckling, occurs in the two-dimensional reconstructed system bearing not whole but a part of [C] **Compartment**. This means that the two-dimensional reconstructed system using cell cytosol is able to afford the measurement of the potential of cytosol, especially, the biochemical reaction network on the [C] **Compartment**. Not only the membrane buckling but also many intracellular membrane dynamics combining [C] **Compartment** and [B] **Energy metabolism**, e.g. endocytosis and exocytosis, are found in amoeba cells. These dynamics have already drawn much attention in terms of the start and the end of the vesicular transportation system [74, 75, 76]. These membrane dynamics involve the deformation of membrane in the nanometer scale. Macropinocytosis, one of the intracellular membrane dynamics, is associated with the micrometer-sized membrane deformation and is closely related to the phosphatidylinositides signaling system [77]. Thus, the further exploration on the interaction and dynamics of the two-dimensional reconstituted system using the cytosol is focused in this Chapter.

On the other side of considering, real amoeba cells have their cellular membrane with single lipid bilayer naturally. Thus it is requisite to prepare a two-dimensional reconstituted system using a single bilayer lipid membrane and the cytosol. Among several preparation methods of the solid supported lipid membrane, so-called small unilamellar vesicle (SUV) ruptured method makes it possible to constitute the unilamellar and more uniform lipid membrane than that formed by the spin-coating method [38, 50, 52, 69]. This method is based on the electrical attractive force between the solid glass surface and lipid affording the supported lipid bilayer (SLB) [55]. Since the *Dictyostelium* lipid has so many species of lipids, the SUV ruptured method is not suitable for preparing *Dictyostelium* lipid SLB.[1]

Moreover, for exploring about the continuity between life system and non-life system (Figure 1.5), the membrane transformation involving life phenomenon (extracted cytosol) and non-life phenomenon (pure lipid SLB) has recently drawn much attention. For example, there are reports on the membrane transition of pure lipid SLB induced by injection of cytosol from *Escherichia coli*. Loose *et al.* presented the observation of the pattern formation and oscillation of proteins MinD and MinE on a SLB and a reaction-diffusion model of the MinD and MinE dynamics that accounts for this experimental observation [72]. In another report, the atomic force microscopy demonstrated that the nanometer-sized pores were formed in the pure phospholipid SLB in presence of *Escherichia coli* cytosol [78]. Furthermore, a SLB containing phosphatidylinositol 4,5 bisphosphate can afford the self-assembly of filopodia-like structures containing actin bundles with Cdc42, N-WASP-WIP, toca-1, Arp2/3 complex, and also the uniform and short polymerized actins [79]. These reports show that the reconstitution method using the pure lipid SLB membrane and the cytosol from prokaryotic cell or purified proteins related to cell motion or dynamics is a powerful tool for measuring the energy and kinetics of membrane transition.

---

[1]Infact, SUV ruptured method using *Dictyostelium* lipid had been tried. Even though SUVs of *Dictyostelium* lipid was formed by the natural swelling method and following ultrasonication and filteration. the SLB membrane was not formed over three days, and no ruptured.

In this chapter, the reconstitution method using the cytosol extracted from *Dictyostelium discoideum*, which is one of the eukaryotes, and a pure phospholipid SLB membrane on a glass substrate is developed using SUV ruptured method. It enables us to approach a question whether the SLB membrane including the lipids related to amoeba locomotion, which was discussed in Chapter 2, exhibits membrane deformation in the presence of the cytosol extracted by *Dictyostelium discoideum*. The SLB membrane was stained by a lipid fluorescence probe, TexasRed-DHPE in order to visualize the uniformness of the SLB membrane. Its dynamics was observed by a confocal laser scanning fluorescence microscope after the injection of the cytosol containing PTEN protein tagged with GFP (Figure 3.1).
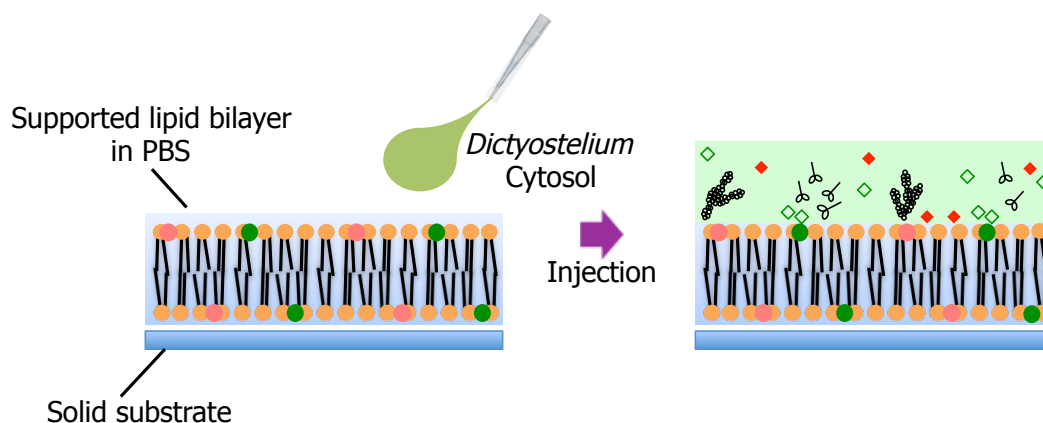
Figure 3.1: Schematic illustration of the supported lipid bilayers consisting of pure lipids and a cytosol extracted from *Dictyostelium discoideum*.

3.2 Materials

1-Palmitoyl-2-oleoyl-3-*sn*-glycero-3-phosphocholine (POPC) were purchased from Wako (Tokyo, Japan).

1-Stearoyl-2-arachidonoyl-*sn*-glycero-3-phospho-(1'-myo-inositol-4',5'-bisphosphate) (18:0-20:4 PI(4,5)P2),

1,2-hexadecanoyl-3-*sn*-glycerophosphatidylinositol-(3,4,5)-trisphosphate (18:0-20:4 PI(3,4,5)P3),

1,2-dihexanoyl-*sn*-glycero-3-phospho-(1'-myo-inositol-4',5'-bisphosphate) (08:0 PI(4,5)P2), and

1,2-dihexanoyl-*sn*-glycero-3-phospho-(1'-myo-inositol-3',4',5'-trisphosphate) (08:0 PI(3,4,5)P3) were purchased from Avanti Polar Lipids (USA).

TexasRed®-1,2-dihexadecanoyl-*sn*-glycero-3-phosphoethanolamine triethylammonium salt (TexasRed-DHPE) were provided from Invitrogen (USA).

3.3 Methods

3.3.1 Preparation of small unilamellar vesicles

The phospholipids were dissolved to be 0.67 mM with 0.04 mol% TexasRed-DHPE in 300 μL of a mixed organic solvent (CHCl$_3$ - MeOH, 2:1, v/v). The solution was poured into a 10 mL round bottom flask. The organic solvent was removed for 5 min by a rotary evaporator (N-1110, EYELA, Japan), equipped with a vacuum pump. The speed of rotation of the evaporator was 180 rpm, the exhaust rate was 1.2 L/min and the temperature was set to 40 °C by a water bath. After a lipid film was formed at the bottom of flask, the flask was placed in a desiccator to remove any residual solvent from the lipid film under reduced pressure (at room temperature for 17 hours).

Next, 2 mL of the phosphate buffered saline (PBS) was heated to 37 °C and was gently poured into the round bottom flask containing the lipid film. The flask was then sealed and incubated at 37 °C for 2 hours. The flask was

shaken by a vortex mixer each 1 hour, and for further dispersing, the sample in the flask was ultrasonicated typically for 1 hour. In order to remove unwanted long tubular vesicles and giant or large vesicles, which are occasionally formed during lipid film hydration, 2 mL of the sample was taken from the vesicle dispersion, and then it was passed through a 0.1 μm IsoporeTM Membrane Filter (Merck Millipore) twice. This filtering treatment afforded SUVs of phospholipids in PBS.

3.3.2   Cover glass washing

For rupturing SUVs on a cover glass, the cover glass was washed carefully in the following protocol (courtesy to Wakamoto Lab. The Univ. of Tokyo). A cover glass (24 mm × 60 mm, No.1, MATSUNAMI, Japan) was set in a rack (SANSYO, Japan) and the rack was placed in a glass vessel (SANSYO, Japan). A washing solution (1/8 Contaminon®LS-II (Wako) and 7/8 MilliQ water) was poured into the vessel and the cover glass was ultrasonicated in the washing solution for 1 hour. After the ultrasonication, the cover glass was rinsed with distilled water (15 times) and the following MilliQ water (3 times). Further rinsing with MilliQ water (ultrasonication for 2 min and following rinsing ×3) was undergone repeatedly (2 times). Next, 100% ethanol was used for the second cleaning step. It was poured into the vessel and the cover glass was ultrasonicated for 30 min. After the ultrasonication, the cover glass was rinsed with MilliQ water (3 times). Further rinsing with MilliQ water (ultrasonication for 2 min and following rinsing ×3) was undergone again repeatedly (2 times). As the third washing solution, 0.1 M NaOH in MilliQ water was used and the cover glass in the vessel was ultrasonicated in 20 minutes. After the ultrasonication, the cover glass was rinsed with MilliQ water (3 times). Further rinsing with MilliQ water (ultrasonication for 2 min and following rinsing ×3) was undergone again repeatedly (4 times). Finally the vessel containing the cover glass was heated in 140 °C for 40 minutes under a dry atmosphere.

3.3.3   Supported lipid bilayer preparation
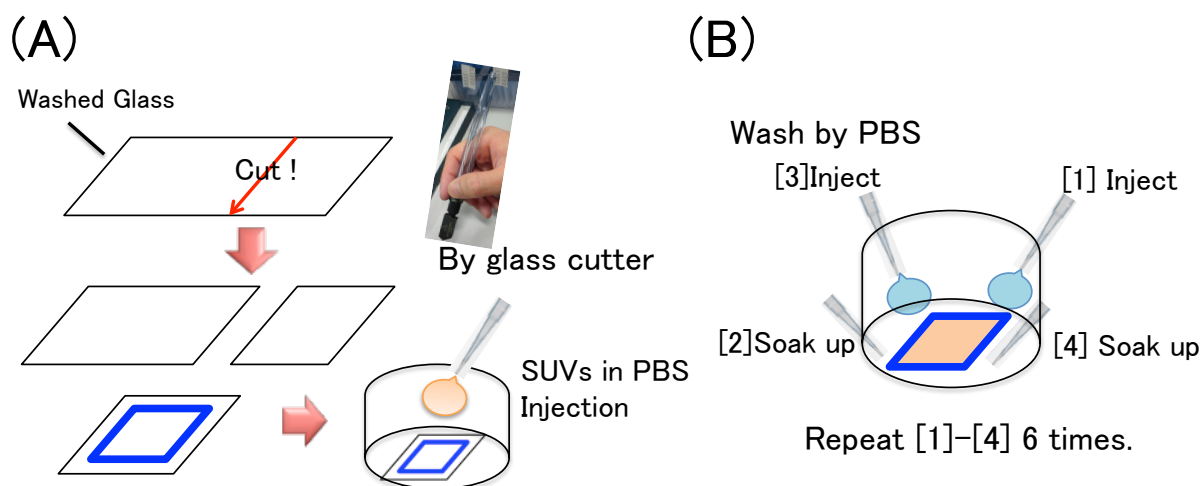
Figure 3.2: Preparation of supported lipid bilayer by SUV ruptured method. (A) Illustration on how to fix the washed glass for the bottom open dish and (B) how to rinse the SLB membrane for removing the surplus SUVs.

First the clean cover glass was cut to fit in size to a bottom-open dish. After setting up a handmade chamber by attaching the cover glass to the bottom-open dish with a double sided tape (Figure 3.2 (A)), 50 μL of the SUV dispersion was injected on the surface of the cover glass and incubated for 30-60 minutes. Second, the chamber was washed six times by addition of PBS (200 μL) at the 4 rims of the cover glass and soaking up it gently, resulting in removing the surplus SUVs (Figure 3.2 (B)).

3.3.4 Fluorescence microscopy observation

The SLB membrane was observed under a confocal laser scanning fluorescence microscope (CSU-X1, IX81, Olympus, Japan) equipped with a 100× objective lens. Red and Green fluorescence images were obtained by using the corresponding band-pass filter and dichroic mirror units (excitation; 520 - 550 nm, emission; > 580 nm and excitation; 470 - 490 nm, emission; 510 - 550 nm).

3.3.5 Cell culture

AX4 cells of the *Dictyostelium discoideum* axenic strain were cultured in modified HL5 medium under shaking at 155 rpm at 22 °C [39]. The AX4 cells co-expressing the Pleckstrin homology domain of cytosolic regulator of adenylyl cyclase (PH-crac) tagged with RFP (PH-crac-RFP) and the phosphatase and tensin homolog deleted from chromosome 10 (PTEN) tagged GFP (PTEN-GFP) were cultured in modified HL5 medium containing G418 (30 μg/mL, Wako) and Hygromycin B (60 μg/mL, Calbiochem) [40].

3.3.6 Cytosol extraction

Cytosolic extracts were prepared from AX4 cells according to the protocol described elsewhere [41, 42]. The cells, which were harvested at the cell density of 7 × 10^6 cells mL^{-1}, washed two times with 80 mL of phosphate buffer (PB), and re-suspended in 500 μL of PB. Cells were disrupted by nitrogen decompression using a cell disruption vessel (model 4639, Parr Instrument, IL, USA) on ice. Cell lysate was centrifuged at 16000 × g for 30 min at 4 °C. The supernatant was isolated and centrifuged again. The supernatant was transferred to a microtube and kept on ice until just before use. When we examined LY294002 as an inhibitor assay, a dimethyl sulfoxide solution (2 μL) of LY294002 (final concentration of 40 μM) was added to the cell suspension of PB (250 μL) with shaking for 30 min just before use for the extraction.

3.4 Results

3.4.1 Supported lipid bilayer membrane formed by rupturing small unilamellar vesicles on the glass

In order to trace the formation of SLB membrane from SUVs stained with 0.04 mol% TexasRed-DHPE, the time-lapse image capture by a confocal laser scanning fluorescence microscope was performed. The focus of the confocal system was set on the surface of the cover glass of the chamber after 50 μL of 0.1 mM POPC SUV dispersion was gently injected on the glass surface. As shown in Figure 3.3, the glass surface was covered by the fluorescent membrane for initial 600-1200 seconds after SUV dispersion injection. The SUV ruptured method for the formation of SLB membrane conventionally enables us heterogeneous films composed of a lipid mixture [38, 50, 52, 69, 72, 78]. When the SUV dispersion of POPC and 2 mol% phosphatidylinositide was dropped on the glass surface, the fluorescent membrane was formed in the same manner as POPC SUVs in initial 1200-1500 seconds after SUV dispersion injection. In order to remove the surplus SUVs, the chamber was washed more than 12 times by PBS (Figure 3.2 (B)).

After washing the chamber which was incubated for 30 minutes after SUV dispersion injection, the fluorescence intensity profile (the mean fluorescence intensity of the area of 81×81μm) along the z-position in Red modes (excitation; 520 - 550 nm, emission; > 580 nm) revealed the single peak with the full width at half maximum < 1μm at the surface of the cover glass (Figure 3.4 (A)). The fluorescence intensity profiles of the fluorescent membranes of other phospholipids formed in the chamber also gave the similar result. The reproducibility of the formation of such flat membrane (Figure 3.4 (B)) was checked at least 9 out of 10 times in all cases. Thus the SUVs in the dispersion was transformed to the SLB membrane via rupturing.
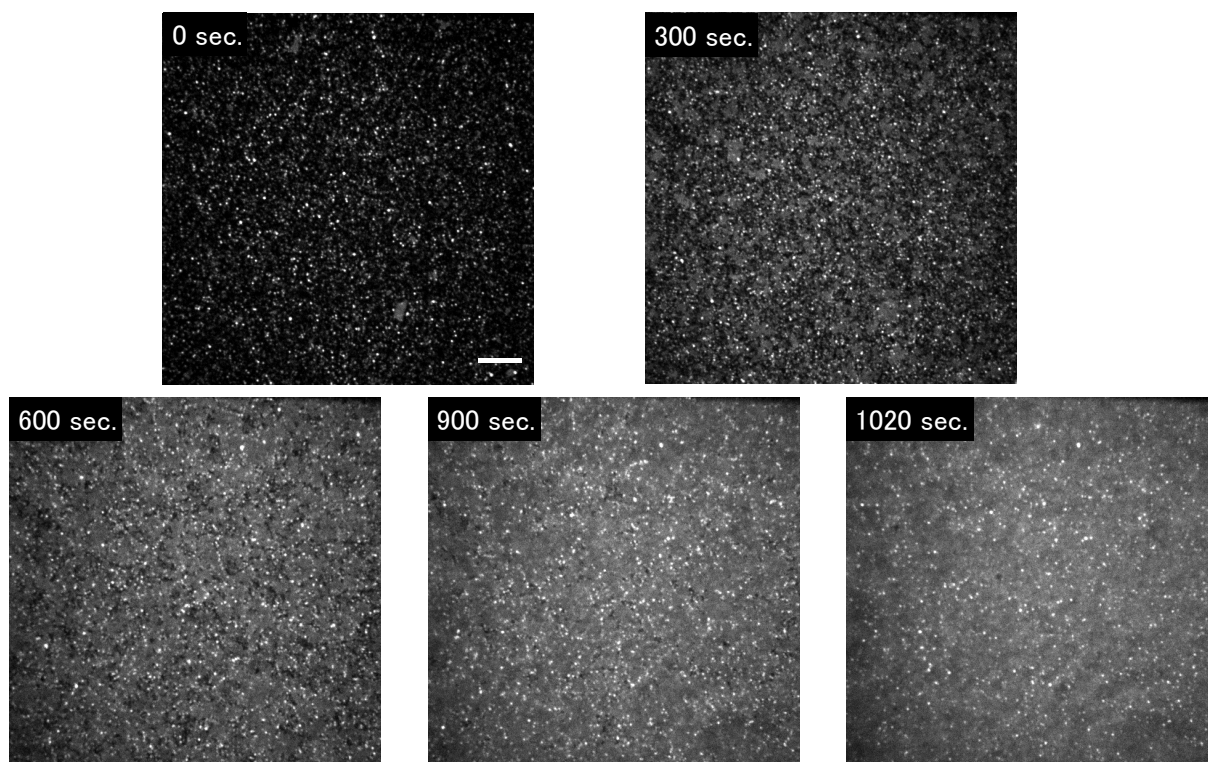
Figure 3.3: Time-course change of fluorescence microscopy images of the glass surface during POPC SUVs rupture. Bar = 10 μm. The POPC SUV was stained with TexasRed-DHPE.
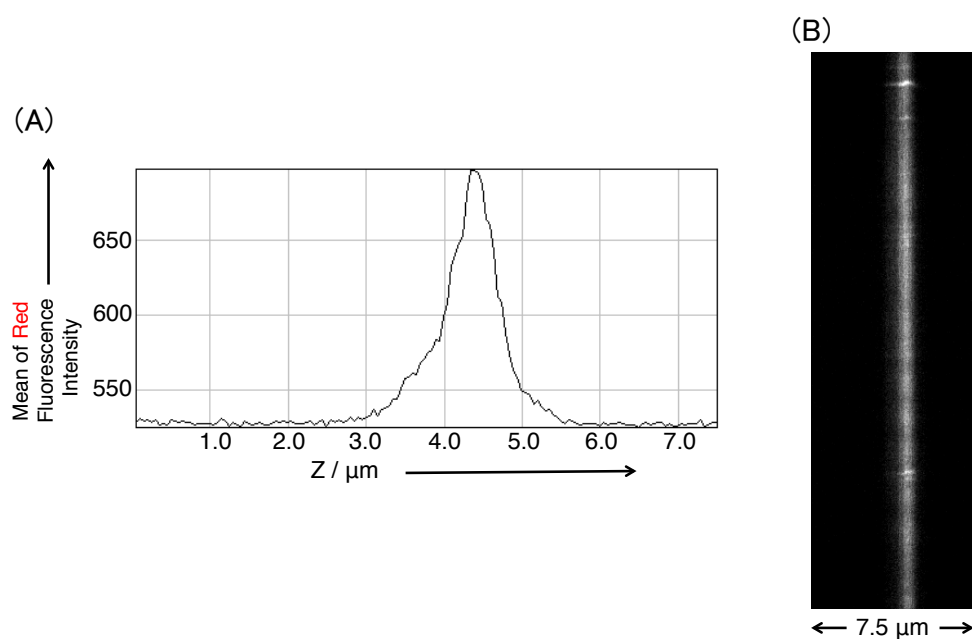
Figure 3.4: POPC SLB membrane formed by SUV ruptured method. (A) Mean fluorescence intensity of Red fluorescence image was plotted along the z position. (B) The cross-section reconstructed fluorescence images of the POPC SLB membrane obtained by confocal laser scanning fluorescence microscopy with Red fluorescence filter units. The images were captured 30 minutes after injection of SUV solution. The SLB membrane was stained with TexasRed-DHPE.

3.4.2 Pore formation on the SLB membrane after injection of cytosol extract

After formation of a SLB membrane in the chamber, the cytosol extracted from *Dictyostelium discoideum* (the PH-crac-RFP/PTEN-GFP co-expressing strain) was injected on the SLB membrane. As shown in Figure 3.5 (A), pore formation on the POPC SLB membrane was observed in initial 444-552 seconds after injection of the cytosol. Then every pore swelled in the x-y plane almost at the same time. As a negative control reference, the pore formation did not occur in the POPC SLB membrane after injection of the cytosol which was boiled in advance. Figure 3.5 (B) shows the time-course change of the standard deviation of Red fluorescence intensity (the area of $81 \times 81 \mu$m) on the POPC SLB membrane. The effect of injection of the cytosol, i.e. the increase of the standard deviation, was observed in initial 60 seconds, plausibly because the fluorescence intensity increased by adsorption of fluorescent proteins. The arrow depicted in Figure 3.5 (B) shows the transition of the SLB membrane. From 400 seconds to 600 seconds, the standard deviation tended to increase while the mean of the fluorescence intensity gradually decreased. This means the increase of the variation in the fluorescence intensity of the SLB membrane because of pore formation (dark spots on the fluorescent image). And, Figure 3.5 (C) shows the profile of the mean fluorescence intensity of Green mode along the z position. Before injection of the cytosol, the fluorescence intensity of the SLB membrane was negligible. The peak was found at the glass surface while a certain value of fluorescence intensity was detected over the glass surface. This result indicates that the green fluorescent molecule, that is PTEN-GFP, was localized on the POPC SLB membrane after injection of the cytosol. To examine the temperature effect, this experiment was performed at low room temperature (21 °C) (note that all other experiments were carried out at 24 - 26 °C). The pore formation on the POPC SLB membrane was observed in initial 1632-3000 seconds after injection of the cytosol (Figure 3.6). The decrease of the temperature caused the delay of the pore formation on the POPC SLB membrane under the cytosol.
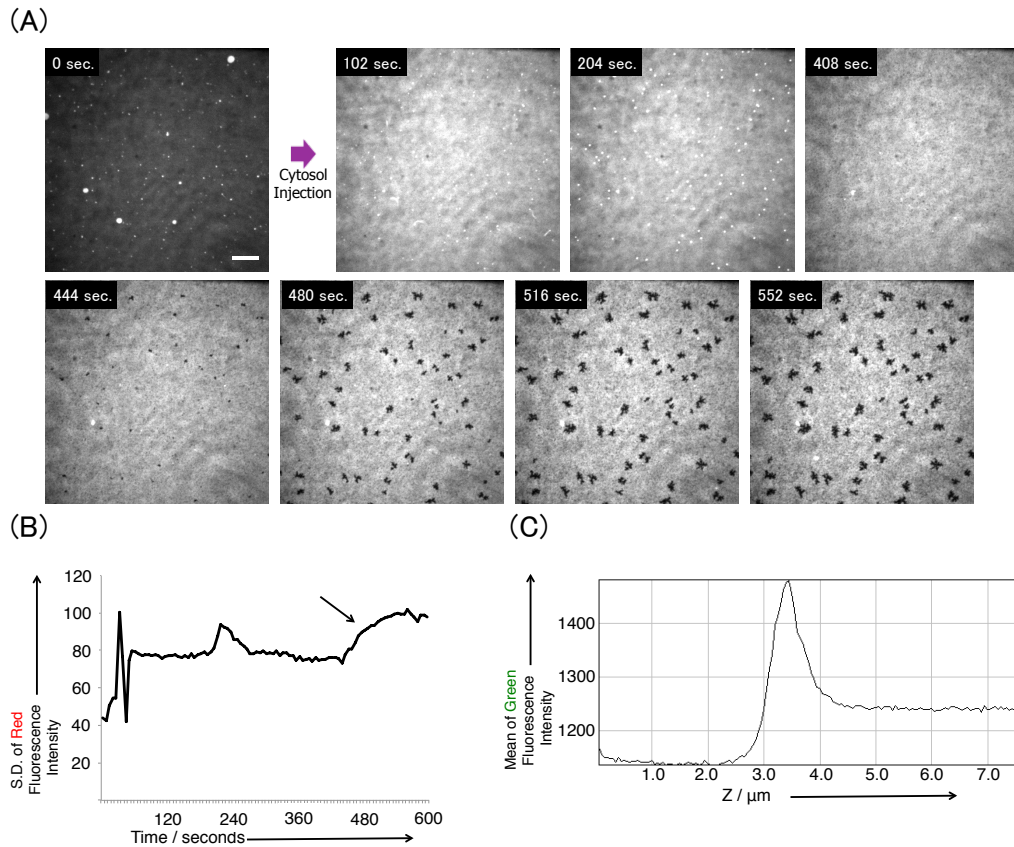
Figure 3.5: Pore formation on the POPC SLB membrane after injection of the cytosol extract of PH-crac-RFP/PTEN-GFP co-expressing cells. (A) Time-course change of microscopy images of the POPC SLB membrane captured by the confocal laser scanning microscopy. The pores on the SLB membrane were remarkably formed for initial 444-552 seconds after cytosol injection (24 - 30 seconds). Bar = 10 μm. (B) Time course change of the standard devision of fluorescence intensity of the microscopy images analyzed by Red fluorescence images. (C) Mean fluorescence intensity of Green fluorescence image was plotted along the z position. The SLB membrane was stained with TexasRed-DHPE.
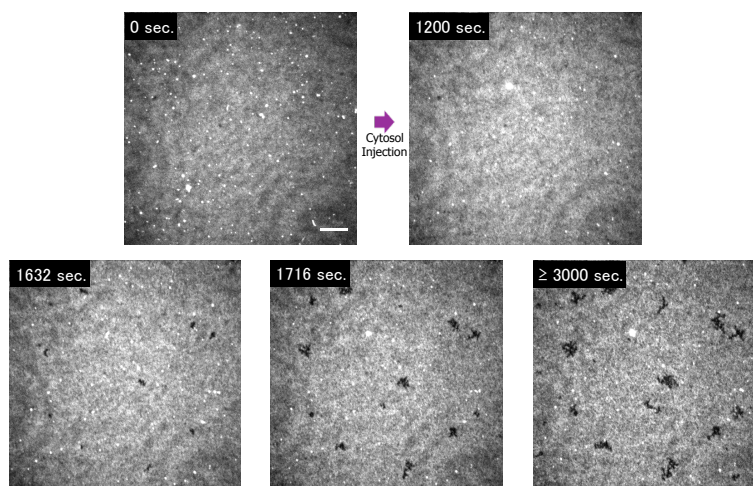
Figure 3.6: Pore formation on the POPC SLB membrane after injection of the cytosol at low room temperature. Time-course change of microscopy images of the POPC SLB membrane in the presence of the cytosol extract of PH-crac-RFP/PTEN-GFP co-expressing cells at 21 °C was monitored by the confocal laser scanning microscopy. The pores on the SLB membrane were remarkably formed for initial 1632-3000 seconds after cytosol injection (24 - 30 seconds). Bar = 10 μm.
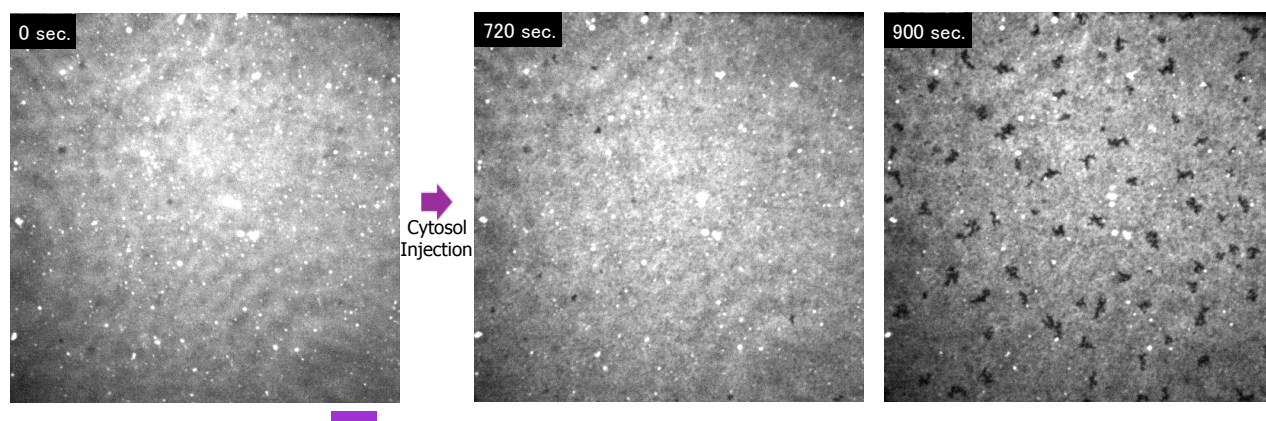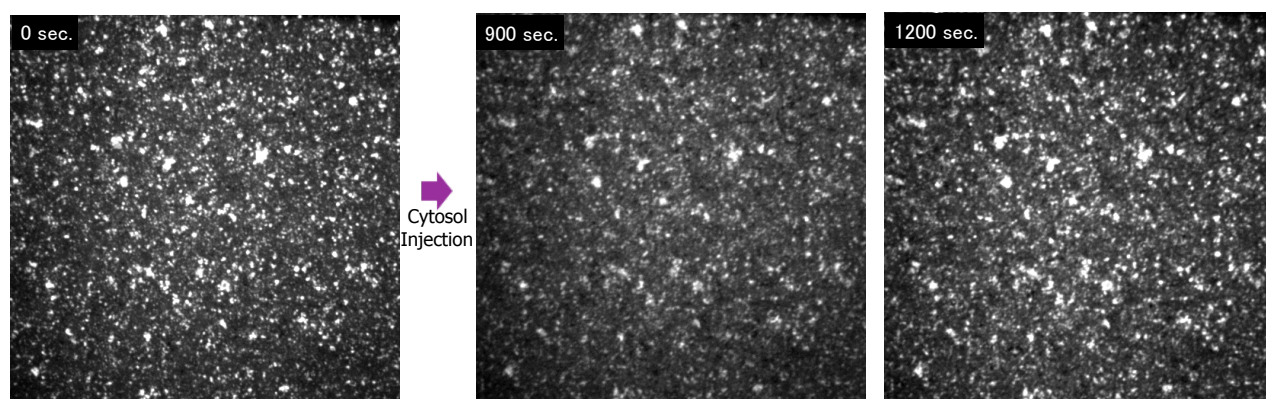
Figure 3.7: POPC/18:0-20:4 PI(4,5)P2 and POPC/18:0-20:4 PI(3,4,5)P3 SLB membrane transition after injection of the cytosol extract of PH-crac-RFP/PTEN-GFP co-expressing cells. (A) Microscopic observation of the time-course change of POPC/18:0-20:4 PI(4,5)P2 SLB membrane. I captured the pictures by confocal laser scanning microscopy. The motion of conformation changing to the pores on the SLB membrane occurred remarkably for initial 720-900 seconds after cytosol injection (24 - 30 seconds). (B) Microscopic observation of the time-course change of POPC/18:0-20:4 PI(3,4,5)P3 SLB membrane. Bar = 10 μm. The time of injection of the cytosol is 24 - 30 seconds. Time course change of the standard devision of intensity analyzed by Red fluorescence images about (C) POPC/18:0-20:4 PI(4,5)P2 and (D) POPC/18:0-20:4 PI(3,4,5)P3 SLB membrane. The SLB membrane was stained with TexasRed-DHPE.

Figure 3.7 (A) shows the time-course change of the fluorescence microscopy images of the SLB membrane of POPC and 2 mol% 18:0-20:4 PI(4,5)P2 after injection of the cytosol. The SLB membrane exhibited the pore formation in initial 720-900 seconds after injection of the cytosol and the pores expanded in the x-y plane. On the other hand, the SLB membrane of POPC and 2 mol% 18:0-20:4 PI(3,4,5)P3 did not change after the injection of the cytosol at 24 - 30 seconds (Figure 3.7 (B)). No pore on the SLB membrane but a slight lipid aggregation was observed. The PTEN-GFP localization of both SLB membranes including phosphatidylinositides was confirmed by the Green mode profile of the fluorescence intensity along the z-position after injection of the cytosol (data not shown). Figure 3.7 (C) and (D) show the time-course change of the standard deviation of Red fluorescence intensity for the SLB membrane of POPC/18:0-20:4 PI(4,5)P2 and POPC/18:0-20:4 PI(3,4,5)P3 respectively. The arrow in Figure 3.7 (C) demonstrates that the pore formation occurred on the POPC/18:0-20:4 PI(4,5)P2 SLB membrane from 720 seconds to 900 seconds. The standard deviation tended to increase in the similar manner to that of the POPC SLB membrane. Moreover, by the image analysis, the distribution of the nearest neighbor distance between the centroids of pores in the captured images of the POPC SLB membrane and the SLB membrane of POPC/18:0-20:4 PI(4,5)P2 was evaluated respectively. The distribution in both cases was almost in the range of 3.3 - 7.3 μm. Namely, the nearest neighbor distance between the centroids of pores did not change as the SLB membrane contained 18:0-20:4 PI(4,5)P2.

The length of the acyl chain of phospholipids is effective to the fluidity of the bilayer membrane. Hence the 08:0 PI(4,5)P2 and 08:0 PI(3,4,5)P3 which have shorter acyl chains than that of 18:0-20:4 PI(4,5)P2 and 18:0-20:4 PI(3,4,5)P3 were also examined to be mixed to the POPC SLB membrane (Figure 3.8). Figure 3.9 (A) shows the fluorescence microscopy image of the SLB membrane of POPC and 2 mol% 08:0 PI(4,5)P2 before and 30 minutes after injection of the cytosol. The pores were formed in the SLB membrane and expanded in the x-y plane. In the case using 2 mol% 08:0 PI(3,4,5)P3, the pore formation was also observed after injection of the cytosol (Figure 3.9 (B)). By using the threshold for adjusting the binarization to the fluorescence microscopy image, the areas of pores were measured.
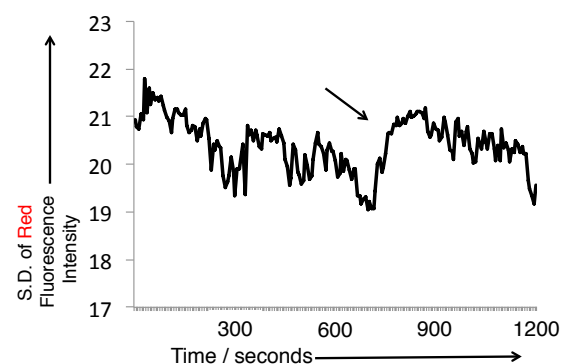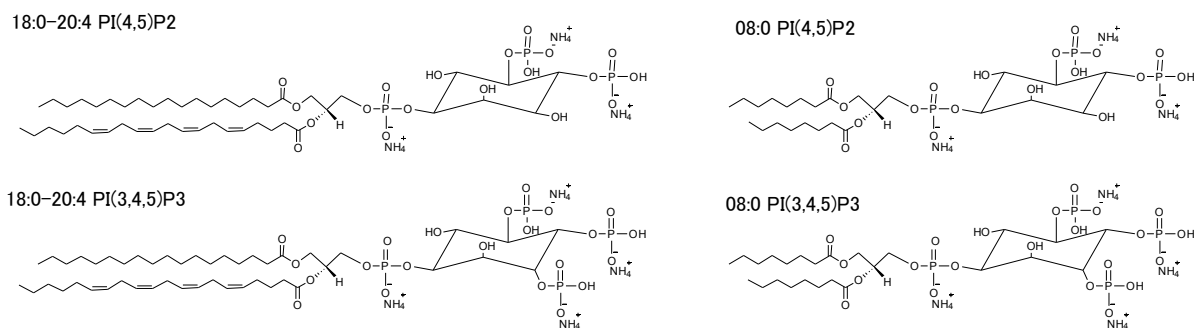

Figure 3.8: Chemical structure of phosphatidylinositides.
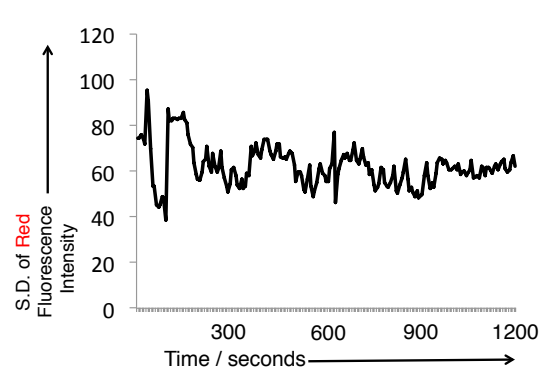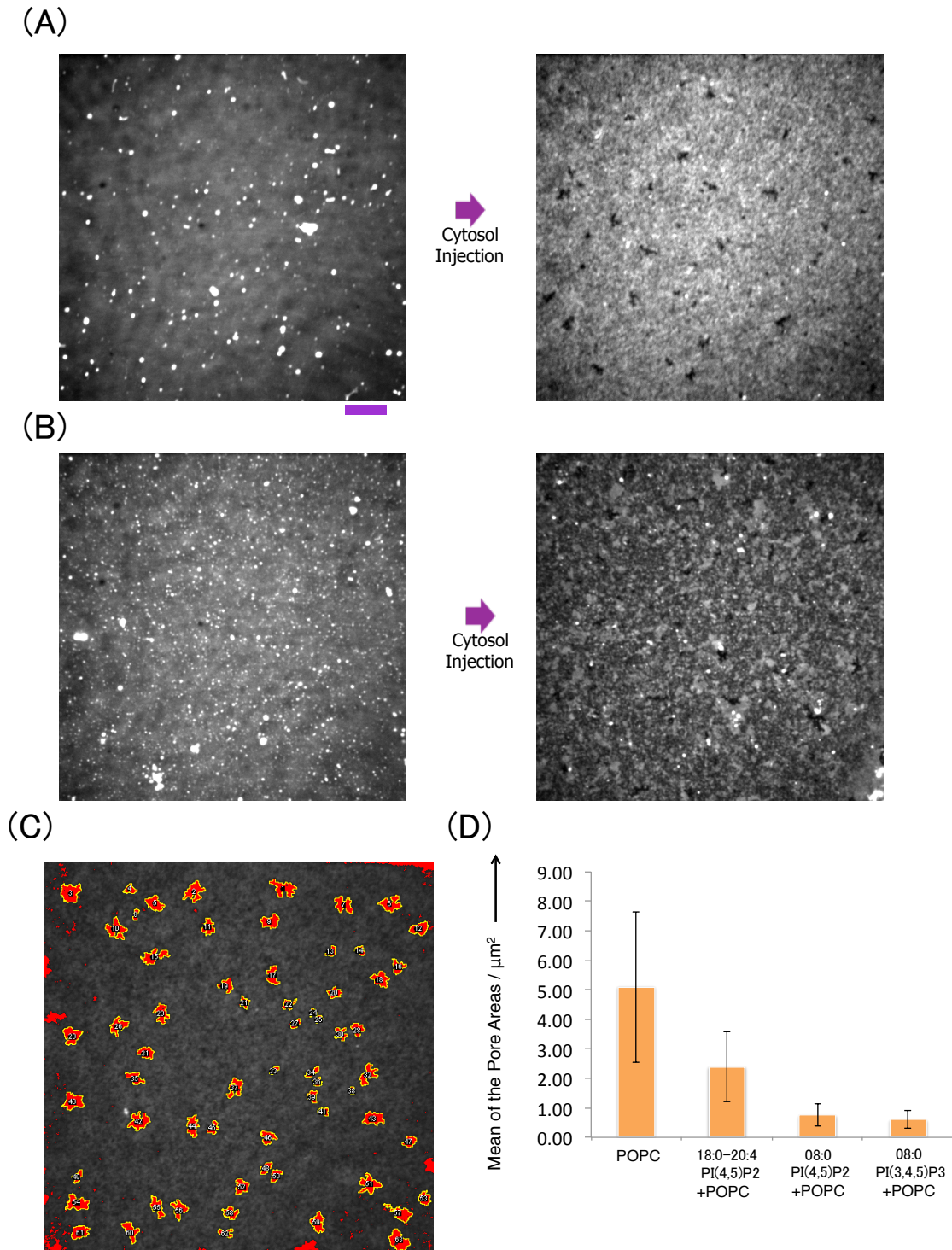
Figure 3.9: POPC/08:0 PI(4,5)P2 and POPC/08:0 PI(3,4,5)P3 SLB membrane transition after injection of the cytosol extract of PH-crac-RFP/PTEN-GFP co-expressing cells and pore size distribution of SLB membrane in each condition. Fluorescence image of (A) POPC/08:0 PI(4,5)P2 and (B) POPC/08:0 PI(3,4,5)P3 SLB membrane images before and after injection of the cytosol. Bar = 10 μm. (C) Area measurement of pores formed at the POPC SLB membrane Figure 3.5 (A) by ImageJ. (D) Distribution of the mean of the pore areas measured at the SLB membrane in each condition. The SLB membrane was stained with TexasRed-DHPE.

The binarization of the POPC SLB membrane with pores 20 min after the injection is shown in Figure 3.9 (C). Figure 3.9 (D) is the diagram of areas of the pores in each SLB membrane observed 25 min after the cytosol injection. The pore size in the POPC SLB membrane was larger than those of any other SLB membranes. This analysis implies that the SLB membrane based on POPC including phosphatidylinositides tended to disturb the pore formation or expansion. Especially the POPC/18:0-20:4 PI(3,4,5)P3 SLB membrane exhibited no pore formation after cytosol injection.

3.4.3 Tubular vesicle formation on SLB membrane after injection of cytosol extract

The SLB membrane in presence of the cytosol also afforded the tubular giant vesicles (tGV). In most cases of tGV formation, the tGVs were formed before the pore formation. Figure 3.10 (A) shows the time-course change of the fluorescence microscopy images of the POPC SLB membrane which was traced immediately after following injection of the cytosol including 3.3 μM LatrunculinA. LatrunculinA is one of the inhibitors of F-actin polymerization (recall the Figure 2.2). The tGVs formed on the POPC SLB membrane in initial 126 seconds and the pore formation occurred in initial 330 seconds after injection of the cytosol. When the cytosol of *Dictyostelium discoideum* with 33.3 μM LY294002, which is the inhibitor of PI3K, was injected on the POPC SLB membrane, the tGVs formed in initial 138 seconds after injection of the cytosol (24 - 30 seconds) and the pore formation occurred in initial 420 seconds after injection of the cytosol (Figure 3.10 (B)). In the case using the cytosol with 100 μM Blebbistatin, which is the inhibitor of Myosin II contraction, many tGVs formed on the POPC SLB membrane in initial 312 seconds after injection of the cytosol (24 - 30 seconds) and the pore formation occurred in more than 1800 seconds after injection of the cytosol (Figure 3.10 (C)). In addition, tGVs were likely formed in the POPC SLB membrane on the surface of the cover glass without the bottom-open dish (Figure 3.10 (D)). In this condition, the pores formed in the SLB membrane were smaller than that observed in Figure 3.5 (A) at 30 minutes after injection of the cytosol. The bottom-open dish used for the chamber appears to resist the slight distorting force to the cover glass surface. The distortion-free surface may allow the pore formation.

3.5 Discussion

The results of pore formation indicated that the cytosol extracted from *Dictyostelium discoideum* has a potential for the membrane transition of even the SLB membrane. In fact, the SLB membrane deformation in nanometer scale have been reported elsewhere. For instance, the atomic force microscopy observation revealed that the formation of nanometer-sized pores in the 1,2-dimyristoyl-*sn*-glycero-3-phosphocholine SLB membrane was caused by poly-*L*-lysine injection [80]. The *Escherichia coli* cytosol expressing pore-forming membrane protein, α-hemolysin, induced the pore formation of POPC SLB membrane in the nanometer scale observed by AFM [78]. These works imply that the proteins or cytosol provoke the SLB membrane of phospholipid resulting in the pore formation. Figure 3.5 (A) and (B) shows the cytosol extracted from *Dictyostelium discoideum* also has a potential of membrane deformation. Note that the pores formed in the POPC SLB membrane expanded to micrometer size. Since PTEN is a well-known membrane-binding protein specifically localizing on 18:0-20:4 PI(4,5)P2 [31], it is important to examine the cytosol injection to the SLB membrane including phosphoinositides for approach to the mechanism of the pore formation. Moreover, the pore formation was sensitive to temperature. Two reasons why the temperature affected the initial timing of the pore formation are raised: (i) the membrane fluidity and (ii) the activity of membrane-binding proteins. The membrane fluidity becomes low as the temperature decreases, especially the membrane transition from liquid crystal phase (fluid) to gel phase (solid-like) occurs [81]. But POPC has its phase transition temperature about 0 °C and the temperature of the experiment condition above-mentioned was much higher than 0 °C. Hence the activity of membrane-binding proteins is plausibly determinant to the pore formation of SLB membrane observed here.
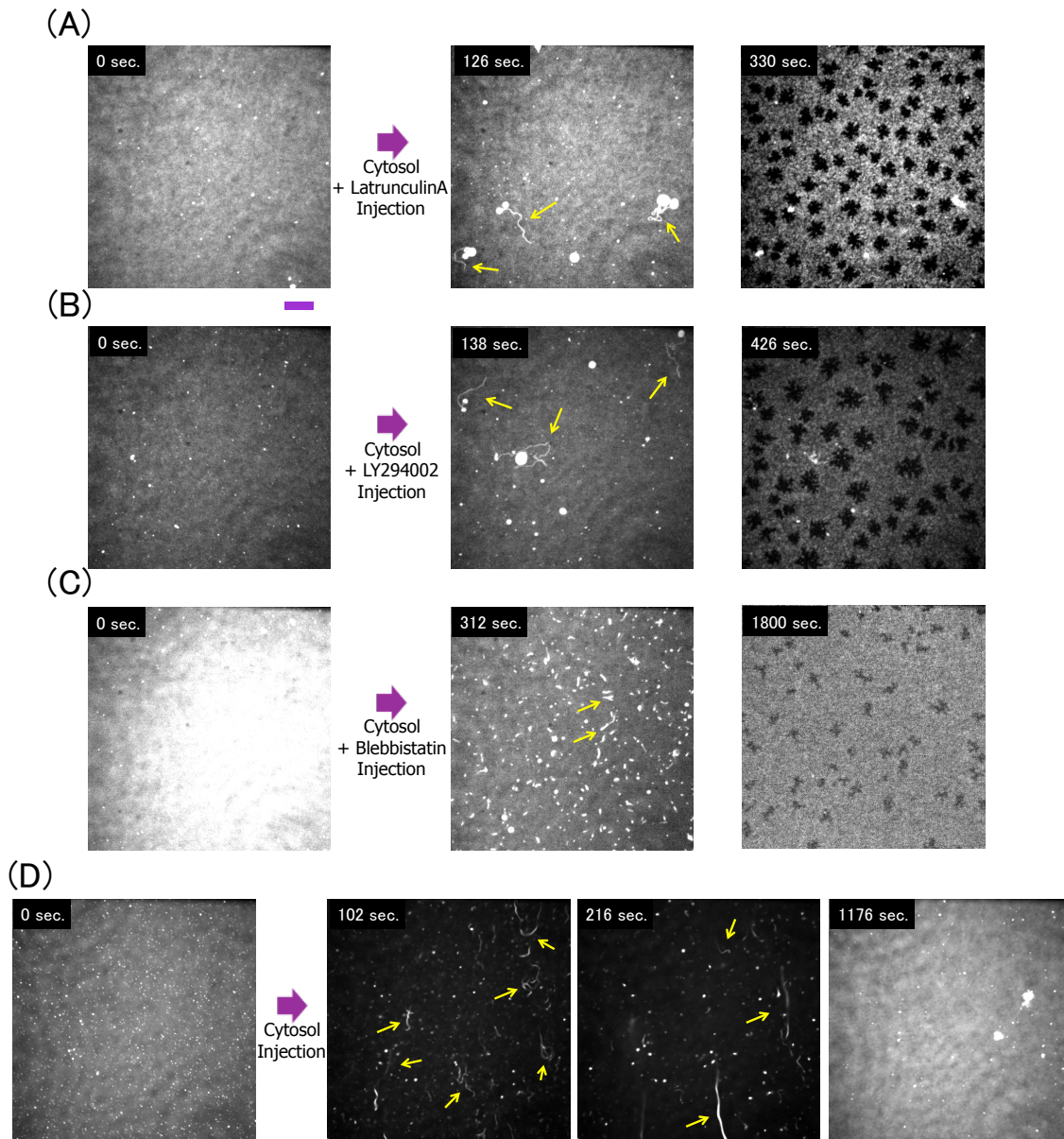
Figure 3.10: Tubular vesicle generation of the POPC SLB membrane after injection of the cytosol extract of PH-crac-RFP/PTEN-GFP co-expressing cells. Time-course change of the fluorescence images of POPC SLB membrane after injection of the cytosol containing 3.3 μM LatrunculinA (A), 33.3 μM LY294002 (B), and 100 μM Blebbistatin(C). (D) Time-course change of the fluorescence images of POPC SLB membrane on the flat slide glass (not using bottom open dish) after injection of the cytosol. Tubular giant vesicles on the SLB membrane were generated remarkably for initial ∼300 seconds after cytosol injection (24 - 30 seconds). The SLB membrane was stained with TexasRed-DHPE. Yellow arrows show tGVs. Bar = 10 μm.
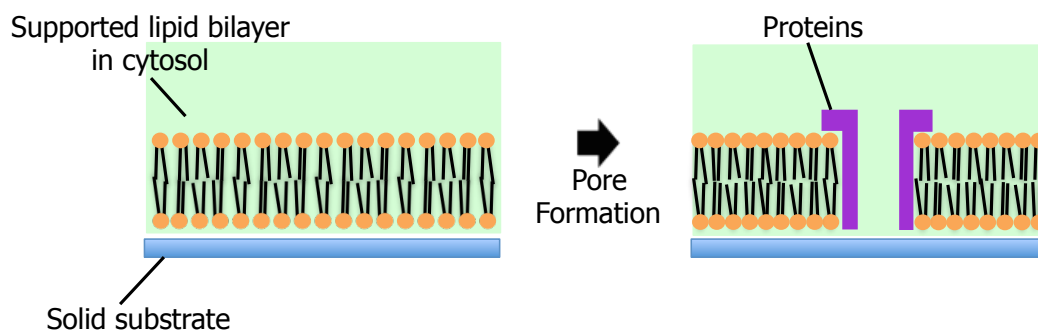
Figure 3.11: Schematic illustration on mechanism of pore formation on the SLB membrane.

The pore formation on cell membrane is often so drastic and destructive for cells that they lose the property connecting the definition of life system, [C] Compartment. In the current results, the phosphatidylinositide played the role to inhibit the potential of the cytosol to completely break the membrane with the micrometer-sized pores. This is probably significant for the symmetry breaking events in amoeba locomotion. The reason why the pores were formed on SLB membrane in presence of the cytosol is probably a certain protein or proteins which can pierce on the SLB membrane and gather each other to exclude the phospholipid molecules (POPC) at the gathering sites (Figure 3.11).

How does the pore stop expanding its size? When some proteins run into the POPC SLB membrane on Poisson's process, gathering the proteins results in making a pore in the SLB membrane and the excluded lipid molecules become dense and packed. This reorientation of lipid molecules on the SLB membrane inhibits more proteins to run into and pore the SLB membrane. Phosphatidylinositides and membrane-binding proteins including PTEN also play a role to decrease the fluidity of the SLB membrane due to their complexation, resulting in preventing the pore formation.

The tGV formation was observed on POPC SLB membrane under the medicine-treated cytosol. The formation time of tGV and its size are similar to the micropinocytosis of amoeba. The model describing the regulation of the macropinocytosis in *Dictyostelium discoideum* depicts that the requirement of the activity of RasS, PIK1, PIK2 and PKB to complete the formation of a macropinosome in micrometer scale for several tens of seconds [77]. This model implies that cytosol extracted from *Dictyostelium discoideum* affects the pure lipid SLB membrane resulting in the pore and tGV formation. In this chapter, by using pure lipid SLB membrane, it was found that the cytosol *Dictyostelium discoideum* evokes the micrometer-sized deformation of membrane which is related not only cell motion but also intracellular motility. The current method revealed that the deformation was tuned by the phosphatidylinositides among many substances to achieve such membrane deformation. Accordingly, the technique in the current method, called as the **Pre-reconstruction** method, would contribute to us as one of in vitro powerful tools for investigation of membrane deformation in terms of cell motion and intercellular motility.

3.6   Summary

In this chapter, the SLB membrane composed of POPC and phosphatidylinositides were constructed through the SUV ruptured method. The injection of the cytosol extracted from *Dictyostelium discoideum* to SLB membrane induced the pore formation and tGV generation on the SLB membrane. The pore formation was inhibited by the phosphatidylinositide. These results imply the cytosol has a potential for membrane transitions in micrometer scale and phosphatidylinositide tunes the deformation.

Chapter 4 Construction of Lipid Membrane of DNA-lipid Conjugate and 2D-3D Transition by Heat Stimulation

4.1 Introduction
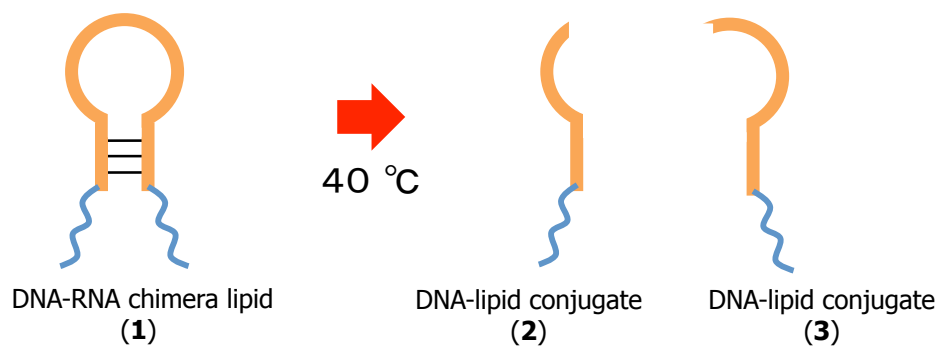
Figure 4.1: Schematic drawing of DNA-lipid conjugate molecule conformation changing by heat stimulation.

In Chapter 2 and 3, the combination of the two-dimensional (2D) lipid membrane and the cytosol as the reconstitution of an amoeba cell membrane enabled us to observe the novel morphological changes in the micrometer scale. The membrane morphological changes were isothermally induced by the cytosol injection. However, since the proteins in the cytosol have the only abilities to specifically bind lipid membranes, the reconstituted systems do not include the information factor regarding to definition of life system. To link the membrane deformation and the information, the simple and chemically pure system has been constituted in this study.

As the candidate molecule carrying information, DNA has drawn much attention since DNA molecules are stable in such aqueous circumstance. But they are so stable when they fold the double helix normally in the secondary structure that they hardly induce morphological change of 2D lipid membrane. In order to link the membrane deformation and DNA information, a stem-loop structure of DNA-RNA chimera was designed and conjugated to lipid molecule here. In the previous reports [82, 83], the stem-loop structure of oligo DNA containing single RNA monomer is able to drastically change its conformation and be hydrolyzed triggered by the binding of an RNA enzyme and a DNA enzyme. Moreover, the structure stability of the stem-loop oligo DNA against heat is controlled by changing the length and sequence constituting in the both stem and loop parts. Thus the micrometer-scale dynamics of a lipid conjugated with the stem-loop oligo DNA-RNA chimera is expected by using both physical stimulation and chemical reaction. It should be noted that this design including the molecular conversion of component molecules of 2D lipid membrane is related not only [C] **Compartment** but also [B] **Energetic metabolism**.

Then the DNA-RNA chimera is designed to be modified by oleic acid. Oleic acid is one of simple fatty acids forming the micrometer-sized vesicle in a buffered solution. It has a non-saturated carbon-carbon bond at the middle of the

alkyl chain, which affords the fluidic phase of membrane. Hence, the chemical conversion of DNA-RNA chimera modified with oleic acid is expected to induce its 2D membrane transition in the micrometer scale. The expected chemical formula is shown in Figure 4.1. The product of the hydrolyzed DNA-RNA chimera modified with oleic acid (**1**) affords two types of DNA-lipid conjugates (**2**, **3**). The chemical conversion is expected to be triggered and accelerated by heat stimulation. Temperature is the important factor for the stability of DNA hybridization and its secondary structure and is the factor of controlling the chemical conversion easier than the enzymes aforementioned.

Moreover, in order to induce the membrane deformation, the DNA-lipid conjugates (**2**, **3**) produced by the hydrolysis of **1** (forming two-dimensional membrane) is expected to form not a nanometer-sized molecular aggregate but a micrometer-sized three-dimensional (3D) structure in the aqueous buffered solution. Concerning about the first stage of origin of life, the temperature stimulation and the following emergence of a boundary in water is indispensable for life system. Thus the sequences of DNA of DNA-RNA chimera **1** and DNA-lipid conjugate **2** and **3** were carefully designed by a software which affords the prediction of DNA melting temperature. The 2D lipid membrane of **1** was prepared by the casting method and wetted by the buffered solution. The heat-induced transition of 2D lipid membrane of **1** was traced by phase contrast microscopy. The transmission electron microscopy and the electrocataphoresis were examined for further revealing the lipid membrane transition in the molecular level.

4.2   Materials

All DNA and DNA-RNA chimera strands in this chapter were synthesized and purified by HPLC and the assignment was performed by mass spectrometry (Sigma-Aldrich). DNA-RNA chimera lipid **1** had the following sequence; 5'-CCGCTATrAGGAAGAGACGG-3' with both 5' and 3' terminals modified by amide bonds which are linked with oleic acid. rA indicates the RNA monomer. DNA-lipid conjugate **2** and **3** had the following sequences; 5'-CCGCTATrA-3' with 5' terminal modified by amide bonds linking to oleic acid, and 5'-GGAAGAGACGG-3' with 3' terminal modified by amide bonds linking to oleic acid, respectively. DNA-lipid conjugate **4** had the following sequence; 5'-CCGCTATAGGAAGAGACGG-3' with both 5' and 3' terminals modified by amide bonds which are linked with oleic acid (Figure 4.2). Squalene and D-fructose were purchased from Wako Pure Chemicals, Inc.
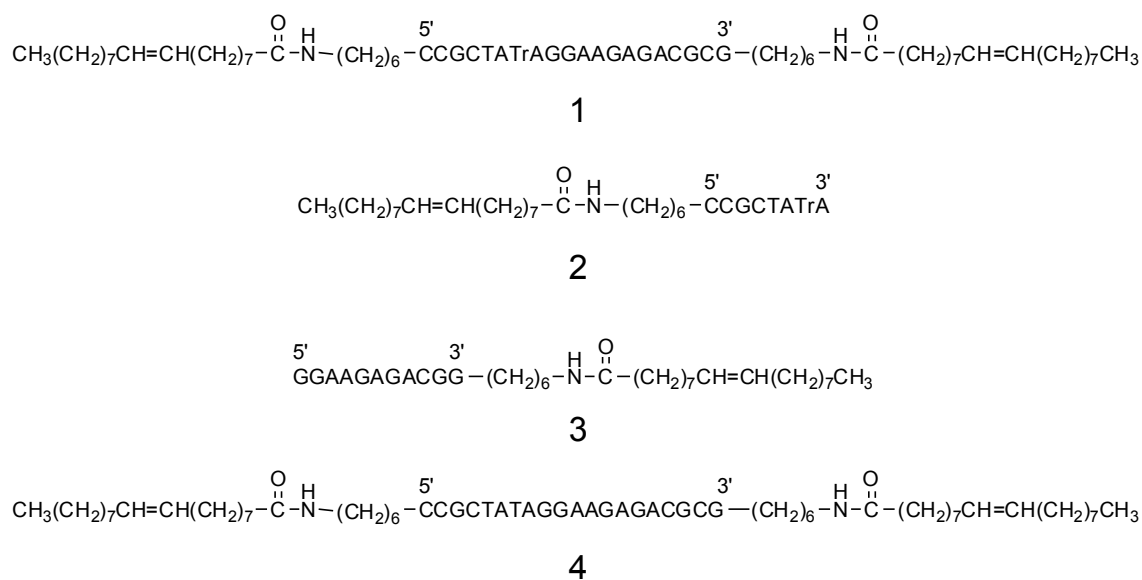

Figure 4.2: Chemical structure of DNA-RNA chimera lipid **1**, DNA-lipid conjugate **2**, **3**, and **4**.

4.3 Methods

4.3.1 Lipid casting on solid substrate

To prepare the casted two-dimensional membrane of DNA-RNA chimera lipid **1** (8.89 μM), $_D$-fructose (88.9 μM), and squalene (0.889 μM) were dissolved in 9 μL of a mixed solvent (H_2O-MeOH-$CHCl_3$, 4:4:1, v/v/v). The solution was gently mixed and injected on a cover glasses (24 mm $\times$ 60 mm, No.3, MATSUNAMI, Japan). The lipid film formed on the cover glass was shaded from light and set in a desiccator, and the residual solvent was completely removed from the lipid film under reduced pressure at room temperature for 17 hours. Then 25 μL of a buffered solution (50 mM HEPES and 10 mM $MgCl_2$) was added onto the lipid cast film and enclosed it by using a frame seal chamber and another cover glass.

4.3.2 Phase contrast microscopy observation

The real-time observation of the transition of the lipid cast film composed of **1** was performed under a phase contrast microscope (IX71, Olympus, Japan) equipped with a CCD camera (DP-72, Olympus, Japan). For the heat stimulation to the lipid cast film, the pocket warmers commercially available ("HOKARON mini ®", Lotte, Japan) were used. The four pocket warmers were shaken well and fixed around the specimen on the microscope stage by a packed tape (Figure 4.3 (A) (B)). The temperature of the specimen was kept at 39.7 - 40.2 °C over 6 hours.

4.3.3 Transmission electron microscopy observation

To clarify the 3D structure after the lipid membrane transition in detail, the transmission electron microscopy was examined. For negative staining, the samples were absorbed to carbon-coated copper grids (400 mesh) and were stained with 1 % uranyl acetate solution for a few seconds. The samples were observed by a transmission electron microscope (JEM-1400Plus; JEOL Ltd., Tokyo, Japan) at an acceleration voltage of 80 kV. Digital images (2048 $\times$ 2048 pixels) were taken with a CCD camera (VELETA; Olympus Soft Imaging Solutions GmbH, Münster, Germany).
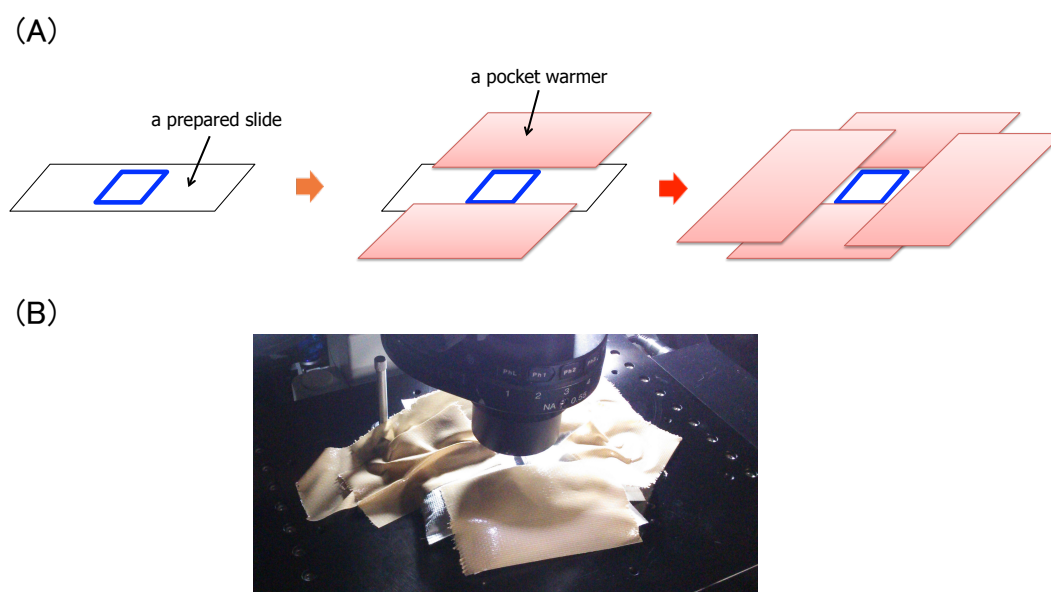

Figure 4.3: Schematic illustration of observation protocol for the casted lipid membrane composed of DNA-lipid conjugate stage constitution for DNA-lipid conjugate on how to place four pocket warmers around the specimen (A) the photograph was show in (B)

4.3.4 Electrocataphoresis

The conversion of DNA-RNA chimera lipid to DNA-lipid conjugate was evaluated by the electrocataphoresis. The gel was constructed of denatured 15 % polyacrylamide (37.5:1) / 8 M urea / 1 × Tris-Borate-EDTA (TBE). The gel after the electrocataphoresis with 200 V for 70 min was dried and the bands were visualized in the presence of SYBR Gold Nucleic Acid Gel Stain ®(Life Technologies).

4.4 Results

4.4.1 Design of the DNA sequence

The DNA-RNA chimera **1** was designed by application of DNA folding form. The prediction of the melting temperature T_M of DNA duplexes affords us to design a new DNA sequence in this manner. We can use the mfold Web Server[1] which predicts T_M of DNA by the application of the nearest-neighbor model [84, 85].

For oligonucleotide duplexes, this software calculates the total values of the standard free-energy changes with additional parameters for the initiation of duplex formation. It combines the initiation parameter including differences between terminal and internal nearest-neighbors and counterion condensation into all other sequence-independent effects. To account for differences between duplexes with terminal A·T vs. terminal G·C pairs, two initiation parameters are introduced: "initiation with terminal G·C" and "initiation with terminal A·T". An additional entropic penalty for the maintenance of the C2 symmetry of self-complementary duplexes is also included. The total differential of Gibbs free energy $\Delta G°$ is given by;

$$\Delta G°(\text{total}) = \sum_i n_i \Delta G°(i) + \Delta G°(\text{init w/ term G} \cdot \text{C}) + \Delta G°(\text{init w/ term A} \cdot T) + \Delta G°(\text{sym}) \quad (4.4.1)$$

where $\Delta G°(i)$ are the standard free-energy changes for the 10 possible Watson-Crick nearest-neighbors, n_i is the number of occurrences of each nearest neighbor i, and $\Delta G°(\text{sym}) = 0.43$kcal/mol if the duplex is self-complementary.

The $\Delta G°$ can also be calculated from $\Delta H°$ and $\Delta S°$ parameters by using the definition of Gibbs free energy;

$$\Delta G° = \Delta H° - T\Delta S° \quad (4.4.2)$$

Here, $\Delta H°$ is the differential of enthalpy and $\Delta S°$ is the differential of entropy. T_M is defined as the temperature at which half of the strands are in the double-helical state and half are in the "random-coil" state. For self-complementary oligonucleotide duplexes, the T_M is calculated from the predicted $\Delta H°$ and $\Delta S°$ and the total oligonucleotide strand concentration C_T, by using the equation;

$$T_M = \frac{\Delta H°}{\Delta S° + R \ln C_T} \quad (4.4.3)$$

where R is the gas constant (1.987 cal/K·mol). Synthetic polymers with simple repeat sequences usually melt in a single cooperative transition (approximately two-state) that is concentration-independent so the $T_M = \Delta H°/\Delta S°$. The minimum value of $\Delta G°$ calculated by sequence information gives us the prediction of the folding secondary structure and T_M of the DNA. The sequence shown in Figure 4.4 finally provided the stem-loop structure with $T_M = 40$ °C in the experimental condition of $[\text{Na}^+] = 0$ M, $[\text{Mg}^{2+}] = 0.01$ M.

---

[1]http://mfold.rna.albany.edu/?q=mfold

10

G — G — A

G   A

A   A

T   G

A   A

T   G

5   C   A   15

G — C

C — G

5' —— C — G —— 3'
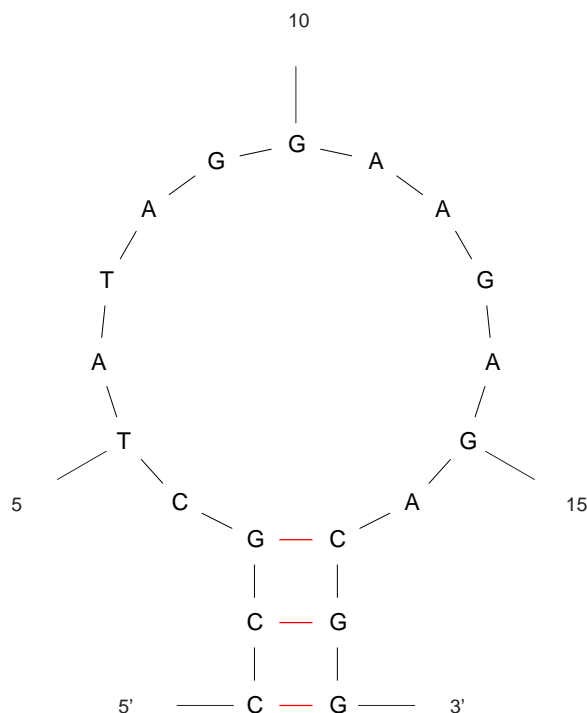
Figure 4.4: The prediction for DNA-RNA chimera **1** T_M value. The conditions are $[Na^+] = 0$ M, $[Mg^{2+}] = 0.01$ M. As a result, assuming a two state model $\Delta G = 0.04$ kcal/mol at 40 °C, $\Delta H = -21.40$ kcal/mol, $\Delta S = -68.4$ cal/(K·mol) and $T_M = 39.2$ °C were evaluated.

4.4.2   3D transition of lipid membrane by heat stimulation

After addition of the buffered solution, the casted lipid membrane of DNA-RNA chimera lipid **1** was observed under the phase contrast microscope. Figure 4.5 (A) shows that time-course of the transition from the casted two-dimensional lipid membrane to three-dimensional structure at 40 °C as the heat stimulation. The emergence of the 3D structures (granules) in the specimen was observed at 450 seconds after heat stimulation. And the granules started gathering at 900 seconds and continued until 2700 seconds. As a reference experiment, the casted lipid membranes composed of DNA-lipid conjugate **2**, **3**, and 1:1 mixture of **2** and **3** were also prepared and observed in the same procedure (in all cases, the final concentration of DNA was arranged to 32 μM DNA) at room temperature. In the specimen containing the casted lipid membrane of 1:1 mixture of **2** and **3**, the formation and aggregation of granules occurred in 60 seconds (Figure 4.5 (B)), which is similar to the situation of DNA-RNA chimera lipid **1**. On the other hand, no transition of the casted lipid membrane composed solely of DNA-lipid conjugate **2** or **3** occurred and only two-dimensional membrane was observed in each specimen (Figure 4.5 (C) and (D)). Even though the casted lipid membrane composed of DNA-lipid conjugate **3** was stimulated by 40 °C incubation, the membrane did not exhibit any deformation (Figure 4.6 (A)).

In order to check the reversibility of the transition, the 3D structure formed in the specimen of DNA-RNA chimera lipid **1** by the heat stimulation (40 °C for 1.5 hours) was incubated for three days at room temperature (Figure 4.6 (B)). Then no change of the three-dimensional structure was observed. Hence, it is implied that the 2D-3D membrane transition was associated by the chemical conversion from **1** to **2** and **3** which was not capable to reverse. As a reference, the casted lipid membrane composed of only DNA-lipid conjugate **3** was also treated by the same heat stimulation and left for three days at room temperature. Figure 4.6 (C) shows that 2D membrane did not deformed but maintained its conformation. Figure 4.7 shows a reference experimental result by using DNA-lipid conjugate with

only DNA sequence (DNA-lipid conjugate **4**). Figure 4.2 shows chemical structure of DNA-RNA lipid conjugate **1** and DNA-lipid conjugate **4**. DNA-RNA chimera lipid **1** has potential to change the structure without cleavage because of the single RNA in the water-soluble head. Figure 4.7 (A) shows the phase contrast microscopy image of 3D structure of DNA-RNA lipid conjugate **1** from the casted two-dimensional lipid membrane at 40 °C for 15 minutes in an incubator. This structure was same as one in Figure 4.5 (A). On the other hand, the casted membrane of DNA-lipid conjugate **4** prepared in the same condition exhibited no change (Figure 4.7 (B)). Taking this result in account, it is deduced that the cleavage of RNA-base in the DNA-RNA lipid conjugate **1** cleaving caused the structure transition.

In order to evaluate the chemical conversion of DNA-RNA chimera lipid **1** in the 2D-3D transition of the casted lipid membrane, the electrocataphoresis was examined. The buffered solution dissolving DNA-RNA chimera lipid **1** (32 μM) was treated with heat stimulation (40 °C, 60 °C, or 95 °C). Each solution of **1** (Lanes 1-3) and the buffered solution of **2** and **3** (Lanes 4,5) were loaded to the gel and the bands were observed under the UV irradiation after the application of voltage and the staining (Figure 4.8). The lanes 1-3 had different bands from lane 4 (DNA-lipid conjugate **2**) and lane 5 (DNA-lipid conjugate **3**). In addition, the lane 3 (treated with 95 °C) had the weaker band than those of lane 1 and 2 (40 and 60 °C respectively). These data are plausibly because the hydrolyzed products of **1**, that is, **2** and **3** exhibited tight self-assembly. It is implied that the heat stimulation of 90 °C treatment to **1** induced the loosening or breakout of the self-assembly of **2** and **3**.
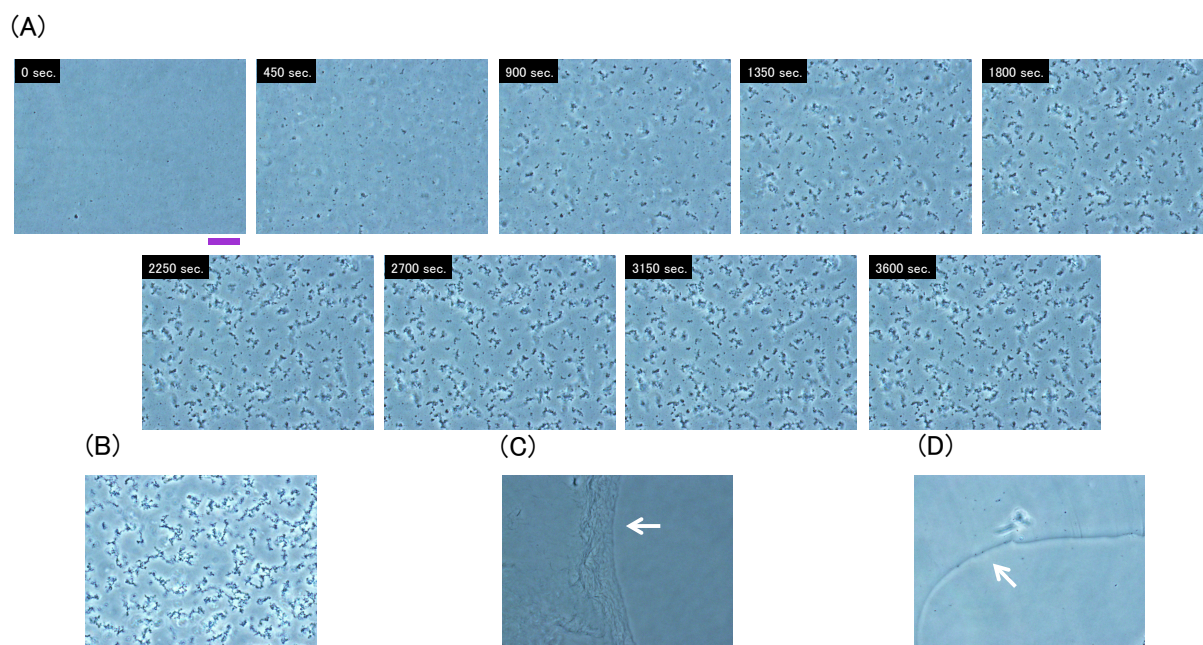
Figure 4.5: DNA-lipid conjugate membrane. (A) Time-course change of microscopy images of the transition of DNA-RNA chimera lipid **1** membrane in the buffer at 40 °C. (B) The microscopy image of the granules of 1:1 mixture of DNA-lipid conjugate **2** and **3** structure in the buffer at room temperature. (C) The 2D casted membrane of only DNA-lipid conjugate **2** in the buffer at room temperature. (D) The 2D casted membrane of only DNA-lipid conjugate **3** in the buffer at room temperature. White arrows show the rims of 2D membrane. Bar = 20 μm.
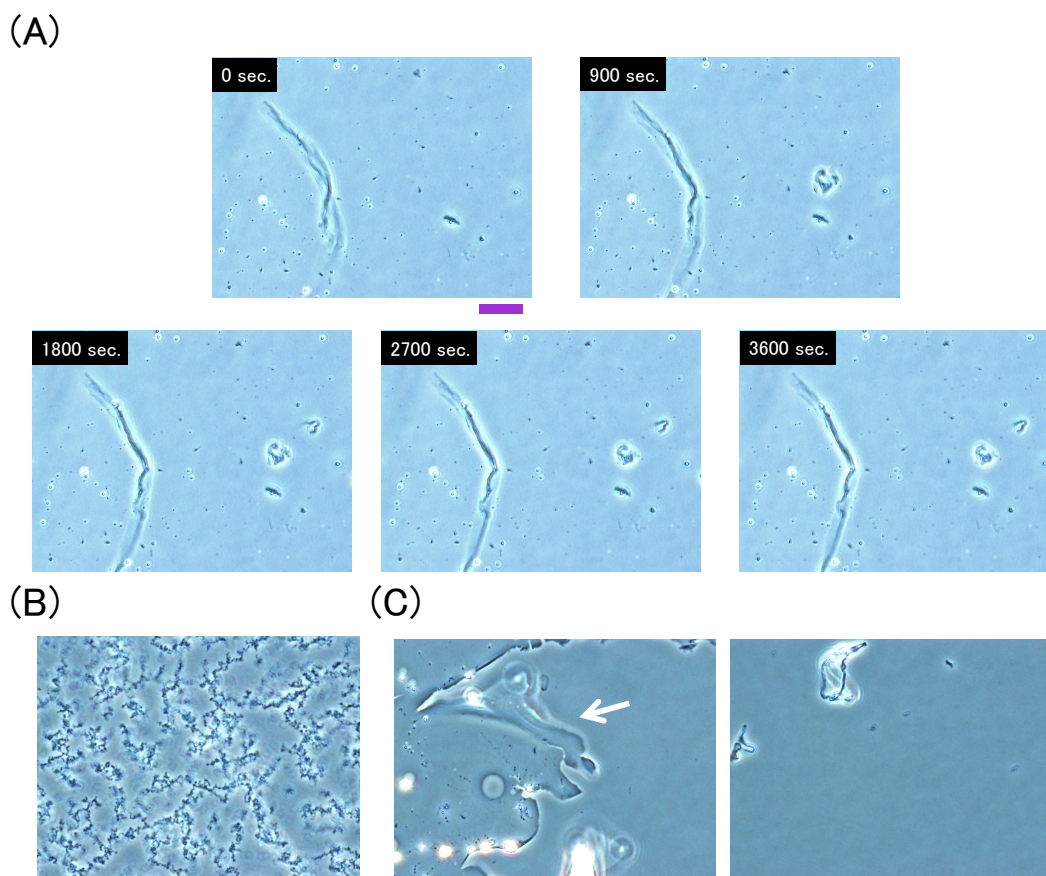
Figure 4.6: Microscopic observation of DNA-lipid conjugate membrane exhibiting no-transition. (A) Time-course change of DNA-lipid conjugate **3** membrane in the buffer at 40 °C incubation. (B) Microscopy image of granules of DNA-RNA chimera lipid **1** incubated at 40 °C for 1.5 hours and left for three days at room temperature. (C) Microscopy image of casted membrane of DNA-lipid conjugate **3** incubated at 40 °C for 1.5 hours and left for three days at room temperature. White arrow shows the rim of the casted membrane. Bar = 20 μm.
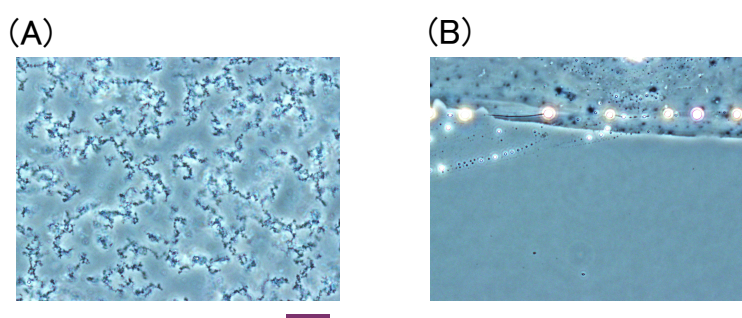
Figure 4.7: Microscopic observation of DNA-lipid conjugate **4** membrane exhibiting no transition. The 2D-3D transition of DNA-RNA chimera lipid **1** was observed in the buffer at 40 °C in 15 minutes (A) while the 2D casted membrane of DNA-lipid conjugate **4** did not change the morphology in the same condition (B). Bar = 20 μm.
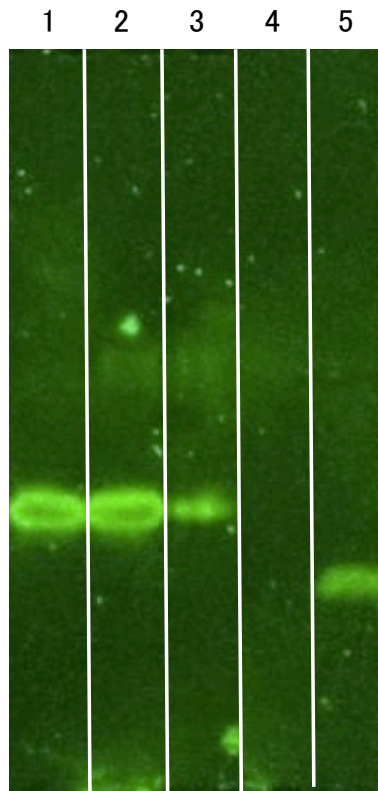
Figure 4.8: Electrocataphoresis result of DNA-lipid conjugates. DNA-RNA chimera lipid **1** was incubated by 40 °C [Lane 1], 60 °C [Lane 2] and 95 °C [Lane 3] in the buffer. DNA-lipid conjugate **2**, and DNA-lipid conjugate **3** was loaded on [Lane 4] and [Lane 5] respectively.

4.4.3 Nanometer-sized self-assembly of DNA-lipid conjugates

It is significant to investigate the self-assembly of the product of **1** after the heat stimulation which induced the 2D-3D transition of the casted lipid membrane. The transmission electron microscopy (TEM) revealed the nanometer scale structures of the DNA-lipid conjugates. Figure 4.9 (A) (B) show the nanomenter-scale TEM image of the specimen of the buffered solution of 32 μM DNA-RNA chimera lipid **1** which was incubated at 40 °C for 15 minutes. Nanometer-sized 3D complex structures and dimples with 200 - 500 nm were clearly observed. The aggregating manner of the structures was resemble to the granule aggregation which was shown in Figure 4.5 (A). Figure 4.9 (C) (D) shows the image of the specimen of the buffered solution of 1:1 mixture of DNA-lipid conjugate **2** and **3** (16 μM per each) which was incubated 40 °C for 15 minutes. The filament structures with their width of 10 - 20 nm and length of 30 - 50 nm their aggregation were found. The aggregation manner of the filament structures is again similar to the granule aggregation observed in Figure 4.5 (B). Note that, although the nanometer-sized self-assembly found in the specimen of the hydrolyzed products of **1** is different from that in 1:1 mixture of DNA-lipid conjugate **2** and **3**, the aggregation manner had been similar. On the other hand, two-dimensional disk-type structures with a textile with width of 300 nm were found in the nanometer-scale TEM image of 32 μM DNA-lipid conjugate **3** which was incubated 40 °C for 15 minutes. The two-dimensional structures observed in the TEM image were able to correspond to the parts of two-dimensional lipid membrane maintained even in the 40 °C treatment, which was observed under the phase contrast microscope (Figure 4.5 (D)).

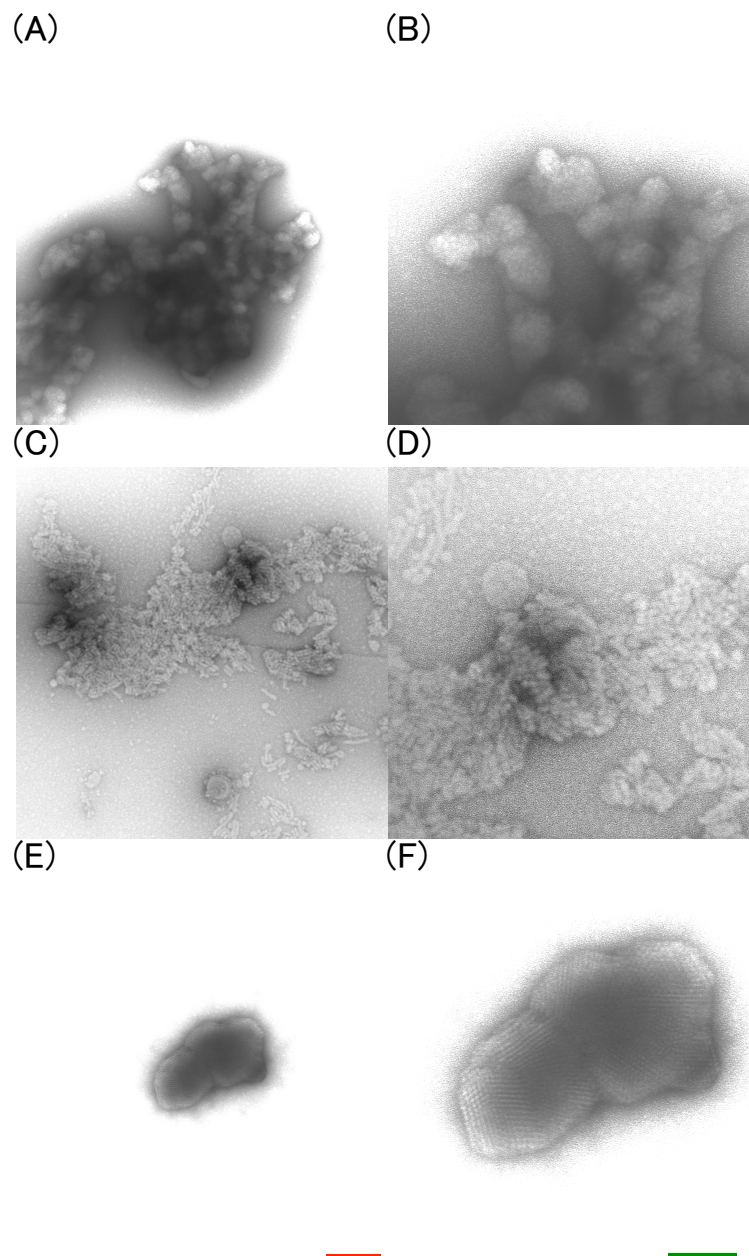Figure 4.9: Transmission electron microscopy images of DNA-lipid conjugate self-assembly. (A)(B) DNA-RNA chimera lipid **1** incubated at 40 °C for 15 minutes in the buffer. (C)(D) 1:1 mixture of DNA-lipid conjugate **2** and **3** incubated at 40 °C for 15 minutes in the buffer. (E)(F) DNA-lipid conjugate **3** incubated at 40 °C for 15 minutes in the buffer. Red bar = 200 nm (A)(C)(E). Green bar = 100 nm (B)(D)(F).

4.5 Discussion

Taking phase contrast microscopy data into account, DNA-RNA chimera lipid **1** was converted to DNA-lipid conjugates **2** and **3** and, as a result, the two-dimensional lipid membrane changed into granule formation and its aggregation as three-dimensional structure. This transition is implied due to the conformation change of membrane molecules involving hydrophobic interaction. Namely, the microscopic observation revealed that 2D-3D membrane transition was induced by heat stimulation.

As the results of TEM images, it can be said that, the buffered solution of DNA-RNA chimera lipid **1** and that of 1:1 mixture of DNA-lipid conjugate **2** and **3** exhibited nanometer-scale self-assembly and their structures were more complicated than that of only DNA-lipid conjugate **3**. By the heat stimulation, DNA-RNA chimera lipid **1** is decomposed to DNA-lipid conjugate **2** and **3** via the breakout at the inserted RNA base "rA", resulting in the 2D-3D transition of the casted lipid membrane.

There have been previous researches on the constitution of the nanometer-sized structures of DNA-modified molecules. Gianneschi group constituted the assembly of DNA-brush copolymers the morphology of which changed from spherical micelle to cylindrical micelle by the injection of the DNA enzyme or the complementary DNA strand [86]. Minseok Kwak and Andreas Herrmann introduced that the linear DNA block copolymer with poly(butadiene) formed vesicles of about 80 nm in diameter. The novel behaviors of self-assembly structures of such amphiphilic oligonucleotides have drawn attention [87]. Sleiman group demonstrated precise self-assembly of hydrophobic polymers and 3D DNA nanostructures. Micelle formation and its aggregation of a DNA polymer conjugate were precisely determined by the DNA cubic structure such like prism as the polar head and the hydrophobic polymer part precisely designed in terms of its length [88]. However, there has been no report on the structure transition in micrometer scale by the chemical conversion of informational materials up to now. Namely, the finding in this chapter is the first experimental result of micrometer-sized molecular self-assembly linked to the information materials. Moreover the transition afforded the emergence of 3D structure by heat stimulation.

Here the results are argued in terms of the Origin of life, especially the "RNA world", because the RNA base in DNA-RNA chimera lipid **1** plays an important role to trigger the three-dimensional body under heat stimulation. In Chapter 1, concerning about the definition of life and origin of life, the role of information materials was described as [**A**] **Self-replication** and [**D**] **Capability to evolve**. Although the RNA world is one of the most important hypotheses, it does not include the fundamental property for life system, i.e. [**C**] **Compartment**. Because a 3D body and its boundary needs to maintain the life system, the structure composed of only RNA is so fragile and degradable that the structure cannot maintain the boundary in an early stage of earth including many heat sources and divalent metal ions. Hence the significance of the current results is one implication that a life system needs DNA to compose and keep its territory in three-dimensional way as well as to make the hereditary information robust for the system. In this sense, the thermal energy of the heat stimulation for the 2D-3D transition is so as an energy source for their bodies indicated in Figure 1.2 (A). Therefore, the findings will contribute an experimental methodology as **Construction** to evaluate how much energy the emergence or the constitution of 3D body structure and its transition containing the information materials taking the minimal condition of life into account.

4.6 Summary

The casted lipid membrane composed of DNA-RNA chimera linked with oleic acid, squalene, and fructose exhibited the transition from two-dimensional structure to three-dimensional structure by the heat stimulation. This transition was plausibly caused by the hydrolysis of DNA-RNA chimera lipid producing two DNA-lipid conjugate molecules and their conformation change, which was discussed with the TEM images of the three-dimensional structures and also electrocataphoresis results.

Chapter 5   General Conclusion

As the general introduction, in Chapter 1, the remained problems of "What is Life?" or "What is the Origin of Life?" were raised. To approach them, this thesis emphasizes the focus point of [C] **Compartment** because the compartment of life system is time-independent factor while other three factors, [A] **Self-replication**, [B] **Energetic Metabolism**, and [D] **Capability to Evolve**, are time-dependent. Hence, to investigate the compartment in terms of the gap between the life and non-life systems, the perturbation approach to the two-dimensional lipid membrane is introduced in this thesis through three techniques (Chapter 2-4 respectively).

Chapter 2 and 3 provide two experimental methods for the reconstituted system of amoeba locomotion. As a model cell, *Dictyostelium discoideum* was adopted and its cytosol was extruded.

In Chapter 2, for using the crude lipid extracted from *Dictyostelium discoideum*, the solid-sustained lipid membrane in a micrometer scale was prepared by the spin coating method. After injection of the cytosol, the membrane deformation and localization of proteins related amoeba locomotion on cell membrane were observed. In other words, the extracts from the dead cells resurged the membrane deformation related to amoeba locomotion by the current method which can be named as the "Frankenstein" method. Namely a part of amoeba motion, which is thought as a perfect life phenomenon, was repaired even using the extracts which were once departed from the successive time line of life. This reconstitution has an impact to the thought that numerous factors and a factor in successive time are peculiar and important in a life phenomenon.

In order to clarify the interaction of these factors more, the supported lipid bilayer membrane containing POPC and phosphoinositide was prepared by the vesicle rapture method and the crude cytosol extracted from *Dictyostelium discoideum* was injected on the SLB membrane. Chapter 3 deals with the results of the cytosol injection, i.e. pore formation, on the SLB membrane. By the analysis on pore formation, the relationship of the cytosol potential and phosphoinositide lipids was revealed. Moreover, the tubular giant vesicles generated from the SLB membrane by the injection of the cytosol including medicines or by a mechanical distortion. Namely, the dead cell cytosol induced the pore formation in the pure lipid SLB membrane the component of which was reduced extremely than that an actual lipid of *Dictyostelium discoideum*. This can afford a minimal model of the amoeba cell membrane. One can affix necessary elements to this model for confirming whether the elements are inevitable or unnecessary. The current result implies that phosphoinositide lipid controlled the potential of the cytosol in the reconstituted system. In a sense that pure lipid SLB membrane is artificially constituted and the extracted cytosol is reconstituted, the current technique is assigned to be the **Pre-reconstruction** method.

The membrane deformation related to cell motion was investigated by the new system replacement or reduction of crude components of cell.

Then, in chapter 4, the **Construction** method approach to membrane deformation using artificial and chemically pure materials was designed to link [C] **Compartment** and other three factors. The casted lipid membrane of a newly designed DNA-RNA chimera lipid exhibited the transition from two-dimensional structure to three-dimensional structure in micrometer scale by heat stimulation. The emergence of the 3D body from the casted lipid membrane was realized by the instability of RNA and temperature controls. This result implies that a life system continues its history by the existence of a DNA to compose territory in three-dimensional way which is not able to be carried out by RNA world hypothesis. Heat stimulation could corresponds to the thermal energy of "food" for their bodies depicted in Figure 1.2 (A). Namely, the molecular design has a potential to explore how much energy the emergence
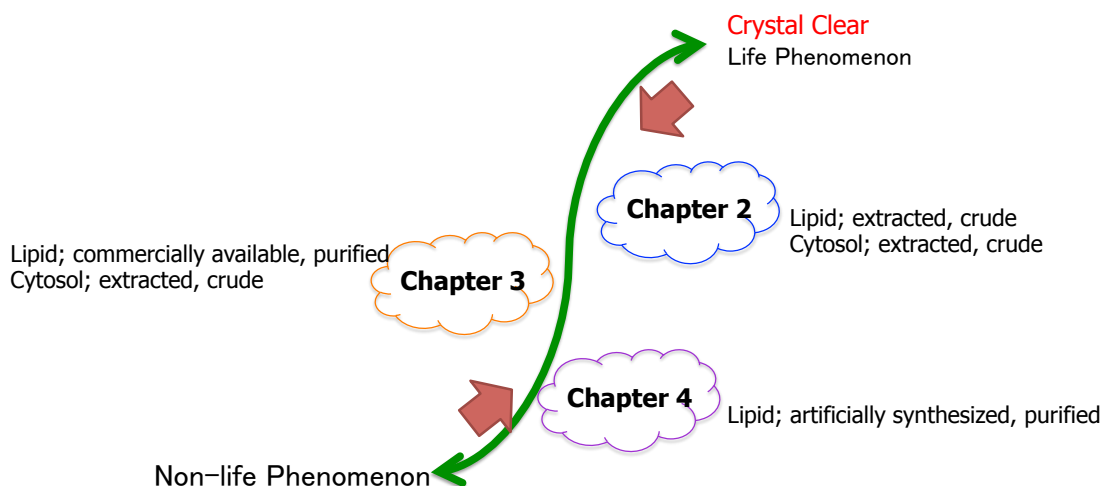
Figure 5.1: Illustration of viewpoints of approaches in this thesis.

of biological body needs.

Finally, the methods and findings are concluded with viewpoints of Figure 1.5. Figure 5.1 demonstrates the mapping of each chapter. *Dictyostelium* lipid patch buckling after injection of cytosol (Chapter 2) is completely assigned to the **Reconstruction** method. The method developed in Chapter 2 is closed to life phenomenon in this thesis. All components were extracted by creation, but the time of life system was not continuous from the history of life. Pore formation on the SLB membrane composed of pure phospholipids after cytosol injection (Chapter 3) is named as the **Pre-reconstruction** method, because the cytosol was crude but the membrane was composed of pure lipids. The 2D-3D transition of DNA-RNA chimera lipid by heat stimulation (Chapter 4) is completely belonging to the **Construction** method. DNA and lipid were related to creation and synthesized artificially, the dynamics are close to physical phenomenon.

All methods described in this thesis rely on the two-dimensional system using lipid membrane films or patches. These have merits in comparison with the reconstruction or construction methods of the encapsulated system using living cells and vesicles. The encapsulated system has the closed boundary separating the body from the outer circumstances, hence the chemical or heat stimulation reaches to the biochemical machinery in diffusion process. Thus the timing of the first stage and the following kinetics of the biochemical machinery linked to the lipid membrane tends to become equivocal. The amount and hydrophobicity/hydrophilicity of the compounds (especially toxic compounds) to be injected are restricted due to the small volume of each compartment and also the living state of the encapsulated system. On the other hand, in the two-dimensional system, the controllable platform to explore the biochemical machinery associated with lipid membranes is realized as a greatest benefit. Namely, the two-dimensional system affords the injection of cytosol or whatever to the lipid membrane at any timing and any ratio because the system is not closed but open. The initial contact of the cytosolic compounds and proteins to the lipid membrane can be easily monitored. For example, in Chapter 2, it was found that PTEN-GFP was localized faster than PH-crac-RFP on *Dictyostelium* lipid patch. In Chapter 3, the fact that PTEN-GFP was localized on even POPC SLB membrane after injection of the cytosol was also described. According to these results, PTEN-GFP is more interactive to the lipid membrane, being clarified for the first time by using the current two-dimensional system. While LY294002 is toxic to the amoeba cells and inhibits the amoeba motion of the cells, the two-dimensional reconstructed system revealed that LY294002 does not influence to the membrane buckling of the *Dictyostelium* lipid patch regardless of the

treatment processes; (i) the cells starving in the presence of LY294002 and (ii) the mixing of an extracted cytosol with LY294002. This result provides us a new insight that the inhibition by LY294002 is activated by three-dimensional encapsulated system of PIP signaling with feedback controls driven by the motion itself. In Chapter 4, the first example of micro-meter sized self-assembly by informational materials was realized and monitored by using the two-dimensional membrane under a phase contrast microscope. Considering the equality of information and energy (refer section 1.1), these DNA-lipid conjugate molecules contribute a controllable device where the emergence of the molecular-based 3D structure is influenced by their sequence information. Therefore, the two-dimensional systems described in this thesis have the strong merit focusing on the direct interaction between lipid membranes and proteins through removing the encapsulation effect (refer section 1.3). Moreover, even though the two-dimensional system is the platform for more physical phenomenon as the initial state, the components and elements exhibited 2D-3D transitions such as membrane buckling (Chapter 2) and tGV formation (Chapter 3). These dynamics or transition were not assigned to a simple swelling process of cell-sized vesicles. In this sense, the two-dimensional system can afford the investigation on the essential part and the very beginning of [**C**] **Compartment** in the "Classical definition of Life". These **Reconstruction** and **Construction** methods as synthetic biology and soft mater science would be contribution for revealing the membrane deformation and comprehending the life systems.

Reference

[1] Hal Tasaki. *Statistical Mechanics 1*. Chapter 1, Baifukan, 2008.

[2] Ashida Masami. *Tokeirikigakuwomanabuhitonotameni*. Chapter 1, Ohmsha, 2006.

[3] Masao Doi. *Introduction to soft matter physics*. Iwanamishuppan, 2010.

[4] Erwin Schrödinger. *WHAT IS LIFE?* Cambridge University Press, 1944.

[5] Alan G. Marshall. *Biophysical Chemistry: Principles, Techniques and Applications*. Chapter 1, john wiley and sons, 1978.

[6] Takahiro Sagawa and Masahito Ueda. Generalized jarzynski equality under nonequilibrium feedback control. *Physical Review Letters*, 104(090602), 2010.

[7] Shoichi Toyabe, Takahiro Sagawa, Masahito Ueda, Eiro Muneyuki, and Masaki Sano. Experimental demonstration of information-to-energy conversion and validation of the generalized jarzynski equality. *Nature Physics*, 6:988–992, 2010.

[8] Kepa Ruiz-Mirazo, Juli Peretó, and Alvaro Moreno. A universal definition of life: Autonomy and open-ended evolution. *Origins of life and evolution of the biosphere*, 34:323–346, 2004.

[9] Joan D Oliver and Randall S Perry. Definitely life but not definitively. *Origins of Life and Evolution of the Biosphere*, 36:515–521, 2006.

[10] Takashi Nakada. Kimagureseibutsugaku, http://www2.tba.t-com.ne.jp/nakada/takashi/origlife/index.html.

[11] Carol E. Cleland and Christopher F. Chyba. Defining 'life'. *Origins of Life and Evolution of the Biosphere*, 32:387–393, 2002.

[12] Tori M Hoehler. An energy balance concept for habitability. *Astrobiology*, 7(6):824–838, 2007.

[13] Walter Gilbert. The RNA world. *Nature*, 319:618, 1986.

[14] Gerald F. Joyce, Alan W. Schwartz, Stanley L. Miller, and Leslie E. Orgel. The case for an ancestral genetic system involving simple analogues of the nucleotides. *Proceedings of the National Academy of Sciences of the United States of America*, 84:4398–4402, 1987.

[15] K Kruger, P J Grabowski, A J Zaug, J Sands, D E Gottschling, and T R Cech. Self-splicing RNA: autoexcision and autocyclization of the ribosomal RNA intervening sequence of Tetrahymena. *Cell*, 31(1):147–157, 1982.

[16] Tracey A. Lincoln and Gerald F. Joyce. Self-sustained replication of an RNA enzyme. *Science*, 323:1229–1232, 2009.

[17] Bianca J Lam and Gerald F Joyce. Autocatalytic aptazymes enable ligand-dependent exponential amplification of RNA. *Nature biotechnology*, 27(3):288–292, 2009.

[18] Jr. Charles Olea, David P. Horning, and Gerald F. Joyce. Ligand-dependent exponential amplification of a self-replicating $_L$-RNA enzyme. *Journal of the American Chemical Society*, 134(8050-8053), 2012.

[19] Michael P. Robertson and Gerald F. Joyce. Highly efficient self-replicating RNA enzymes. *Chemistry & Biology*, 21:238–245, 2014.

[20] Martin M. Hanczyc, Taro Toyota, Takashi Ikegami, Norman Packard, and Tadashi Sugawara. Fatty acid chemistry at the oil-water interface: Self-propelled oil droplets. *Journal of the American Chemical Society*, 129:9286–9291, 2007.

[21] Taro Toyota, Naoto Maru, Martin M. Hanczyc, Takashi Ikegami, and Tadashi Sugawara. Self-propelled oil droplets consuming "fuel" surfactant. *Journal of the American Chemical Society*, 131:5012–5013, 2008.

[22] Daniel Segré, Dafna Ben-eli, David W. Deamer, and Doron Lancet. The lipid world. *Origins of Life and Evolution of the Biosphere*, 31:119–145, 2001.

[23] Dennis E. Discher and Adi Eisenberg. Polymer vesicles. *Science*, 297:967–973, 2002.

[24] J. C. M. van Hest, D. A. P. Delnoye, M. W. P. L. Baars, M. H. P. van Genderen, and E. W. Meijer. Polystyrene-dendrimer amphiphilic block copolymerswitha generation-dependent aggregation. *Science*, 268:1592–1595, 1995.

[25] Peter Walde, Katia Cosentino, Helen Engel, and Pasquale Stano. Giant vesicles: Preparations and applications. *ChemBioChem*, 11:848–865, 2010.

[26] Keitaro Ishikawa, Kanetomo Sato, Yasufumi Shima, Itaru Urabe, and Tetsuya Yomo. Expression of a cascading genetic network within liposomes. *FEBS letters*, 576(3):387–390, 2004.

[27] Shin-ichiro M Nomura, Kanta Tsumoto, Tsutomu Hamada, Kazunari Akiyoshi, Yoichi Nakatani, and Kenichi Yoshikawa. Gene expression within cell-sized lipid vesicles. *Chembiochem*, 4(11):1172–1175, 2003.

[28] Timothy S. Gardner, Charles R. Cantor, and James J. Collins. Construction of a genetic toggle switch in *Escherichia coli*. *Nature*, 403:339–342, 2000.

[29] Yi Elaine Huang, Miho Iijima, Carole A. Parent, Satoru Funamoto, Richard A. Firtel, and Peter Devreotes. Receptor-mediated regulation of PI3Ks confines PI(3,4,5)P3 to the leading edge of chemotaxing cells. *Molecular Biology of the Cell*, 14:1913–1922, 2003.

[30] Dirk Dormann, Gerti Weijer, Carole A Parent, Peter N Devreotes, and Cornelis J Weijer. Visualizing PI3 kinase-mediated cell-cell signaling during *Dictyostelium* development. *Current biology*, 12(14):1178–1188, 2002.

[31] Miho Iijima and Peter Devreotes. Tumor suppressor PTEN mediates sensing of chemoattractant gradients. *Cell*, 109(5):599–610, 2002.

[32] Carole A. Parent, Brenda J. Blacklock, Wendy M. Froehlich, Douglas B. Murphy, and Peter N. Devreotes. G protein signaling events are activated at the leading edge of chemotactic cells. *Cell*, 95:81–91, 1998.

[33] Arpita Upadhyaya, Jeffrey R. Chabot, Albina Andreeva, Azadeh Samadani, and Alexander van Oudenaarden. Probing polymerization forces by using actin-propelled lipid vesicles. *Proceedings of the National Academy of Sciences of the United States of America*, 100(8):4521–4526, 2003.

[34] Nobuhito Mori, Kaori Kuribayashi, and Shoji Takeuchi. Artificial flagellates: Analysis of advancing motions of biflagellate micro-objects. *Applied Physics Letters*, 96:083701, 2010.

[35] Yukinori Nishigami, Masatoshi Ichikawa, Toshiya Kazama, Ryo Kobayashi, Teruo Shimmen, Kenichi Yoshikawa, and Seiji Sonobe. Reconstruction of active regular motion in amoeba extract: dynamic cooperation between sol and gel states. *PLoS One*, 8(8):e70317, 2013.

[36] E. Helfer, S. Harlepp, L. Bourdieu, J. Robert, F. C. MacKintosh, and D. Chatenay. Buckling of actin-coated membranes under application of a local force. *Physical Review Letters*, 87(8):088103, 2001.

[37] Rudolf Merkel, Rudolf Simson, Doris A. Simson, Melanie Hohenadl, Alexei Boulbitch, Eva Wallraff, and Erich Sackmann. A micromechanic study of cell polarity and plasma membrane cell body coupling in *Dictyostelium*. *Biophysical Journal*, 79:707–719, 2000.

[38] Ulrike Mennicke and Tim Salditt. Preparation of solid-supported lipid bilayers by spin-coating. *Langmuir*, 18:8172–8177, 2002.

[39] D. J. Watts and J. M. Ashworth. Growth of myxamoebae of the cellular slime mould *Dicyostelium discoideum* in axenic culture. *Biochemical Journal*, 119:171–174, 1970.

[40] Daisuke Taniguchi, Shuji Ishihara, Takehiko Oonuki, Mai Honda-Kitahara, Kunihiko Kaneko, and Satoshi Sawai. Phase geometries of two-dimensional excitable waves govern self-organized morphodynamics of amoeboid cells. *Proceedings of the National Academy of Sciences of the United States of America*, 110(13):5016–5021, 2013.

[41] Hiroshi Watarai, Yoshimasa Inagaki, Naomi Kubota, Kazumi Fuju, Jun Nagafune, Yasunori Yamaguchi, and Toshihiko Kadoya. Proteomic approach to the identification of cell membrane proteins. *Electrophoresis*, 21:460–464, 2000.

[42] Thomas Gregor, Koichi Fujimoto, Noritaka Masaki, and Satoshi Sawai. The onset of collective behavior in social amoebae. *Science*, 328(5981):1021–5, 2010.

[43] J. R. Bartles, B. T. Pardos, and W. A. Frazier. Reconstitution of discoidin hemagglutination activity by lipid extracts of *Dictyostelium discoideum* cells. *The Journal of Biological Chemistry*, 254:3156–3159, 1979.

[44] Satoru Funamoto, Kristina Milan, Ruedi Meili, and Richard A. Firtel. Role of phosphatidylinositol 3' kinase and a downstream pleckstrin homology domain–containing protein in controlling chemotaxis in *Dictyostelium*. *The Journal of Cell Biology*, 153:795–809, 2001.

[45] Carole A. Parent and Peter N.Devreotes. Molecular genetics of signal transduction in *Dictyostelium*. *Annual Review Biochemisty*, 65:411–440, 1996.

[46] A. D. Bangham, M. M. Standish, and J. C. Watkns. Diffusion of univalent ions across the lamellae of swollen phospholipids. *Journal of Molecular Biology*, 13:238–252, 1965.

[47] Céline Billerit, Gavin D. M. Jeffries, Owe Orwar, and Aldo Jesorka. Formation of giant unilamellar vesicles from spin-coated lipid films by localized IR heating. *Soft Matter*, 8:10823–10826, 2012.

[48] Yoshio Okahata, Tomoya Tsuruta, Kuniharu Ijiro, and Katsuhiko Ariga. Langmuir-blodgett films of an enzyme-lipid complex for sensor membraned. *Langmuir*, 4:1373–1375, 1988.

[49] Thais F Schmidt, Luciano Caseli, Tapani Viitala, and Osvaldo N Oliveira, Jr. Enhanced activity of horseradish peroxidase in langmuir-blodgett films of phospholipids. *Biochimica et biophysica acta*, 1778(10):2291–2297, 2008.

[50] Marie-Paule Mingeot-Leclercq, Magali Deleu, Robert Brasseur, and Yves F Dufrêne. Atomic force microscopy of supported lipid bilayers. *Nature Protocols*, 3(10):1654–1659, 2008.

[51] Marie-Cécile Giocondi, Daisuke Yamamoto, Eric Lesniewska, Pierre-Emmanuel Milhiet, Toshio Ando, and Christian Le Grimellec. Surface topography of membrane domains. *Biochimica et biophysica acta*, 1798(4):703–718, 2010.

[52] Andrea Alessandrini and Paolo Facci. Unraveling lipid/protein interaction in model lipid bilayers by atomic force microscopy. *Journal of Molecular Recognition*, 24(3):387–396, 2011.

[53] Elisa Elizondo, Jannik Larsen, Nikos S. Hatzakis, Ingrid Cabrera, Thomas Bjørnholm, Jaume Veciana, Dimitrios Stamou, and Nora Ventosa. Influence of the preparation route on the supramolecular organization of lipids in a vesicular system. *Journal of the American Chemical Society*, 134:1918–1921, 2012.

[54] Jannik Larsen, Nikos S. Hatzakis, and Dimitrios Stamou. Observation of inhomogeneity in the lipid composition of individual nanoscale liposomes. *Journal of the American Chemical Society*, 133:10685–106887, 2011.

[55] Gerald Wiegand, Noah Arribas-Layton, Heiko Hillebrandt, Erich Sackmann, and Peter Wagner. Electrical properties of supported lipid bilayer membranes. *The Journal of Physical Chemistry B*, 106:4245–4254, 2002.

[56] John S. Ellingson. Changes in the phospholipid composition in the differentiating cellular slime mold, *Dictyostelium discoideum*. *Biochimica et biophysica acta*, 337(1):60–67, 1974.

[57] E. Yavin and A. Zutra. Separation and analysis of ^{32}P - labeled phospholipids by a simple and rapid thin-layer chromatographic procedure and its application to cultured neuroblastoma cells. *Analytical Biochemistry*, 80:430–437, 1977.

[58] G. Weeks and F. G. Herring. The lipid composition and membrane fluidity of *Dictyostelium discoideum* plasma membranes at various stages during differentiation. *Journal of Lipid Research*, 21:681–686, 1980.

[59] Rodolphe Marie, Silvan Schmid, Alicia Johansson, Louise Ejsing, Maria Nordström, Daniel Häfliger, Claus Bv Christensen, Anja Boisen, and Martin Dufva. Immobilisation of DNA to polymerised SU-8 photoresist. *Biosensors & bioelectronics*, 21(7):1327–32, 2006.

[60] Keyur Shah, W.C. Shin, and R.S. Besser. Novel microfabrication approaches for directly patterning PEM fuel cell membranes. *Journal of Power Sources*, 123:172–181, 2003.

[61] Du Yeol Ryu, Kyusoon Shin, Eric Drockenmuller, Craig J Hawker, and Thomas P Russell. A generalized approach to the modification of solid surfaces. *Science*, 308(5719):236–239, 2005.

[62] Sang Ouk Kim, Harun H. Solak, Mark P. Stoykovich, Nicola J. Ferrier, Juan J. de Pablo, and Paul F. Nealey. Epitaxial self-assembly of block copolymers on lithographically defined nanopatterned substrates. *Nature*, 424:411–414, 2003.

[63] Jui-Fen Chang, Baoquan Sun, Dag W. Breiby, Martin M. Nielsen, Theis I. Sölling, Mark Giles, Iain McCulloch, and Henning Sirringhaus. Enhanced mobility of poly(3-hexylthiophene) transistors by spin-coating from high-boiling-point solvents. *Chemistry of Materials*, 16:4772–4776, 2004.

[64] Adam Cohen Simonsen and Luis A. Bagatolli. Structure of spin-coated lipid films and domain formation in supported membranes formed by hydration. *Langmuir*, 20(9720-9728), 2004.

[65] Aurora Dols-Perez, Laura Fumagalli, Adam Cohen Simonsen, and Gabriel Gomila. Ultrathin spin-coated dioleoylphosphatidylcholine lipid layers in dry conditions: A combined atomic force microscopy and nanomechanical study. *Langmuir*, 27:13165–13172, 2011.

[66] Mikkel Herholdt Jensen, Eliza J. Morris, and Adam Cohen Simonsen. Domain shapes, coarsening, and random patterns in ternary membranes. *Langmuir*, 23(15):8135–8141, 2007.

[67] Fredric M. Menger and Miglena I. Angelova. Giant vesicles: Imitating the cytological processes of cell membranes. *Accounts of Chemical Research*, 31(12):789–797, 1998.

[68] M Haugwitz, A A Noegel, J Karakesisoglou, and M Schleicher. *Dictyostelium* amoebae that lack G-actin-sequestering profilins show defects in F-actin content, cytokinesis, and development. *Cell*, 79(2):303–314, 1994.

[69] Andrea Alessandrini, Heiko M. Seeger, Alessandro Di Cerbo, Tommaso Caramaschi, and Paolo Facci. What do we really measure in AFM punch-through experiments on supported lipid bilayers? *Soft Matter*, 7:7054–7064, 2011.

[70] Abdellah Menikh, Samuel P Mickan, Haibo Liu, Robert Maccoll, and X-C Zhang. Label-free amplified bioaffinity detection using terahertz wave technology. *Biosensors & bioelectronics*, 20(3):658–662, 2004.

[71] Michael S. Jablin, Mikhail Zhernenkov, Boris P. Toperverg, Manish Dubey, Hillary L. Smith, Ajay Vidyasagar, Ryan Toomey, Alan J. Hurd, and Jaroslaw Majewski. In-plane correlations in a polymer-supported lipid membrane measured by off-specular neutron scattering. *Physical Review Letters*, 106(138101), 2011.

[72] Martin Loose, Elisabeth Fischer-Friedrich, Jonas Ries, Karsten Kruse, and Petra Schwille. Spatial regulators for bacterial cell division self-organize into surface waves in vitro. *Science*, 320:789–792, 2008.

[73] M D Mager and N A Melosh. Single-step process to reconstitute cell membranes on solid supports. *Langmuir*, 26(7):4635–4638, 2010.

[74] Chris A. Kaiser and Randy Schekman. Distinct sets of SEC genes govern transport vesicle formation and fusion early in the secretory pathway. *Cell*, 61:723–733, 1990.

[75] Peter Novick, Charles Field, and Randy Schekman. Identification of 23 complementation groups required for post-translational events in the yeast secretory pathway. *Cell*, 21(1):205–215, 1980.

[76] Thomas Weber, Boris V. Zemelman, James A. McNew, Benedikt Westermann, Michael Gmachl, Francesco Parlati, Thomas H. Söllner, and James E. Rothman. SNAREpins: Minimal machinery for membrane fusion. *Cell*, 92:759–772, 1998.

[77] James Cardelli. Phagocytosis and macropinocytosis in *Dictyostelium*: Phosphoinositide-based processes, biochemically distinct. *Cell & Molecular Biology*, 2:311–320, 2001.

[78] Jerome Chalmeau, Nadezda Monina, Jonghyeon Shin, Christophe Vieu, and Vincent Noireaux. α-hemolysin pore formation into a supported phospholipid bilayer using cell-free expression. *Biochimica et biophysica acta*, 1808(1):271–278, 2011.

[79] Kwonmoo Lee, Jennifer L Gallop, Komal Rambani, and Marc W Kirschner. Self-assembly of filopodia-like structures on supported lipid bilayers. *Science*, 329(5997):1341–1345, 2010.

[80] Seungpyo Hong, Pascale R. Leroueil, Elizabeth K. Janus, Jennifer L. Peters, Mary-Margaret Kober, Mohammad T. Islam, Bradford G. Orr, Jr. James R. Baker, and Mark M. Banaszak Holl. Interaction of polycationic polymers with supported lipid bilayers and cells: Nanoscale hole formation and enhanced membrane permeability. *Bioconjugate Chemistry*, 17:728–734, 2006.

[81] Ichiro Hatta and Masayuki Murata. *Biological membrane dynamics series・New biophysics*. Kyoritsushuppan, 2000.

[82] R R Breaker and G F Joyce. A DNA enzyme that cleaves RNA. *Chemistry & Biology*, 1(4):223–229, 1994.

[83] R R Breaker and G F Joyce. A DNA enzyme with Mg^{2+}-dependent RNA phosphoesterase activity. *Chemistry & Biology*, 2(10):655–660, 1995.

[84] Michael Zuker. Mfold web server for nucleic acid folding and hybridization prediction. *Nucleic Acids Research*, 31(13):3406–3415, 2003.

[85] Jr. John Santalucia. A unified view of polymer, dumbbell, and oligonucleotide dna nearest-neighbor thermodynamics. *Proceedings of the National Academy of Sciences of the United States of America*, 95:1460–1465, 1998.

[86] Miao-Ping Chien, Anthony M. Rush, Matthew P. Thompson, and Nathan C. Gianneschi. Programmable shape-shifting micelles. *Angewandte Chemie International Edition*, 49:5076–5080, 2010.

[87] Minseok Kwak and Andreas Herrmann. Nucleic acid amphiphiles: synthesis and self-assembled nanostructures. *Chemical Society Reviews*, 40:5745–5755, 2011.

[88] Christopher J. Serpell, Thomas G. W. Edwardson, Pongphak Chidchob, Karina M. M. Carneiro, and Hanadi F. Sleiman. Precision polymers and 3D DNA nanostructures: Emergent assemblies from new parameter space. *Journal of the American Chemical Society*, 136:15767–15774, 2014.

Acknowledgement

I am most grateful to Prof. Taro Toyota for supervising my doctoral dissertation.

I want to express my sincere appreciation and gratitude to Prof. Satoshi Sawai and Assistant Prof. Nao Shimada for the collaboration and valuable discussions.

I would like to thank Prof. Yuichi Wakamoto, Dr. Akihiko Nakajima, Mr. Fumihito Fukujin, Prof. Hiroyuki Noji, Prof. Kazuhito Tabata, and all Sawai Laboratory members for the precious discussions about especially Chapter 2 and 3.

I also thank Assistant Prof. Koh-ichiro Shohda, Ms. Maasa Yokomori and all Toyota Laboratory members, especially Mr. Kiyoto Omata, Mr. Muneyuki Matsuo, Mr. Yuki Kazayama, and Assistant Prof. Taisuke Banno for the valuable suggestions and comments about Chapter 4.

Special thanks go out to Dr. Juan Castro Mannuel (Waseda University), Prof. Ken Takai (Japan Agency for Marine-Earth Science and Technology), Prof. Kunihiko Kaneko, Prof. Takahiro Sagawa, Prof. Tadashi Sugawara (Kanagawa University), Prof. Akira Suyama, Prof. Tetsuro Nikuni (Tokyo University of Science), Prof. Koji Fukushima, Prof. Martin Hanczyc (University of Trento), Prof. Akira Shimizu, Prof. Albert J. Libchaber (Rockefeller University), Assistant Prof. Yusuke T. Maeda (Kyoto University), Prof. Hiroyuki Kitahata (Chiba University), Prof. Tatsunari Sakurai (Chiba University), Mr. Mikihiro Hashimoto, Mr. Georg Tremmel, Prof. Kheya Sengupta (Centre Interdisciplinaire de Nanoscience de Marseille), and Prof. Shugo Nakamura.

Finally, I would like to express my heartfelt gratitude to my family, all my friends, and you.

List of Publication

Kei Takahashi and Taro Toyota

Autonomous Buckling of Micrometer-Sized Lipid-Protein Membrane Patches Constructed by *Dictyostelium discoideum*

Journal of Biological Engineering, **9**:3, 21 January 2015

Kei Takahashi and Taro Toyota

Membrane Transition of Solid-supported Lipid Bilayer under Amoeba Cytosol

to be prepared.